STARS

University of Central Florida

STARS

Electronic Theses and Dissertations, 2004-2019

2016

Biophysical Sources of 1/f Noises in Neurological Tissue

Alan Paris
University of Central Florida

Part of the Medical Biophysics Commons

Find similar works at: https://stars.library.ucf.edu/etd

University of Central Florida Libraries http://library.ucf.edu

STARS Citation

University of Central Florida

STARS
Showcase of Text, Archives, Research & Scholarship

BIOPHYSICAL SOURCES OF 1/F-TYPE NOISES IN NEUROLOGICAL SYSTEMS

by

ALAN PARIS
B.S. in Mathematics, Massachusetts Institute of Technology, Cambridge MA, 1984
M.S. in Mathematical Logic, Cornell University, Ithaca NY, 1988

A dissertation submitted in partial fulfilment of the requirements
for the degree of Doctor of Philosophy
in the Modeling and Simulation Program
in the College of Graduate Studies
at the University of Central Florida,
Orlando, Florida

Fall Term
2016

Major Professors: Azadeh Vosoughi, George Atia

ABSTRACT

High levels of random noise are a defining characteristic of neurological signals at all levels, from individual neurons up to electroencephalograms (EEG). These random signals degrade the performance of many methods of neuroengineering and medical neuroscience. Understanding this noise also is essential for applications such as real-time brain-computer interfaces (BCIs), which must make accurate control decisions from very short data epochs. The major type of neurological noise is of the so-called **$1/f^\theta$-type**, whose origins and statistical nature has remained unexplained for decades. This research provides the first simple explanation of $1/f^\theta$-type neurological noise based on biophysical fundamentals. In addition, noise models derived from this theory provide validated algorithm performance improvements over alternatives.

Specifically, this research[1] defines a new class of formal latent-variable stochastic processes called **hidden quantum models** (HQMs) which clarify the theoretical foundations of ion channel signal processing. HQMs are based on **quantum state processes** which formalize time-dependent observation. They allow the quantum-based calculation of channel conductance autocovariance functions, essential for frequency-domain signal processing. HQMs based on a particular type of observation protocol called **independent activated measurements** are shown to be distributionally equivalent to hidden Markov models yet without an underlying physical Markov process. Since the formal Markov processes are non-physical, the theory of activated measurement allows merging energy-based Eyring rate theories of ion channel behavior with the more common phenomenological Markov kinetic schemes to form **energy-modulated quantum channels**. These unique biophysical concepts developed to understand the mechanisms of ion channel kinetics have the potential of revolutionizing our understanding of neurological computation.

To apply this theory, the simplest quantum channel model consistent with neuronal membrane voltage-clamp experiments is used to derive the activation eigenenergies for the Hodgkin-Huxley K^+ and Na^+ ion channels. It is shown that maximizing entropy under constrained activation energy yields noise spectral densities approximating $S(f) \sim 1/f^\theta$, thus offering a biophysical explanation for this ubiquitous noise

---

[1]Portions of this abstract have appeared in [1–3].

component. These new channel-based noise processes are called **generalized van der Ziel–McWhorter** (GVZM) power spectral densities (PSDs). This is the only known EEG noise model that has a small, fixed number of parameters, matches recorded EEG PSDs with high accuracy from 0 Hz to over 30 Hz without infinities, and has approximately $1/f^{\theta}$ behavior in the mid-frequencies.

In addition to the theoretical derivation of the noise statistics from ion channel stochastic processes, the GVZM model is validated in two ways. First, a class of mixed autoregressive models is presented which simulate brain background noise and whose periodograms are proven to be asymptotic to the GVZM PSD. Second, it is shown that pairwise comparisons of GVZM-based algorithms, using real EEG data from a publicly-available data set, exhibit statistically significant accuracy improvement over two well-known and widely-used steady-state visual evoked potential (SSVEP) estimators.

Dedicated to my heroes and teachers Johannes Kepler and Norbert Wiener and most of all to my Professor, Dr. Anil Nerode, who continued to believe in me long after I stopped believing in myself.

We have contributed to the initiation of a new science which . . . embraces technical developments with great possibilities for good and for evil. We can only hand it over to the world that exists about us . . . We do not even have the choice of suppressing these new technical developments. They belong to the age, and the most any of us can do by suppression is to put the development of the subject in the hands of the most irresponsible and most venal of our engineers . . . There are those who hope that the good of a better understanding of man and society which is offered by this new field of work may anticipate and outweigh the incidental contribution we are making to the concentration of power (which is always concentrated, by its very conditions of existence, in the hands of the most unscrupulous). I write in 1947 and I am compelled to say it is a very slight hope.

Norbert Wiener, Cybernetics

ACKNOWLEDGMENTS

TABLE OF CONTENTS

LIST OF FIGURES

LIST OF TABLES

LIST OF ACRONYMS

AR   Autoregressive.

AR-GVZM   Autoregressive generalized van der Ziel - McWhorter process (Sec. 5.2.6: Eq. 5.12).

ARMA-N N–periodic autoregressive – moving average (Appendix F: Def. 42).

BCI   Brain-computer interface (Sec. 1.1, Sec. 2.3).

EEG   Electroencephalogram, electroencephalography.

FPR   False positive rate (Sec. 6.6: Def. 29).

GVZM   Generalized van der Ziel - McWhorter autocovariance (Sec. 5.1: Def. 20), power spectral density (Sec. 5.2.4: Def. 21), and noise model. (Sec. 5.2.7: Def. 22).

HAMM   Hidden activated measurement model (Sec. 3.4: Def. 12).

HARM   Hidden autoregressive model (Sec. 5.2.1: Examp. 9).

HH   Hodgkin-Huxley.

HMM   Hidden Markov model (Sec. 2.1.2).

HQM   Hidden quantum model (Sec. 3.3: Def. 10).

MIT   Massachusetts Institute of Technology.

PSD   Power spectral density (Appendix F: Def. 44).

ROC   Receiver operating characteristics (Chap. 6).

SSVEP   Steady-state visual evoked potential (Sec. 1.1, Sec. 2.3).

TPR   True positive rate (Sec. 6.6: Def. 29).

UCF   University of Central Florida, Orlando FL.

CHAPTER 1: INTRODUCTION
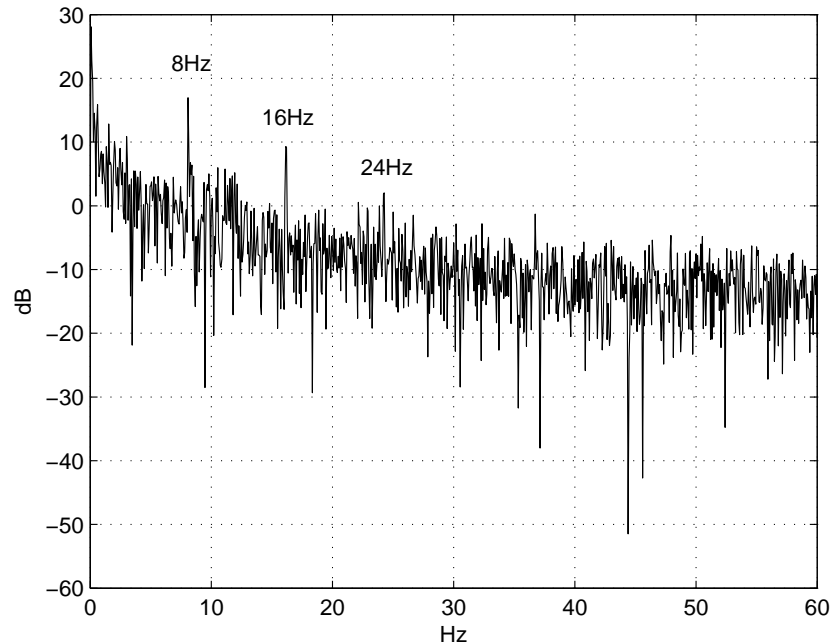
Figure 1.1: Recorded EEG single-epoch periodogram from a 15-second, 8Hz SSVEP experiment showing the stimulus frequency and two harmonics.

1.1   Research History: γ–band Steady State Visual Evoked Potentials

This research originated in meetings held in July, 2013 between the author and professors Azadeh Vosoughi and George Atia of the University of Central Florida's (UCF) department of Electrical and Computer Engineering during which we discussed the possibility of real-time, steady-state visual evoked potential (SSVEP) brain computer interfaces (BCI) [4–6] using stimulus frequencies above 30Hz. The great advantage of such high frequency (γ–band) stimuli is that they dramatically reduce the discomfort, fatigue, and the potential for seizures caused by the long-term viewing of low-frequency flashing. These problems are especially acute for fully paralyzed patients [7] who cannot look away from the bright flashes. This is the central reason that SSVEP BCIs have not been offered as a practical solution to the problem of control and communication in the disabled population, even though the hardware and software technology is simple and reliable (Fig. 1.1;

1

see also [8]).

Super-30Hz stimuli are known to produce measurable brain responses [9] and can be utilized, to some extent, for BCI control [10–13]. However, their overwhelming advantage is not only that high-frequency flashing is less fatiguing but, as with animations and video, it actually becomes less and less noticable as the frequency increases. At some (possibly subject-dependent) level, the stimuli frequency is so high that the subject has no **conscious** awareness of any flashing even though there is indisputable evidence that the brain continues to synchronize with signals at as high as 100Hz. [9].

Successful detection of γ–band stimuli opens a world of applications for SSVEP BCIs well beyond the disabled population. For example, one can imagine brain-based gaming control [14] in which avatars, weapons, and virtual locations are flashing at distinct, yet consciously invisible, frequencies so that a glance at an object or place is sufficient to initiate activity. One can even envision a physical SSVEP-control home or work environment where strobe lights invisibily illuminate objects and places and in which a disabled person can navigate a wheelchair by merely looking at the desired location. There are numerous other transformational, BCI-inspired applications which will be within reach once the γ–barrier is broken. For these reasons, commercial BCI companies are actively investigating γ–band detection and estimation of SSVEP signals [15].

The new approach proposed by the author in 2013 was a sensitive audio and image technique called *homomorphic signal processing* or *ceptral analysis* (pronounced "kepstral") [16] which exploited the response harmonics (see Fig. 1.1) resulting from brain non-linearity [8, 9]. The hope was this would prove effective in spite of the well-known response attenuation at high stimulus frequencies. However, we found that cepstral analysis failed on the high-frequency SSVEP detection problem due to the level of noise inherent in short-epoch neurological signals, even after many months of intense development. Fig. 1.2 is a typical example of 28Hz SSVEP stimulus showing how the resulting spectral spike is nearly indiscernable from the noise peaks. We found that the sophistication of the cepstral technique actually limited its usefulness in the presence of strong noise.

The traditional method for reducing neurological noise is *multi-epoch averaging* [17, 18], usually over sev-
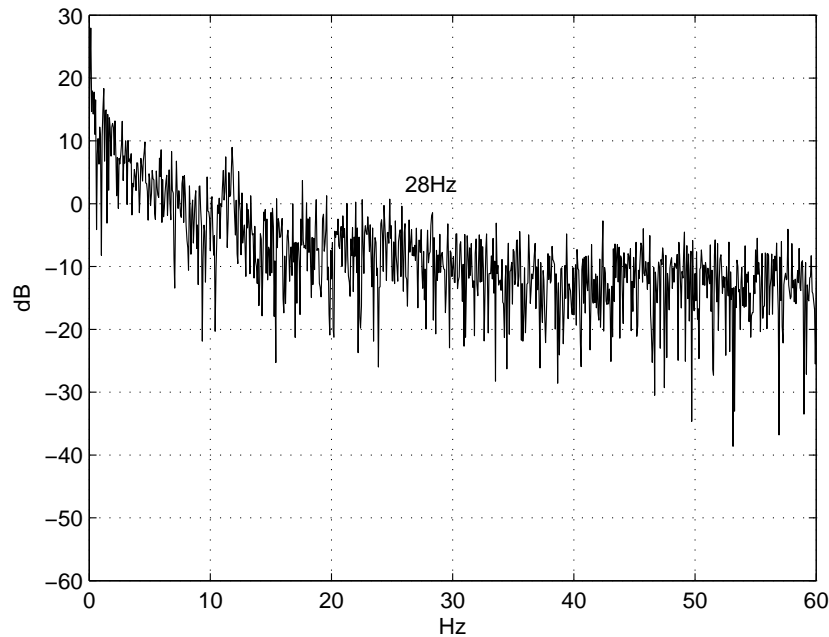
Figure 1.2: Recorded EEG single-epoch periodogram from a 15-second, 28Hz SSVEP experiment showing the 28Hz response nearly lost in brain background noise. The α–band power around 12Hz is also evident.

eral minutes, in the frequency domain (or time domain if precise phase-synchronization is posssible). However, a basic target for effective real-time control is to use the shortest sampling periods possible. For example, a highly-cited SSVEP BCI paper [5] limited these periods to no more than 8 seconds (see Sec. 7.1). We allowed ourselves sampling periods up to 15 seconds (Chap. 7) for development purposes but these were still too short for splitting into epochs while maintaining adequate frequency resolution.

Recognizing that the significance of background neurological noise is much larger than any particular BCI application, we decided to confront this noise head-on by proceeding simultaneously in two, nearly opposite, directions:

- Drilling down into electroencephalogram (EEG) cortical sources to understand the biophysical mechanisms which give rise to dominant noise components.

- Expanding outward using the knowledge gained about noise generation mechanisms in order to create superior SSVEP detection and estimation algorithms.

As will be seen (Chap. 4, Chap. 5, Chap. 7), we have achieved considerable success in both these directions. This has brought the original γ–band BCI application finally within range of laboratory work [19, 20] .

1.2   On the Mathematical Modeling of Neurological Systems

Linearity seems elegant only when one has not seen an even more attractive, essentially non-linear generalization.   *Roger Penrose*

Sec. 1.4 sets out the objective scientific goals of this research but some general remarks concerning mathematical modeling are necessary because they reveal the larger purpose of this work.

Great mathematical abstractions and algorithms do not derive from merely choosing a few ready-made techniques from a standard toolbox and then applying them to new data, although this must certainly be part of an initial exploration. One only needs to recall Newton who invented calculus not as an act of pure mathematics (although he was also a brilliant pure mathematician) but because the one-dimensional, constant acceleration models of Galileo were inadequate to account for planetary motion.

The mathematician Norbert Wiener was one of the founding geniuses of 20th signal processing who, as far back as the early 1920's, developed the first mathematically rigorous theory of random noise processes and their use as signal sources [21], a profoundly original theory whose applications continue even into 21st century quantum field theory [22]. However, his abstract mathematical model of random processes was proposed after a deep prior study of the work of Einstein, Perrin and others [23] on the physical Brownian motions which he was trying to explain. Similarly, it is not well-known that Wiener's work on the causal linear filtering, interpolation, and extrapolation of time series [24], which required the creative development of abstract harmonic analysis in the complex plane and which continues to play a central role in signal processing, was developed during World War II to solve the particular problem of aiming anti-aircraft guns to shoot down rapidly-moving enemy aircraft.

Within neuroscience, Hodgkin and Huxley (HH) developed their famous non-linear, 2nd –order partial dif-

ferential equation for action potentials as well as its first numerical solutions [25] only after they had first learned everything that was possible to learn about nerve conduction using 1950's laboratory technology [26]. As a result of this depth, and though continually modified and generalized over the years, the HH conduction model continues to form a foundational paradigm of neuroscience over 60 years after it was first proposed.

On the other hand, one only need consider the neuroscience proposals of Roger Penrose and his collaborators to see neuroscience modeling gone awry. During the 1980's Penrose, published some fascinating verbal speculations on the relation between quantum coherence, general relativity, and human consciousness [27] (and see his very insightful quotation above). However, by the early 2000's, these speculations had untethered from neuroscience reality to form a vastly complex mathematical/physical dreamworld of "microtubules" as the seat of consciousness [28]. This is in spite of regular, and highly-public, expert refutations by neuroscientists [29, 30] and physicists [31].

It is the author's strongly-held opinion, to take just one example, that epilectic seizure identification, prediction, and control will not be advanced by researchers who see neurology as merely another source for abstract data on which to exercise their favorite, off-the-shelf, statistical algorithms. Rather, the signal processing of epilectic seizure signals will be advanced by researchers who are passionately interested in **curing epilepsy**. In this way, the mathematical techniques will grow naturally from epilepsy research itself.

With that philosophical background, it must be stated that the "hidden agenda" of this research is the demonstration by example that organic, mathematical growth based on ever-advancing neuroscience knowledge is the most valid approach to modeling. The problem of γ–band SSVEP BCI affords a perfect test case for this. Specifically, the author created the hidden activated quantum process theory of Chap. 3, the energy-gated quantum ion channel model of Chap. 4, the noisy tissue and generalized van der Ziel – McWhorter (GVZM) autocovariance formulas of Chap. 5, the SSVEP BCI applications of Chap. 7, and even the SSVEP algorithm statistical comparison methodology of Chap. 6 to solve specific technical problems involved in γ–band SSVEP BCI. It is the author's strong belief that, although created with this single-minded, practical focus, the methods subsequently will prove useful in many other areas of neurological signal processing.

1.3 Brain Background Noise

Signals recorded from living neurological tissue are extremely noisy at all scales from individual ion channels [32] through collections of one or more neurons [33–35] up to scalp-recorded EEGs [36] (Fig. 1.2) Data taken from [37]). As a result, the theory of neurological noise continues to be a thriving area for research [38], with theoretical and practical implications for neurological signal processing, neuroscience, and medical neurology.

Neuronal noise is a major factor limiting the success of neuroengineering applications such as brain-computer interfaces (BCI) [4, 7] and automatic seizure detection and control [39, 40]. In particular, high-power $1/f$-type noise is omnipresent in all measurements of the electromagnetic properties of neurons [38, 41, 42] from the compartment level [43–45] through axonal transmission [33, 46], up to EEG [36, 47].

Neurological noise cannot be eliminated from *in vivo* studies because it originates directly from the biological mechanisms themselves [35, 48, 49] and may even be an essential component of neuronal computation [50–52]. Moreover, unlike inorganic sources of data for signal processing, neuronal noise obviously cannot be reduced through cooling or improved manufacture.

On the other hand, the statistics of neuronal noise also can provide useful indirect constraints on dynamic neuron models and has led to major advances in pure neuroscience [53] and medicine [54, 55].

In fact, the traditional model of an information-carrying signal corrupted by interfering noise is problematic for neurological sources since the conceptual classification into signal vs. noise remains a topic of controversy [50]. Therefore understanding the definitions, mechanisms, and statistical properties of neuronal noise is of critical importance for both theory and applications neurological signal processing [35, 38]. However, there has been no completely satisfying abstract model of neurological $1/f$-type noise.

For example, it is well-known (e.g., [35]) that a properly-weighted sum of noise spectra of the so-called **Lorentzian** [41] form $S_{f_0}(f) \propto 1/(1 + (f/f_0)^2)$, where f_0 are appropriately-chosen "cut-off frequencies", can approximate $1/f$ noise spectrum in neuronal tissue . However no general procedures exist in the

literature for selecting the number of Lorentzians, their weighting coefficients, or the cut-offs.

1.4   Goals of this Research

The main goal of this report is to present an abstract, biophysically-consistent model of neural tissue by considering **populations of quantum ion channels in thermal equilibrium** (cf. Sec. 5.1) and use these tissue models to better understand the statistics of the $1/f$-type noise which they generate. In particular, we will investigate a new class of stationary processes called **generalized van der Ziel – McWhorter noise** (Sec. 5.2.7) which arise directly from the the new models by a generalization of the weighted Lorenztian mechanism and which form a very flexible parametric model for $1/f$-type noise in neurological applications.

In this paper we examine the statistical characteristics of EEG periodograms [16, 56]. Specifically, we present a new model for the statistical properties of EEG background processes which, for the purpose of many applications, may be regarded as "brain noise". To the best of our knowledge, it is the first simple and general noise model in the EEG literature which closely matches recorded EEG periodograms from near 0 Hz to over 30 Hz. We then validate this new model using three different and complementary approaches. Our research on neurological noise is focused on three main goals:

● *Improving the performance of real-time neurological algorithms:* Certain neurological signal processing tasks, such as extracting event-related potentials (ERPs), increase signal-to-noise ratios by averaging many epochs of data recorded over long experimental periods [17]. However, time-frequency algorithms, which assume high levels of nonstationarity [40], and BCIs [5, 6], which are meant to provide disabled patients with a sense of real-time control, must work with much shorter, single-trial epochs.

Ordinary linear filtering of such short epochs is problematic, since there is evidence that the brain's responses are highly nonlinear [39], and because the target signals can be nearly indistinguishable from the background (cf. Fig. 1.2). Such poorly-fitting models of the detailed statistical characteristics of brain processes reduces the precision of detection/estimation procedures and makes model validity uncertain.

Our particular interest is developing real-time SSVEP BCI algorithms which are accurate into the γ-band,

above 30 Hz, a region of the EEG spectrum which is dominated by noise.

• *Creating statistically-realistic simulations of neurological signals:* A common research practice is to add artificial noise sources to neurological simulations in order to increase their realism and to measure the performance of models and algorithms [35]. Good simulations of neurological signals are essential for the development and testing of medical and BCI algorithms, especially for critical applications to human neurology [39, 40] in which experimentation is highly restricted.

• *Generating new insight into underlying neurological processes:* Statistical models of neurological noise have had remarkable success in providing indirect tests of neuroscience hypotheses. This was spectacularly true for the elucidation of the acetycholine neurotransmission mechanisms in the 1970's by Katz & Miledi [53]. But noise models continue to enhance our understanding of neurological illness [54, 55], cognitive processes [51], and may even explain brain nonlinearity [57].

CHAPTER 2: LITERATURE REVIEW

2.1 Quantum Ion Channels

Abstract mesoscale models of neurological tissue and signals[1] are a key bridge between the hyper-detailed nanoscale structural and behavioral analyses of ion channels obtained by modern biochemical techniques [58] and the overly-simplified macroscale (i.e., neuron-level) synthetic neuron models pioneered by Mc-Colloch and Pitts [59] in the 1940's which are the basis for current neural network technology. Improved models in the mesoscale have significance for biological neuroscience and neurology, neurological signal processing and engineering, as well as synthetic neural networks for massive computation.

There has been enormous progress made in terms of **concrete** or protein-structural models of neuronal ion channels [58]. Such concrete understanding of the nanomechanical and biochemical behavior of these channels is essential for pure neuroscience and its applications to neuropharmacology. However, there is simultaneously an expanding need for **abstract** mathematical channel models because the detailed architecture of concrete models makes them inappropriate as the elementary units needed for signal processing, biometic networks, neuroengineering, and whole-brain neurology.

A very successful direct abstraction of the activation-energy basis of structural channels was made through the theory of **Eyring rate channels** [60] (cf. Sec. 2.2.4). Although subject to recent criticism [61] they still form a dominant conceptual framework for understanding aggregate conductance properties of membranes [34, 62]. However, the absence of a kinetic mechanism limits their usefulness for understanding dynamic processes such as neuronal noise.

On the other hand, throughout the 60's, 70's, and 80's, the ion channel kinetics discovered by Hodgkin and Huxley [25, 63] were abstracted by Fitzhugh, Clay, Hill and Chen, DeFelice *et al.*, and others [32, 64–72] to form the core of the highly successful standard **Markov process model of neuronal noise** [34]. These models were purely phenomenological in the sense that the all-important **transition probabilities**

---

[1] Portions of this section have appeared in [1].

between states were derived to match experimental conductance curves without an underlying biophysical framework. Nevertheless, such models accounted for some of the spectral structure of membrane noise.

However, since that time, very few general classes of alternative abstract stochastic channel models have been investigated even though the standard models are known to have difficulty explaining the ubiquitous $1/f$–**type noise** in neurological tissue [32] (cf. Sec. 2.2.5).

(See also [73–76].)

2.1.1 Quantum Mechanics and Signal Processing

A subtle limitation of standard formulations of quantum mechanics is that it has difficulty with the concept of sampling a physical system over time because of unsolved metaphysical problems concerning the role of the **observer** and **wavefunction collapse**. (Refer to Appendix A for a summary of quantum mechanics.) This is seen most clearly in the paradoxical "watched pot theorem" [77] which seems to imply that sampled quantum systems are always frozen into their initial states.

As a consequence, while standard quantum mechanics has no trouble defining what is meant by the state $\Psi(t)$ of a system at a single time t, the ambiguities resulting from the Measurement Problem makes it difficult to assign meaning to a state $\Psi(t_1, t_2)$ which is supposed to represent the system at two distinct times $t_1 < t_2$ (cf. Chap. 3 for a complete discussion).

This causes enormous practical problems for signal processing in quantum systems because the standard autocovariance function

$$R_A(t_1, t_2) \overset{\text{def}}{=} \mathsf{E}\left[(A_{t_1} - \mu_A(t_1)) \cdot (A_{t_2} - \mu_A(t_2)) \mid \Psi(t_1, t_2)\right]$$

on which the entire theory of power spectra rests is thus ill-defined.

More generally, it is essential for ion channel signal processing to be able to calculate the higher moments $\mathsf{E}[A_1(t_1) \cdots A_n(t_n) \mid \Psi(\cdot)]$ of observables $A_1, \cdots A_n$ at distinct times $t_1 < \cdots < t_n$ for systems prepared

10

in quantum state Ψ.

The calculation of $\mathsf{E}\left[A_1\left(t_1\right)A_2\left(t_2\right)\mid\Psi\left(\,\cdot\,\right)\right]$ requires knowledge of **every measurement made by the observer during the closed interval** $[t_1, t_2]$ because every such measurement caused the system to collapse into a measurement state at the moment it was made (Appendix A Def. **??**). Different observer behaviors would lead to completely different average values of the product $A_1\left(t_1\right)\cdot A_2\left(t_2\right)$. So a concept of a state which intuitively corresponds to $\Psi\left(t_1, t_2\right)$ can only be defined in the context of the knowledge of the **observer's actions through time** and must implicitly encode that knowledge into some form of **measurement protocol**.

This is in contrast to the calculation of $\mathsf{E}\left[A_1\left(t_1\right)\mid\Psi\right]$ at time t_1 for which the closed "interval" $[t_1, t_1]$ leaves room for, at most, a single measurement. For this reason, completely general observer-independent statements such as Born's Axiom (Appendix A Def. 32) are possible at a single time, but not over a non-trivial time interval.

See Sec. 3.1: Remark 6 for a further discussion of this issue and our solution to it.

2.1.2 Classical Stochastic Processes

Several observations first need to be made concerning general stochastic processes. In particular, we need to make conceptual distinctions between **formal** and **concrete** processes and also between **physical** and **simulated** processes.

2.1.2.1 Process Classification

By an (absolutely continuous, real-valued, Borel [78]) **formal** stochastic process $\{X_t\}_{T_1\leqslant t\leqslant T_2}$ on the time interval $[T_1, T_2]$ we mean the specification of a family

$$\{p_{t_1,\cdots,t_n}\left(x_1,\cdots,x_n\right)\mid T_1\leqslant t_1<\cdots<t_n\leqslant T_2, 0\leqslant n<\infty\}$$

of probability distributions on $\mathbb{R}$ satisfying the **Kolmogoroff consistency** or **marginalization** conditions: $p_\emptyset\,(\,) = 1$ for $n = 0$ and

$$p_{t_1,\cdots,\widehat{t_i},\cdots,t_n}\,(x_1,\ldots,\widehat{x_i},\ldots,x_n) = \int\limits_{-\infty}^{\infty} p_{t_1,\cdots,t_i,\cdots,t_n}\,(x_1,\ldots,x_i,\ldots,x_n)\ dx_i \qquad (2.1)$$

for every $n > 0$, $T_1 \leqslant t_1 < \cdots < t_n \leqslant T_2$, and $1 \leqslant i \leqslant n$, where the caret $\widehat{\cdot}$ indicates a item deleted from a list (cf. Appendix G). Thus the **form** of the probability distribution functions through time are given.

On the other hand, by a **concrete** stochastic process [56, 79] we mean the specification of an underlying sample space Ω with probability measure $\mathsf{Prob}\,(\,\cdot\,)$ [80] together with a collection $\{X_t\,(\omega)\,|\,\omega \in \Omega\}_{T_1 \leqslant t \leqslant T_2}$ of (Borel) random variables X_t on Ω. A concrete process (with absolutely continuous probability) always generates a unique formal process given by

$$p_{t_1,\cdots,t_n}\,(x_1,\cdots,x_n) \stackrel{\text{def}}{=} \frac{\partial^n}{\partial x_1 \cdots \partial x_n}\,\mathsf{Prob}\,\{\omega \in \Omega\,|\,X_{t_1}\,(\omega) \leqslant x_1,\cdots,X_{t_n}\,(\omega) \leqslant x_n\}.$$

However, the converse (i.e., that every formal process comes from at least one concrete process) requires a strong theorem due to Kolmogoroff [79] which utilizes subtle topological properties of the real numbers.[2] (There are, in fact, well-defined and consistent formal processes with non-real values which have no underlying sample space $(\Omega, \mathsf{Prob}\,(\,\cdot\,))$ [80] so are not concrete in the above sense.)

Moreover, Kolmogoroff's Theorem has no **uniqueness** guarantee and this brings us to the second distinction.

By a **physical** process we mean an actual mechanism in nature which generates random values whose frequency distributions we are studying. By a **simulated** process we mean an abstract or computer-based concrete process which yields the same formal distribution functions as the physical process.

Because of the lack of uniqueness in Kolmogoroff's Theorem, even if the formal distributions are known exactly, there may be many distinct simulations none of which may actually represent the underlying physical

---

[2]E.g., that $\mathbb{R}$ is a locally compact metric space.

process.

2.1.2.2 Latent Processes and Hidden Markov Models

A **hidden stochastic model** explains the dependencies in a **manifest** random process $\{X_t\}_{T_1 \leqslant t \leqslant T_2}$ in terms of an underlying, **latent** process $\{Y_t\}_{T_1 \leqslant t \leqslant T_2}$ with **prior** formal distribution functions

$$\{\pi_{t_1,\cdots,t_n}(y_1,\ldots,y_n)\}_{T_1 \leqslant t_1 < \cdots < t_n \leqslant T_2}$$

and a **conditional** distribution function $f(x \,|\, y)$ chosen so that the **posterior** distribution functions of $\{X_t\}$ are

$$p_{t_1,\cdots,t_n}(x_1,\ldots,x_n) = \int \cdots \int f(x_1 \,|\, y_1) \cdots f(x_n \,|\, y_n) \, \pi_{t_1,\cdots,t_n}(y_1,\ldots,y_n) \, dy_1 \cdots dy_n. \qquad (2.2)$$

Intuitively, one can think of the Y process as dealing numbered cards from a finite pack (thus showing dependent choices) while the X process consists of independent selections from numbered urns corresponding to the Y cards dealt.

When the latent process is a formal discrete-state, continuous-time process I with prior distributions

$$\{\pi_{t_1,\cdots,t_n}(i_1,\ldots,i_n)\}_{a \leqslant t \leqslant b}$$

and we are given conditional distributions $f_i(x) \overset{\text{def}}{=} f(x \,|\, i)$ then the posterior distribution functions may be written

$$p_{t_1,\cdots,t_n}(x_1,\ldots,x_n) \overset{\text{def}}{=} \sum_{i_1,\cdots,i_n} f_{i_1}(x_1) \cdots f_{i_n}(x_n) \, \pi_{t_1,\cdots,t_n}(i_1,\ldots,i_n). \qquad (2.3)$$

In the special case in which the latent process I is Markov, i.e., the ratios

$$\frac{\pi_{t_1,\cdots,t_n}(i_1,\ldots,i_{n-1},i_n)}{\pi_{t_1,\cdots,t_{n-1}}(i_1,\ldots,i_{n-1})} \overset{\text{def}}{=} \pi_{t_n \,|\, t_{n-1}}(i_n \,|\, i_{n-1}) \qquad (2.4)$$

do not depend on $t_1, \ldots, t_{n-2}$, then Eq. 2.4 constitutes a formal **hidden Markov model** (HMM) [81]. By the discussion above, for every formal HMM there exists at least one concrete discrete-state Markov process $\{I_t \mid t \in T\}$ with distributions Eq. 2.4. However, in Sec. 3.3, we will show that formal HMM distributions can also arise from systems with no latent physical or concrete Markov process.

2.1.2.3 *Notes on Markov Matrices*

There are two common methods for specifying continuous-time Markov transition probability matrices, both of which we will use.

Probabilities themselves generally will be denoted by expressions such as $\mathbf{\Pi}(l, k)$, with entries $\mathbf{\Pi}(l, k)_{ji} = \mathsf{Prob}[I_l = j \text{ and } I_k = i]$ and $\mathbf{\Pi}(l|k)$ with entries $\mathbf{\Pi}(l|k)_{ji} = \mathsf{Prob}[I_l = j, \text{ given } I_k = i]$. Thus, for example, $\mathbf{\Pi}(l|k) \cdot \mathbf{\Pi}(k, m) = \mathbf{\Pi}(l, m)$, while $\mathbf{\Pi}(l|k) \cdot \mathbf{\Pi}(k|m) = \mathbf{\Pi}(l|m)$, both for $l \geqslant k \geqslant m$. This notation works for both discrete-time processes $\mathbf{\Pi}(l, k)$ and continuous-time processes $\mathbf{\Pi}(t, s)$.

However, continuous transition matrices are often specified by the **rate matrix K** from which the probabilities are obtained by solving the differential equation

$$\frac{\partial}{\partial t}\mathbf{\Pi}(t, s) + \mathbf{K} \cdot \mathbf{\Pi}(t, s) = 0.$$

This is especially common in chemical kinetics [82]. For example, the classic Hodgkin-Huxley "α/β" matrices of Sec. 4.4.2, Eq. 4.8 are rate matrices in this sense [34].

Given a fixed **stochastic matrix P** [79] (i.e., the conditional probability matrix $\mathbf{P}(1|0)$ of a discrete-time, time-homogenous Markov process), the standard conversion to a rate matrix is given by

$$\mathbf{K} = \lambda \left(\mathbf{I} - \mathbf{P} \right), \tag{2.5}$$

where $\lambda > 0$ is a **Poisson rate**. Note that $\mathbf{K}$ will have reduced rank because $[1, \ldots, 1] \cdot \mathbf{K} = \mathbf{0}$.

Since $0 \leqslant \mathbf{P} \leqslant 1$, we will always generate a $\mathbf{K}$ with nonpositive off-diagonal entries while the diagonal entries are nonnegative and $\leqslant \lambda$. Thus every $\mathbf{P}$ generates a valid $\mathbf{K}$. However, not every $\mathbf{K}$ will generate a valid $\mathbf{P}$ via the equation $\mathbf{P} = \mathbf{I} - (1/\lambda) \mathbf{K}$ because of the previous entry constraints.[3]

2.1.2.4 *Classical Simplicial Processes*

Eq. 2.4 can be given a suggestive form, useful subsequently for understanding the quantum generalization in Sec. 3.3 of hidden layers.

Define[4] a K–component **simplicial process** to be a real (continuous- or discrete-time) stochastic process $\mathbf{X}(t)$, written as a $(K \times 1)$ column vector, which satisfies the following relations: for all times t, $\mathbf{X}(t) \geqslant 0$ and $\sum_k X_k(t) = 1$ with probability 1.

Remark 1. The condition $\sum_k X_k(t) = 1$ implies the component random variables cannot be independent. In particular, their covariance matrix must be singular.

For example, let $S(t) \in \{1, 2, \ldots, K\}$ be a discrete-state process and define $X_k(t) = 1$ if $S(t) = k$ and $X_k(t) = 0$ otherwise, for $k = 1, \ldots, K$. Then $\mathbf{X}(t)$ is simplicial. We call $\mathbf{X}(t)$ the **indicator process** associated with $S(t)$.

Let $\mathbf{f}(g) = [f_1(g), \cdots, f_K(g)]$ be a $(1 \times K)$ row vector of probability distribution functions. Let $\mathbf{X}(t)$ be a K–component simplicial process. We define a scalar stochastic process $G(t)$ to be a **hidden simplicial process** with conditionals $\mathbf{f}$ and hidden process $\mathbf{X}$ if, for all distinct times $t_1, \ldots, t_n$, the joint probability distribution $p_{t_1,\ldots,t_n}(g_1, \ldots, g_n)$ of G is given by the expression

$$p_{t_1,\ldots,t_n}(g_1, \ldots, g_n) =$$
$$\mathsf{E}[(\mathbf{f}(g_1) \mathbf{X}(t_1)) \cdots (\mathbf{f}(g_n) \mathbf{X}(t_n))], \tag{2.6}$$

---

[3]But note that negative probabilities may have a rational interpretation in quantum mechanics [83].

[4]Portions of this section have appeared in [3].

where $\mathsf{E}\left[\,\cdot\,\right]$ is the expectation operator. (Note that every factor $\mathbf{f}\left(g_i\right)\cdot\mathbf{X}\left(t_i\right)$ is a scalar so that the products are well-defined.)

Remark 2. The intuition for Eq. 2.6 is that the value $G\left(t\right)$ is determined by a two-layer procedure. First, a random list of mixing coefficients $x_1 = X_1\left(t\right),\dots,x_K = X_K\left(t\right)$ is generated. Then $G\left(t\right)$ itself is selected from the mixed distribution $x_1 f_1\left(g\right) + \cdots + x_K f_K\left(g\right)$. The simplicial conditions on $\mathbf{X}\left(t\right)$ assure this procedure is well-defined.

When $\mathbf{X}\left(t\right)$ is the indicator process of a continuous- or discrete-time Markov process, it is easy to verify that $G\left(t\right)$ is precisely the same as an HMM defined by Eq. 2.4 above.

The weak 2nd–order properties of hidden simplicial models are easy characterized:

Theorem 1. *Let $G\left(t\right)$ be a K–component hidden simplicial model with conditionals $\mathbf{f}$ and hidden process $\mathbf{X}$. Define the $\left(K\times 1\right)$ vector $\mathbf{P_X}\left(t\right) = \mathsf{E}\left[\mathbf{X}\left(t\right)\right]$ and the $\left(K\times K\right)$ matrix $\mathbf{P_X}\left(t,s\right) = \mathsf{E}\left[\mathbf{X}\left(t\right)\cdot\mathbf{X}\left(s\right)^{\text{T}}\right]$. Then the autocovariance $C_G\left(t,s\right)$ [56] of G is given by:*

$$C_G\left(t,s\right) = \mu_{\mathbf{f}}\cdot\mathbf{P_X}\left(t,s\right)\cdot\mu_{\mathbf{f}}{}^{\text{T}} + \delta\left(t-s\right)\sigma_{\mathbf{f}}^2\cdot\mathbf{P_X}\left(t\right),$$

where $\mu_{\mathbf{f}}$ and $\sigma_{\mathbf{f}}^2$ are column vectors of the means and standard deviations of the conditional distributions and $\delta\left(\,\cdot\,\right)$ is the Dirac delta function.

2.1.3 Latent Quantum Stochastic Processes in Ion Channels

This section distinguishes between theoretical statistical models of ion channels given by **Kolmogoroff's Theorem** [79] and the **physical processes** which gives rise to the observed behavior.

These distinctions are key to understanding the ion channel literature. It has been known since the 1960's [64] that the physical stochastic processes represented by channel permiabilities or conductances have the formal structure of hidden Markov models. By Kolmogoroff's Theorem, these conductance processes can certainly be **simulated** by underlying concrete Markov processes.

As a result, channel researchers have always assumed there are Markov processes controlling the successive transitions of the physical conformations of channels. But this is actually an unwarranted step since we cannot know if any particular simulated channel process is the actual physical process driving the distributional evolution because there is no general uniqueness corollary of Kolmogoroff's Theorem.

In fact, the physically-based quantum activated measurement processes which are defined in Sec. 3.4 will be proven to give rise to **formal** hidden Markov models (i.e., HMM distribution functions) yet with no underlying physical Markov process.

Therefore, if all we know about a channel is its formal permiability or conductance distribution, there is no scientific way to choose between a hidden quantum model (HQM) and a hidden Markov model as the physical process. However, when the results of this research are considered which prove HQM's can give rise to $1/f$-type noise (Sec. 5.2.4) while HMM's apparently cannot (Sec. 2.2.5), the evidence will clearly favor the new HQM channel processes.

Thus, based on our research, the theoretical existence of simple concrete simulations may have completely distorted the historical understanding of ion channel behavior.

2.2 Mathematical Models of Noisy Tissue

Because of its power and ubiquity in all neural recordings[5], from the individual channel level up to cortical electroencephalograms (EEG), the study of neuronal noise continues to be a major field of research [38, 42, 43].

Most of the noise created by the electrical activity in neural tissue can be characterized as $\mathbf{1/f}$**-type noise**; that is, its power spectrum is of the general form $1/f^\theta$ over a significant range of frequencies f for some constant θ. Data taken from [37]).

Ion channels are protein-based micromachines densely embedded in all neuron membranes, which create

---

[5]Portions of this section have appeared in [3].

and control the transmission of information by regulating the passage of ions in response to neurotransmitters, local voltages, or external stimuli such as temperature, pressure, or photon reception [34].

Soon after Hodgkin & Huxley explained the generation of action potentials by the K^+/Na^+ channel system [25], researchers began to model membrane conductance fluctuations as resulting from simple Markov processes governing the open/close kinetics of the embedded ion channels [32]. These conductance fluctuations were recognized as a potential source of neurological noise, at least at the neuron level [34].

However, as will be discussed in detail in Sec. 2.2.5, since the 1970's it has been thought that $1/f$-type neural noise must originate somewhere other than ion channels because hidden Markov models generate autocovariance functions of the wrong form [32, 41, 65–67].

2.2.1 $1/f$-type Noises

The dominant form of noise in passive electrical circuits has power spectra of the form $S(f) \approx \sigma_0^2 T + bP/f^\theta$, where f is frequency, T is an equivalent temperature of the circuit, P is the net power drawn by the circuit, and σ_0^2, b, θ are circuit-defined constants [41]. In most analyses, the spectral exponent θ is taken to be precisely equal to 1. Often the defining relation $S(f) \approx \sigma_0^2 T + bP/f^\theta$ holds only over a portion of the spectrum large enough to cover the region of interest. We shall refer to the class of all such models as **$1/f$-type noises** [84–88]. The flat, temperature-proportional noise floor term $S_J(f) \sim \sigma_0^2 T$ is the classic **Johnson noise** and is explainable in terms of thermal motions of electric carriers [89]. However the power-dependent $1/f^\theta$ term, first studied by Bernamont [90], is less easily understood and has been a key topic within noise research for nearly a century [85, 86].

2.2.2   Modeling EEG Noise and Noise PSDs

EEG noise has often been modeled using PSDs [16, 56] that are power law functions [57, 88] of the form $S(f) \propto 1/f^\theta$ for some $0 \leqslant \theta < 2$. Neurological noise PSDs at all scales have long been claimed [32, 35, 91] to have the general characteristics of such "$1/f$–type noise" [88] even though such models include the

18

obvious contradiction of a biological system with infinite low frequency power density and even infinite total power if $\theta < 1$.

Autoregressive (AR) [6] and autoregressive-moving average (ARMA) models of [56] of EEG recordings are commonly used, in particular to simulate noise for the SSVEP detection algorithm in [92]. Such models are useful approximations but yield PSDs which are rational functions and are more appropriate for linear systems. However, as mentioned previously, brain responses are known to be non-linear [39, 57].

One useful approach has been modeling the random variations of noise periodograms around their mean PSD. In many cases, the periodogram values $S_x(k)$ of a discrete-time random process $x(n)$ are independent, scaled $\chi^2(2)$ random variables [93], whose expected value $\mathsf{E}[S_x(k)]$ is the mean spectral power at the frequency index k [56]. This holds exactly for many important special cases, such as white Gaussian noise and causal periodic ARMA processes. (cf. Appendix F for the definition and proof of this property.) In more general situations, the $\chi^2(2)$ distribution is approached only asymptotically as the data length increases. However the result still has very broad applicability [56].

The technique of detecting SSVEP responses for BCI applications by performing statistical testing of the periodogram (often called the Spectral F-Test (SFT)) was developed by several research groups in the mid-1990's [94] and is based on "hidden periodicity" methods dating back to the 1940's [56]. The idea has been used regularly, notably in [37, 92] which enhanced the flexibility of the original SFT procedure.

2.2.3   The van der Ziel and McWhorter Mechanism

In the 1950s, McWhorter [95], van der Ziel [96], and Du Pre [97] began to consider general mechanisms of $1/f$-type noise generation in semiconductors based on a distribution of independent bound charges each of which decays randomly from its activated to its inactivated state. The relation between a charge's decay time τ and its activation energy E was hypothesized on quantum mechanical grounds to be of the form $\tau = \tau_0\, e^{E/\,k_B T}$, where τ_0 is a time constant, T is the ambient absolute temperature, and k_B is Boltzmann's constant. General thermodynamic arguments then imply a population distribution of decay times propor-

tional to $1/\tau$ over some finite range $[\tau_1, \tau_2]$ [98]. As these researchers showed, such populations give rise to noise spectra of the form

$$S_{\text{VZM}}(f) \propto \frac{1}{f} \tan^{-1} \left[\frac{2\pi f (\tau_2 - \tau_1)}{1 + \tau_1 \tau_2 (2\pi f)^2} \right] \tag{2.7}$$

which reach finite asymptotic values as $f \to 0$, fall off like $1/f^2$ as $f \to \infty$, but are very closely of the form $1/f$ for $1/(2\pi\tau_2) < f < 1/(2\pi\tau_1)$.

The van der Ziel - McWhorter formalism is one of the most general and flexible mechanisms for explaining the ubiquitous $1/f$-type noises in nature. Subsequently (Sec. 5.1), we will present much more general forms of van der Ziel - McWhorter (VZM) conductance noise in neural tissue which, in the simplest case, results from a population of independent ion channel processes, each of which has autocovariance of the form $R(\tau) \propto e^{-|\tau|/\upsilon}$ and which has time-constant population distribution $p(\upsilon) \propto 1/f^{2-\theta}$. Such neural membrane noises yield conductance spectra $S_{\text{GVZM}(\theta)} \approx 1/f^\theta$ over a significant range of frequencies. We will prove that the simple relation

$$\upsilon = \upsilon_0 \, e^{E/k_B T} \tag{2.8}$$

is the formal bridge between our general quantum energy-modulated channel models and $1/f$-type noises in neural tissue.

2.2.4   The Eyring Rate Theory of Ion Channels

A highly-abstracted, non-kinetic form of structural channels which accounts for certain conductance properties is derived from **Eyring rate theory** [34, 60, 62] which is a steady-state model of a neuron ion channel that posits a flux of ions moving along a "bumpy" energy profile from the channel's entrance to its exit. The bumps occur at linearly-arranged stations along the channel's interior.

When an ion is in station i, it is at the bottom of a potential well of known energy level E_i. In order to move onto station $i + 1$, it must acquire activation energy $E_{i,i+1} - E_i > 0$ from the thermal environment, where $E_{i,i+1} > E_i, E_{i+1}$ is an energy barrier. Based on general thermodynamic considerations, the rate at which

ions make this transition (or the probability that a single ion does so) is the **Eyring rate**,

$$r_i = r_0 \, e^{-(E_{i,i+1} - E_i)/k_B T},$$

(2.9)

where T and k_B are as above and r_0 is a scaling factor. Since the energies $E_{i,i+1}(V), E_i(V), E_{i+1}(V)$ are assumed to be functions of the control or **gating** variable V (e.g., the membrane voltage, chemical ligand density, etc.), these Eyring rates will themselves be determined by V. As is well known [34, 62], this model along with simple linear functional relations for the barrier energies $E_{i,i+1}$ can account for steady-state flux formulas such as the Goldman-Hodgkin-Katz Equation [60].

However, the standard theory does not have a kinetic mechanism [72]; i.e., a model of random channel changes such as Markov kinetics which accounts for Hodgkin-Huxley [25] and similar transient behavior caused by sudden changes in the gating variable. Moreover, the theory only predicts the mean flux at each level of the gating parameter (from which the conductance may be infered), not deviations from the mean which is what the noise signal is.

But if we rephrase the Eyring rate relation (2.9) in terms of time, we can say that the average **waiting time** v_i for an ion to pass from station i to station $i + 1$ is given by $v_i = v_0 \, e^{(E_{i,i+1} - E_i)/k_B T}$, an expression obviously reminiscent of the McWhorter semiconductor relation $v = v_0 \, e^{E/k_B T}$ (2.8) which led to VZM noise. By incorporating energy levels into a generalized Markov kinetic model, we use this shared relation to connect Eyring rates and channel noise. (cf. Sec. 4.4.2).

2.2.5   Markov Ion Channels and Neural Membranes as Sources of Noise

It has been known at least since the 1960's that neuron membranes *in vitro* also give rise to $1/f$-type noise although the biochemical mechanism remains controversial [35].

In the early 1970's, Terrell Hill and Yi-Der Chen published a classic series of articles [32, 65–70] which investigated the statistics of various Markov process models of ion channel kinetics for neuron membranes. In particular, they derived the autocorrelation formula Appendix E, Eq. E.4 for the conductance noise of

21

a population of independent, identical, 4-subunit Hodgkin-Huxley [25] K^+/Na^+ neuron channels which change their physical conformations randomly in accordance with the steady-state distribution of the Markov process [62, 72]. In their models, only when all 4 subunits are in a "permissive" conformation is the channel open for the passage of ions through the neural membrane. Otherwise, it is considered closed or fully blocking.

One of their stated goals was to **exclude** the possibility that such Markov kinetics could give rise to $1/f$-type spectra by considering various modifications of their basic model. These modifications included interaction energies between Markov states as well as "leaky" channels (refinements we will later adopt for our models). In addition, they considered a scheme closely related to the van der Ziel – McWhorter mechanism, as they state,

"... not because we believe in it but because it is well known in semiconductor physics that a sufficiently broad distribution ... in $[\upsilon]$ values of the form $[1/\upsilon]$, corresponding to a constant or flat distribution in activation energies for the $[\upsilon]$ process, will give $[S(f)] \sim 1/f$." [95, 98, 99]. [Notation adjusted.]

According to Hill and Chen, analysis of these modified models

"... confirms the generally held view that the observed $[S(f)] \sim 1/f$ is associated primarily with K^+ current through open K^+ channels and not with the open-close kinetics of these channels" [32];

i.e., the source of $1/f$-type randomness in the K^+ current is not the channels' opening and closing behavior but some still unexplained mechanism.

So far as the present authors are aware, this conclusion of Hill and Chen has not been seriously questioned since their work appeared. At present, it is taken for granted that there must be an additional, unknown random process at work in neural membranes governing the flow of ions which accounts for $1/f$-type noise (but cf. [35]). One common explanation is some mysterious scale-similarity property of neuronal tissue [52, 100] which, in other contexts, is known to give rise to $1/f$ spectra [88]. However, there seems

to be no evidence for such scale similarity and, as we will show, there are far more cogent explanations for $1/f$-type neuronal noise.

We believe that general biophysical principles, such as thermodynamic equilibrium, can provide these needed objective optimization principles. In particular, we will prove in Appendix E that entropy maximization in a population of quantum ion channels can give rise to approximate $1/f$-type noise.

2.3   Steady-State Visual Evoked Potentials and Brain-Computer Interfaces

A sudden stimulus[6] such as a touch, a sound, or a bright flash will elicit a detectable brain reaction called an **event-related potential** [17] or **evoked potential** (EP). Such EPs typically last on the order of 500 ms before disappearing, and may be reinvoked after a short refractory period. However, if the stimuli are repeated at a regular rate faster than about 2Hz, the EPs will not have time to decay and the brain's reaction will be a periodic signal called a **steady-state evoked potential** with fundamental frequency the same as the stimulus'. In particular, a periodic visual stimulus will cause an SSVEP [101].

These stimulus-dependent brain frequencies can be used to control brain-computer interfaces (BCI) [6] by flashing lights at various distinct frequencies simultaneously in different locations on a computer screen or LED device. The strongest SSVEP response peak detected corresponds to the location on which the subject's attention is most focused and usually represents the selection.

Low frequency visual stimuli generally induce harmonics [9] (cf. Fig. 7.4) which also may be used for BCI detection [8]. Thus the corresponding subject selections can be identified by simple algorithms. It is worth remarking that such harmonic responses prove conclusively that the brain is a nonlinear system since pure linear systems cannot generate harmonics. On the other hand, higher frequencies, especially those which approach the γ-band, are much more difficult to detect because their response power is close to that of the background, and all harmonics (if they exist at all) are lost in the γ-band noise. This is seen clearly in Fig. 7.4 which shows the 28 Hz brain response is almost indistinguishable from background noise. (However,

---

[6]Portions of this section have appeared in [2].

note that our new GVZM-based algorithms in Chap. 7 detect the 28 Hz peak even in this difficult data set.)

CHAPTER 3: HIDDEN ACTIVATED QUANTUM MEASUREMENT MODELS

[I]t may well be that a fuller understanding of the brain will require ... more extensive theories going beyond quantum mechanics.

David Bohm and Basil Hiley, <u>The Undivided Universe</u> [102]

In this chapter, the new approach to quantum stochastic processes will be outlined. The most important result, presented in Sec. 3.4, Thm. 3, is a mechanism by which a hidden, quantum mechanical, layer can give rise to a manifest process in our measuring instruments (such as current meters and so forth) that **appears** to have been generated by a classical, discrete-state Markov process. This classical compatibility is critical for the new ion channel model presented in Chap. 4 because of the overwhelming experimental evidence, going all the way back to the pioneering work of Hodgkin, Huxley, Katz, and others [26, 64], which demonstrates the applicability of such processes to ion channel electrochemistry.

The theory is presented in a sequence of theoretical sections.

- The foundational concept of **formal quantum state processes**, on which the entire theory rests, is defined in Sec. 3.1, Def. 1. Several key examples of quantum state processes are presented.

- An abstract formalization, termed **activated measurement**, of the dissipative quantum process of energy absorption followed by state collapse, is presented in Sec. 3.2. These activated measurements will be posited later as the hidden engine of quantum ion channel kinetics.

- In Sec. 3.3, **conditional quantum fields**, which are are the connecting link between between the manifest classical layer and the hidden quantum layer, are defined. This classical/quantum complex forms a **hidden quantum model**.

- Finally, Sec. 3.4 encapsulates the previous sections in the concept **hidden activated measurement models** whose attributes are summarized in Thm. 3.

A summary of the quantum mechanical background necessary for understanding the concepts and notation is presented in Appendix A. See Appendix B for a discussion of tensor products and the partial trace. Appendix G contains all notational symbols and conventions. Note that, for simplicity of presentation, Hilbert spaces are generally assumed to be separable. Thus, when $\mathbb{H}$ is non-trivial, $1 \leqslant \mathbf{dim}\left(\mathbb{H}\right) \leqslant \aleph_0$.

3.1 Quantum State Processes

In this section, a type of quantum stochastic processes called **formal quantum state processes** are defined (Def. 1). Examples are presented including a formulation of the Schrödinger equation as a state process (Examp. 1). The other examples explore the concept of a **coherent family** of state operators which is essential for defining the **activated measurement processes** of Sec. 3.4.

The theories of general quantum [77, 103, 104] and statistical mechanics [105, 106], as well as stochastic processes [79, 82], have a vast and accessible literature. We use a minimalist quantum theory compatible with any detailed quantum model of ion channels.[1]

Let $\mathbb{H}$ be a fixed separable complex Hilbert space with inner product $\langle \cdot \,|\, \cdot \rangle$ [109]. The space $\mathbb{H}$ is the **configuration space** of the quantum system. Vectors $\psi \in \mathbb{H}$ (or, sometimes $|\psi\rangle$), are called **wavefunctions**, **pure states**, or "**kets**" in Dirac's terminology [110]. In order to simplify the presentation of quantum-based reasoning, we fix a particular orthonormal basis for $\mathbb{H}$ so that all vectors are (possibly infinite) columns of complex numbers, dual vectors (Dirac's "**bras**" [110]) are rows, and continuous linear operators are (possibly infinite) square matrices. In this way, operators act by matrix multiplication, the inner product $\langle \psi | \phi \rangle$ is just $\psi^{\mathrm{H}} \cdot \phi$, where $(\,\cdot\,)^{\mathrm{H}}$ denotes the hermitian transpose (i.e., the adjoint [111]), and the projection operator $\mathbf{P}_\psi$ onto a unit vector $|\psi\rangle$ is the rank-1 matrix $\mathbf{P}_\psi = |\psi\rangle\langle\psi| = \psi \cdot \psi^{\mathrm{H}}$. Moreover, we will generally consider only bounded, normal operators which are **compact** [109, 111] (so that orthonormal bases

---

[1]Since protein macromolecules are very large systems, it may be advantageous to base quantum ion channel models on Bohm & Hiley's alternative foundation for quantum mechanics which uses non-local **quantum potentials** [102]. In fact, David Bohm and his colleagues have speculated for decades on the relation between non-locality, quantum potentials, and mind (e.g., [102] and [107]). The highly controversial [29, 31] theories of Penrose [27, 108] and Penrose & Hameroff [28] must be mentioned in this regard as well. We shall, however, avoid these fascinating excursions in favor of more standard quantum "metaphysics."

of eigenvectors and countable spectral decomposition exist) and even **non-degenerate** (so eigenspaces are 1-dimensional) when convenient. We will often treat $\mathbb{H}$ as finite-dimensional to simplify formulas. These simplifications are replaceable by appropriate functional analysis generalizations [103, 109, 111, 112].

Definition 1. Let $(T, \leqslant, t_0)$ be a quasi-ordered[2] set with least element t_0. The elements $t \in T$ will be refered to as "times". Let $\mathbb{H}$ be the configuration space of a quantum system. A **formal quantum state process** $\boldsymbol{\Psi}\left(\,\cdot\,\right)$ on T is a family

$$\left\{\boldsymbol{\Psi}\left(t_1, \ldots, t_n\right) \mid t_0 \leqslant t_1 < \cdots < t_n,\ t_1, \ldots, t_n \in T,\ 0 \leqslant n < \infty\right\}$$

of non-negative definite, self-adjoint, trace class operators [111] on $\mathbb{H}^{\otimes n} \overset{\text{def}}{=} \overbrace{\mathbb{H} \otimes \cdots \otimes \mathbb{H}}^{n}$ satisfying the marginalization conditions: $\boldsymbol{\Psi}\left(\emptyset\right) = 1$ for $n = 0$ and

$$\boldsymbol{\Psi}\left(t_1, \ldots, \widehat{t_k}, \ldots, t_n\right) = \mathbf{tr}_k\left(\boldsymbol{\Psi}\left(t_1, \ldots, t_k, \ldots, t_n\right)\right), \tag{3.1}$$

for all $t_1 < \cdots < t_k < \cdots t_n, 1 \leqslant k \leqslant n$, where $\mathbf{tr}_k\left(\,\cdot\,\right)$ is the partial trace along the kth dimension and, as before, the caret $\widehat{\cdot}$ above a symbol indicates an item deleted from a list. (Cf. Appendix B for the definitions of tensor products and partial trace.)

Remark 3. The $n = 0$ condition $\boldsymbol{\Psi}\left(\emptyset\right) = 1$ implies that every $\boldsymbol{\Psi}\left(t_1, \ldots, t_n\right)$ is a **state** on $\mathbb{H}^{\otimes n}$; i.e., $\mathbf{tr}(\boldsymbol{\Psi}\left(t_1, \ldots, t_n\right)) = 1$.

Remark 4. Quantum marginalization is the quantum mechanical generalization of the Kolmogoroff consistency conditions Eq. 2.1 for classical formal stochastic processes.

Remark 5. It is important to interpret Def. 1 correctly with respect to observers and measurements. The process $\boldsymbol{\Psi}\left(\,\cdot\,\right)$ must be interpreted as excluding any further disturbances to the system. It implicitly "codes" every measurement or observation that has been or will be made on the system during the times T. Any additional observation would change the process itself. However, probability and expectation calculations such as **Born's Law** [77] $\mathsf{E}\left[A \mid \boldsymbol{\Psi}\right] = \mathbf{tr}\left(\mathbf{A} \cdot \boldsymbol{\Psi}\right)$, where $\mathsf{E}\left[\,\cdot\,\right]$ denotes the frequentist average (or expected) value,

---

[2]i.e.; $t \leqslant t$ and $r \leqslant s, s \leqslant t$ imply $r \leqslant t$.

are allowed because they do not constitute measurements or observations in the strict quantum mechanical sense.

Definition 2. Let $\Psi\left(\,\cdot\,\right)$ be a formal quantum state process on T. Let $\mathcal{A}$ be a $*$–algebra [103, 112] of observables of the system. For every $A \in \mathcal{A}$, let $\mathbf{A}$ denote the operator on $\mathbb{H}$ which corresponds to A. The algebra $\mathcal{A}$ is a called **correlatable by** $\Psi\left(\,\cdot\,\right)$ if, for all times $t_1 < \cdots < t_n$ and every $A_1, \ldots, A_n \in \mathcal{A}$, with associated operators $\mathbf{A}_1, \ldots, \mathbf{A}_n$, the product $A_1 \cdots A_n$ has a frequentist average value $\mathsf{E}\left[A_1 \cdots A_n \mid \Psi\left(t_1, \ldots, t_n\right)\right]$ in systems prepared in state $\Psi\left(t_1, \ldots, t_n\right)$ and which satisfies the **Generalized Born Law**

$$\mathsf{E}\left[A_1 \cdots A_n \mid \Psi\left(t_1, \ldots, t_n\right)\right] = \mathbf{tr}\left(\mathbf{A}_1 \otimes \cdots \otimes \mathbf{A}_n \,\cdot\, \Psi\left(t_1, \ldots, t_n\right)\right). \tag{3.2}$$

Definition 3. A **concrete quantum state process**[3] consists of a formal quantum state process $\Psi\left(\,\cdot\,\right)$, a $*$–algebra $\mathcal{A}$ of observables which are correlatable by $\Psi\left(\,\cdot\,\right)$, and a time-dependent observable function $A : [a, b] \to \mathcal{A}$. The **moments** of A are the values

$$\mathsf{E}\left[A\left(t_1\right) \cdots A\left(t_n\right) \mid \Psi\right]$$

Remark 6. It must be noted that Eq. 3.2 is a non-trivial generalization of the standard axioms of quantum mechanics. It cannot be derived from standard formulations since none of those assign a meaning to the concept of statistical moments $\mathsf{E}\left[A\left(t_1\right) \cdots A\left(t_n\right) \mid \Psi\right]$ at distinct times. Interpreting this concept is certainly challenging as we are not allowed to imagine performing actual measurements at times $t_1, \ldots, t_n$ to calculate the product $A\left(t_1\right) \cdots A\left(t_n\right)$ since every such measurement would cause wavefunction collapse and thus invalidate the given state $\Psi\left(t_1, \ldots, t_n\right)$.

We do not minimize these foundational issues. Nevertheless, conventional quantum formulations were created with a view to physical applications, for which the statistics and dynamics at a single time t are sufficient. On the other hand, and bearing in mind the quote from Bohm & Hiley which began this section,

---

[3]The concept of a concrete quantum state process is related to the "totally symmetric quantum stochastic processes" of Accardi, Frigerio, & Lewis [113]. In addition, there are numerous alternative definitions of the concept "quantum stochastic process' in the literature" (e.g. [114]) whose relation to one another is complex. For this reason, we coined the term "quantum state process" and used the simplest definition which can be adapted to random quantum channel kinetics.

neurological signal processing simply cannot do without the concept of correlated behavior at distinct times, most importantly in order to calculate autocovariance functions. For this reason the notion of a correlatable $*$–algebra $\mathcal{A}$ of observables (Def. 2) was introduced: we regard the problem of identifying the algebra $\mathcal{A}$ of appropriate observables for a particular quantum state process $\mathbf{\Psi}(\cdot)$ as a key part of the formalization of any application area.

Similar remarks apply to the definition of hidden quantum models Sec. 3.3, Def. 10, which is meant to bridge the gulf separating underlying quantum-level processes from macroscopic classical instrument readings. Such a concept is needed, at the minimum, to explain the excellent fit of classical Markov kinetics to the ion channel noise measurements in which we were particularly interested.

Example 1. The Schrödinger Process: Let $\mathbf{H}$ be the time-independent Hamiltonian of a physical system [77,103,104,110] and T be the real-valued time interval $[0,\infty)$. Then **Schrödinger's Equation** for the state $\mathbf{\Psi}$ can be written as

$$\frac{\partial \mathbf{\Psi}}{\partial t} + \frac{2\pi\sqrt{-1}}{h}\left[\mathbf{\Psi},\mathbf{H}\right] = 0,$$

where h is Planck's Constant and $[\,\cdot\,,\,\cdot\,]$ denotes the commutator $[\mathbf{A},\mathbf{B}] \stackrel{\text{def}}{=} \mathbf{A}\mathbf{B} - \mathbf{B}\mathbf{A}$. Note that, since $\mathbf{\Psi}$ is of trace class and $\mathbf{H}$ is bounded, then $[\mathbf{\Psi},\mathbf{H}]$ is also of trace class [111] and $\mathbf{tr}\left[\mathbf{\Psi},\mathbf{H}\right] = 0$. It then follows that the operators

$$\mathcal{S}_t\left[\,\cdot\,\right] \stackrel{\text{def}}{=} e^{-t\left(2\pi\sqrt{(-1)}/h\right)\left[\,\cdot\,,\mathbf{H}\right]},$$

for $t \geqslant 0$, sends states to states. Moreover, for any initial state $\mathbf{\Psi}_0$, $\mathcal{S}_t\left[\mathbf{\Psi}_0\right]$ solves Schrödinger's Equation.

Now define

$$\mathbf{\Psi}\left(t_1,\ldots,t_n\right) \stackrel{\text{def}}{=} \mathcal{S}_{t_1}\left[\mathbf{\Psi}_0\right] \otimes \cdots \otimes \mathcal{S}_{t_n}\left[\mathbf{\Psi}_0\right],$$

for $t_1 < \cdots < t_n$ and $n \geqslant 0$. Then $\mathbf{\Psi}(\cdot)$ is a formal quantum state process. We can take $\mathcal{A}$ to be all possible obervables under the **Schrödinger measurement protocol**: never measure anything during the interval $[0,\infty)$. Thus the system will never be disturbed away from its pure quantum evolution. We will

then have, for any observable function $A : [0, \infty) \to \mathcal{A}$, moments

$$\mathsf{E}\left[A\left(t_1\right) \cdots A\left(t_n\right) \mid \boldsymbol{\Psi}\right] = \mathbf{tr}\left(\mathbf{A}\,\boldsymbol{\Psi}\left(t_1\right)\right) \cdots \mathbf{tr}\left(\mathbf{A}\,\boldsymbol{\Psi}\left(t_n\right)\right)$$

$$= \mathsf{E}\left[A\left(t_1\right) \mid \mathcal{S}_{t_1}\left[\boldsymbol{\Psi}_0\right]\right] \cdots \mathsf{E}\left[A\left(t_n\right) \mid \mathcal{S}_{t_n}\left[\boldsymbol{\Psi}_0\right]\right],$$

so the observable evolves dynamically and is uncorrelated at distinct times.

Example 2. Diagonalizable State Processeses: Let $A\left(t\right) \equiv A$, a constant observable at all times $t \in T$. Assuming A is compact [109, 111], there is a countable set $\{\mathbf{P}_i \mid i = 1, 2, \ldots\}$ of projection operators onto the eigenspaces of A. Let $\{\pi_{t_1, \cdots, t_n}\left(i_1, \ldots, i_n\right)\}_{a \leqslant t \leqslant b}$ be any formal discrete-state random process (Sec. 2.1.2.1). Define

$$\boldsymbol{\Psi}\left(t_1, \cdots, t_n\right) \overset{\text{def}}{=} \sum_{i_1, \cdots, i_n} \pi_{t_1, \cdots, t_n}\left(i_1, \ldots, i_n\right) \boldsymbol{\Psi}_1 \otimes \cdots \otimes \boldsymbol{\Psi}_n, \tag{3.3}$$

where $\boldsymbol{\Psi}_i \overset{\text{def}}{=} \mathbf{P}_i / \mathbf{tr}\left(\mathbf{P}_i\right)$ is the ith eigenstate. Then $\boldsymbol{\Psi}\left(t_1, \cdots, t_n\right)$ is a quantum state process.

Definition 4. A quantum state process $\boldsymbol{\Psi}$ is called **diagonalizable** if there is a compact observable A and and a formal discrete-state random process $\{\pi_{t_1, \cdots, t_n}\left(i_1, \ldots, i_n\right)\}_{a \leqslant t \leqslant b}$ such that $\boldsymbol{\Psi}$ is of the form Eq. 3.3.

Diagonalizable state processes will be key for Sec. 3.4, Thm. 3. Critically, diagonalizable processes satisfy

$$\mathbf{tr}\left(\mathbf{A} \otimes \cdots \otimes \mathbf{A} \cdot \boldsymbol{\Psi}\left(t_1, \ldots, t_n\right)\right) = \sum_{i_1, \cdots, i_n} \alpha_{i_1} \cdots \alpha_{i_n}\, \pi_{t_1, \cdots, t_n}\left(i_1, \ldots, i_n\right), \tag{3.4}$$

where α_i is the ith eigenvalue of A. From this formula we can see that A has certain attributes in common with a classical process $X\left(t\right)$ whose distribution function is $\mathsf{Prob}\left[X\left(t_1\right) = \alpha_{i_1}, \ldots, X\left(t_n\right) = \alpha_{i_n}\right] = \pi_{t_1, \cdots, t_n}\left(i_1, \ldots, i_n\right)$; namely, they both share the same moments $\mathsf{E}\left[X\left(t_1\right) \cdots X\left(t_n\right)\right]$ as given by Eq. 3.4. This is the first example which shows that a classical-looking process actually may derive from a hidden layer governed by quantum, rather than classical, probability.

Definition 5. Coherence: A state $\boldsymbol{\Psi}$ is **coherent with an observable** A (or simply A–**coherent**) if it commutes with the operator $\mathbf{A}$ associated with A: $\boldsymbol{\Psi} \cdot \mathbf{A} = \mathbf{A} \cdot \boldsymbol{\Psi}$. The A–coherent states form a closed, convex subset $\mathcal{S}\left(A\right) \subseteq \mathcal{S}\left(\mathbb{H}\right)$ of the set of all states of the configuration Hilbert space $\mathbb{H}$. The **Measurement**

(or Observation or Projection or ...) **Law** [77] states, in the simplest cases, that a measurement of A, while the system is in state $\mathbf{\Psi}$, will leave the system in the A–coherent state

$$\mathbf{\Psi}' = \sum_i \mathbf{P}_i \cdot \mathbf{\Psi} \cdot \mathbf{P}_i,$$

where, as in Examp. 2, $\mathbf{P}_i$ is the projection onto the ith eigenspace of $\mathbf{A}$.

We will use the term "coherent" if the operator A is clear from context.

Example 3. Coherent Families: An **coherent transition** is function $\mathcal{P}[\cdot] : \mathcal{S}(A) \to \mathcal{S}(A)$ which pre-serves mixtures: $\mathcal{P}[\sum a_i \mathbf{\Psi}_i] = \sum a_i \mathcal{P}[\mathbf{\Psi}_i]$, for $a_i \geqslant 0$, $\sum a_i = 1$.

A **coherent family on** T is a collection $\{\mathcal{P}_{t|s} \mid t \geqslant s, \ t, s \in T\}$ of coherent transitions satisfying:

$$\begin{cases} \mathcal{P}_{t|t} = \text{identity} \\ \mathcal{P}_{t|s} \circ \mathcal{P}_{s|r} = \mathcal{P}_{t|r}, & \text{for } t \geqslant s \geqslant r, \end{cases} \tag{3.5}$$

where $\circ$ denotes composition.

Given an A–coherent family $\mathcal{P}_{t|s}$, let $\mathbf{\Psi}_i$ be the ith eigenstate of A and let $\mathbf{\Psi}_0$ be any coherent state. Define

$$\mathcal{P}(t_n, \cdots, t_1) \stackrel{\text{def}}{=} \sum_{i_{n-1}, \cdots, i_1} \mathcal{P}_{t_n|t_{n-1}} \left[\mathbf{\Psi}_{i_{n-1}} \right] \otimes \cdots \otimes \mathcal{P}_{t_2|t_1} \left[\mathbf{\Psi}_{i_1} \right] \otimes \mathcal{P}_{t_1|a} \left[\mathbf{\Psi}_0 \right]. \tag{3.6}$$

(Note that time sequence $t_n, \cdots, t_1$ has been written in reverse order for clarity.)

As will be seen in the proof of Sec. 3.3, Thm. 2, $\mathcal{P}(\cdot)$ is a quantum state process that can generate Markov-like behavior at the classical level.[4]

Example 4. Discrete-time Coherent Generators: Let T be the discrete-time points $T = \{0, 1, 2, \ldots\}$. Let

---

[4]But see [115, 116] and [117] for alternative approaches to quantum Markov processes.

$\mathbf{\Pi}[\,\cdot\,]$ be a coherent transition. For time points $l \geqslant k$, define

$$\mathbf{\Pi}_{l \mid k}[\,\cdot\,] \overset{\text{def}}{=} \mathbf{\Pi}^{l-k}[\,\cdot\,] \overset{\text{def}}{=} \overbrace{\mathbf{\Pi}[\cdots \mathbf{\Pi}[\,\cdot\,]]}^{l-k},$$

the $(l-k)$–fold composition of $\mathbf{\Pi}$. The simple relation $(m-l) + (l-k) = (m-k)$ shows that $\mathbf{\Pi}_{l \mid k}[\,\cdot\,]$ forms a coherent family. The induced $\mathbf{\Pi}(l_n, \ldots, l_1)$ is called the **discrete-time quantum state process generated by $\mathbf{\Pi}$**.

Example 5. Continuous-time Coherent Generators: Let T be the real-valued time interval $[0, \infty)$. Let $\mathbf{\Pi}[\,\cdot\,]$ be a coherent transition and let $\lambda > 0$ be a constant. For $t \geqslant s$, define, by expanding in a Taylor series, the operator

$$\mathbf{\Pi}^{\lambda}_{t \mid s}[\,\cdot\,] \overset{\text{def}}{=} e^{\lambda(t-s)(\mathbf{\Pi}[\,\cdot\,] - \mathbf{I})}, \tag{3.7}$$

where $\mathbf{I}$ denotes the identity transition. From the expansion

$$\mathbf{\Pi}^{\lambda}_{t \mid s}[\,\cdot\,] = \sum_{k=0}^{\infty} e^{-\lambda(t-s)} \frac{\lambda^k (t-s)^k}{k!} \mathbf{\Pi}^k[\,\cdot\,], \tag{3.8}$$

where, as before, $\mathbf{\Pi}^k[\,\cdot\,]$ denotes k successive applications of $\mathbf{\Pi}[\,\cdot\,]$, it is easy to show that $\mathbf{\Pi}^{\lambda}_{t \mid s}[\,\cdot\,]$ is also a coherent transition. The composition conditions Eq. 3.5 follow from the properties of the exponential and the simple equation $(t-s) + (s-r) = (t-r)$. Therefore $\mathbf{\Pi}^{\lambda}_{t \mid s}$, for $t \geqslant s$, defines a coherent family.

(Equation 3.8) clearly shows that, from a classical perspective, $\mathbf{\Pi}^{\lambda}(t_n, \ldots, t_1)$ can be thought of as the result of applying the generator $\mathbf{\Pi}[\,\cdot\,]$ according to a Poisson process with rate constant λ; that is, the probability of precisely k applications of $\mathbf{\Pi}[\,\cdot\,]$ during the time interval $[s, t]$ is $e^{-\lambda(t-s)} \lambda^k (t-s)^k / k!$. Of course, as with Examp. 3, this classical conception does not represent the actual quantum behavior inside the hidden layer. Nevertheless, it may **appear** to be a valid description at the manifest, classical level. The induced $\mathbf{\Pi}^{\lambda}(t_n, \ldots, t_1)$ is called the **continuous-time quantum state process, with Poisson rate λ, generated by $\mathbf{\Pi}$**.

3.2 Activated Measurement Processes

In this section we present an important type of quantum operation called **activated measurement** which is meant to abstract the double procedure of absorption of energy while in a coherent state of an observable A followed by the measurement of A itself. This collapses the system into a new coherent state and may also return energy back to the environment. As will be seen, activated measurement affords an example of a generator for a coherent family (Sec. 3.1, Examp. 4).

Definition 6. An **activator** for an observable A is a bounded linear operator $\mathbf{Q}$ such that, for every coherent state $\boldsymbol{\Psi}$ of A, the operator $\mathbf{Q}\boldsymbol{\Psi}\mathbf{Q}^{\mathrm{H}}$ is a state ; that is, $\mathbf{tr}\left(\mathbf{Q}\boldsymbol{\Psi}\mathbf{Q}^{\mathrm{H}}\right) = 1$. (Recall $(\,\cdot\,)^{\mathrm{H}}$ denotes the hermitian transpose. Note that the operation $\mathbf{Q}\left(\,\cdot\,\right)\mathbf{Q}^{\mathrm{H}}$ preserves non-negative definiteness.) We call $\mathbf{Q}\boldsymbol{\Psi}\mathbf{Q}^{\mathrm{H}}$ an **activated state** of A.

Example 6. Unitary operators $\mathbf{U}$ are activators for every observable since

$$\mathbf{tr}\left(\mathbf{Q}\boldsymbol{\Psi}\mathbf{Q}^{\mathrm{H}}\right) = \mathbf{tr}\left(\boldsymbol{\Psi}\mathbf{Q}^{\mathrm{H}}\mathbf{Q}\right) = \mathbf{tr}\left(\boldsymbol{\Psi}\mathbf{I}\right) = 1.$$

As a result, if $\mathbf{Q}$ is an activator for A and $\mathbf{U}$ is unitary then $\mathbf{U}\mathbf{Q}$ is also an activator for A. In particular, the dynamic operator $\mathbf{U}\left(t\right) = e^{-\frac{2\pi}{\hbar}\sqrt{-1}\mathbf{H}t}$, with $\mathbf{H}$ the system's time-independent Hamiltonian, is an activator for every observable.

Remark 7. A good image of activation is **shaking dice in a cup** before they are rolled. A biophysical example is an ion channel absorbing thermal energy from the membrane environment, causing it to become excited.

Lemma 1. *Let A be an observable. If the linear operator $\mathbf{Q}$ is an activator for A then $\|\mathbf{Q}\psi\| = \|\psi\|$ for every eigenvector of $\mathbf{A}$. If A is compact [111] (in particular if $\mathbb{H}$ is finite), the converse holds.*

Proof. Let $\mathbf{Q}$ be an activator and ψ be an eigevector of A. Then $\boldsymbol{\Psi} \overset{\mathrm{def}}{=} \psi\psi^{\mathrm{H}}/\|\psi\|^2$ is a coherent state of A. By hypothesis

$$1 = \mathbf{tr}\left(\mathbf{Q}\boldsymbol{\Psi}\mathbf{Q}^{\mathrm{H}}\right) = \frac{1}{\|\psi\|^2}\mathbf{tr}\left((\mathbf{Q}\psi)(\mathbf{Q}\psi)^{\mathrm{H}}\right) = \frac{1}{\|\psi\|^2}\|\mathbf{Q}\psi\|^2.$$

Conversely let A be compact and let $\mathbf{Q}$ preserve the norms of eigenvectors of A. Since A is compact, it has a discrete spectrum $\{\alpha_i \mid 1 \leqslant i \leqslant \dim(\mathbb{H})\}$ and every eigenspace for $\alpha_i \neq 0$ is finite-dimensional [109]. Let $\psi_1, \ldots, \psi_{d_i}$ be an orthonormal basis for each finite-dimensional eigenspace. Then the projection operator onto such an eigenspace is

$$\mathbf{P}_i = \sum_{i=1}^{d_i} \psi_i \psi_i^{\mathrm{H}}$$

and every term $\psi_i \psi_i^{\mathrm{H}}$ is a coherent state. From this we see that $\mathbf{tr}(\mathbf{P}_i) = d_i$ and

$$\mathbf{tr}(\mathbf{Q}\mathbf{P}_i\mathbf{Q}^{\mathrm{H}}) = \sum_{i=1}^{d_i} (\mathbf{Q}\psi_i)(\mathbf{Q}\psi_i)^{\mathrm{H}} = \sum_{i=1}^{d_i} \|\mathbf{Q}\psi_i\|^2 = \sum_{i=1}^{d_i} 1 = d_i = \mathbf{tr}(\mathbf{P}_i)$$

since $\|\mathbf{Q}\psi_i\| = \|\psi_i\| = 1$ by hypothesis. So $\mathbf{Q}(\cdot)\mathbf{Q}^{\mathrm{H}}$ preserves the trace of every finite-dimensional projection $\mathbf{P}_i$. A general A-measurement state is a mixture $\mathbf{\Psi} = \sum_i a_i \mathbf{P}_i$, for which $a_i \geqslant 0$ and $\sum_i a_i \mathbf{tr}(\mathbf{P}_i) = 1$. All projections in the sum for which $a_i \neq 0$ must be finite dimenensional or else the sum would not be of trace class. Thus

$$\mathbf{tr}(\mathbf{Q}\mathbf{\Psi}\mathbf{Q}^{\mathrm{H}}) = \sum_i a_i \mathbf{tr}(\mathbf{Q}\mathbf{P}_i\mathbf{Q}^{\mathrm{H}}) = \sum_i a_i \mathbf{tr}(\mathbf{P}_i) = 1$$

and so $\mathbf{Q}\mathbf{\Psi}\mathbf{Q}^{\mathrm{H}}$ is a state. Therefore $\mathbf{Q}$ is an activator for A. $\qquad\square$

Remark 8. Thus $\mathbf{Q}$ is an activator for a compact observable A if and only every column of the matrix of $\mathbf{Q}$ in the orthonormal basis for A has norm 1. This is a useful criterion.

Activated states for A are quantum states but generally not A–**coherent** states. In a coherent state we can regard A as having some particular but unobserved value but activation causes quantum interference and so the possible A–eigenstates superpose. This motivates the following:

Definition 7. Let $\mathbf{Q}$ be an activator for observable A and let $\mathbf{\Psi}$ be a coherent state of A. An **activated measurement** of A consists of activating $\mathbf{\Psi}$ by $\mathbf{Q}$ followed by measuring (but not observing) A. This yields a new coherent state of A denoted $\mathbf{\Psi}' = \mathcal{M}_A^{\mathbf{Q}}[\mathbf{\Psi}]$.

Remark 9. Continuing the simile of Remark 7, the measurement subsequent to activation corresponds to turning the cup upside down on the table **without lifting it to see the result**. (If the cup were lifted, this

would constitute an "observation" and the system would collapse further to the particular wavefunction of A corresponding the value observed.)

The activated measurement operator may be written explicitly as

$$\mathcal{M}_A^{\mathbf{Q}}[\boldsymbol{\Psi}] = \int\limits_{\mathbf{Sp}(\mathbf{A})} \boldsymbol{\Psi}_\alpha \mathbf{Q} \boldsymbol{\Psi} \mathbf{Q}^{\mathrm{H}} \boldsymbol{\Psi}_\alpha \, d\alpha, \tag{3.9}$$

where $\mathbf{Sp}\,(\mathbf{A})$ is the spectrum of A and where $\boldsymbol{\Psi}_\alpha \overset{\text{def}}{=} \mathbf{P}_\alpha / \mathbf{tr}\,(\mathbf{P}_\alpha)$ is the α eigenstate.

Since $\mathcal{M}_A^{\mathbf{Q}}[\,\cdot\,]$ is an A–coherent transition (Examp. 3), we can apply the theory developed in Sec. 3.1 to define a continuous quantum state process (Examp. 5) generated by the activator $\mathbf{Q}$:

Definition 8. The **coherent family generated by the activator Q**, with rate constant $\lambda > 0$, is

$$\mathcal{M}_{t|s}^{\mathbf{Q}}[\,\cdot\,] \overset{\text{def}}{=} e^{\lambda(t-s)\left(\mathcal{M}_A^{\mathbf{Q}}[\,\cdot\,]-1\right)}, \tag{3.10}$$

for $t \geqslant s$.

The **activated measurement process generated by the activator Q** is defined, as in Eq. 3.6 by

$$\mathcal{M}^{\mathbf{Q}}\,(t_n,\cdots,t_1) \overset{\text{def}}{=} \sum_{i_{n-1},\cdots,i_1} \mathcal{M}_{t_n|t_{n-1}}^{\mathbf{Q}}\left[\boldsymbol{\Psi}_{i_{n-1}}\right] \otimes \cdots \otimes \mathcal{M}_{t_2|t_1}^{\mathbf{Q}}\left[\boldsymbol{\Psi}_{i_1}\right] \otimes \mathcal{M}_{t_1|a}^{\mathbf{Q}}\left[\boldsymbol{\Psi}_0\right], \tag{3.11}$$

where $\boldsymbol{\Psi}_i, \; i = 1, 2, \ldots$ is a basis of eigenstates of A.

3.3   Hidden Quantum Models

In this section, we show how a hidden quantum layer can control a manifest classical process at the observational level.

Definition 9. Let $\mathbb{X}$ be a measure space thought of as the possible observational values of a manifest process X. A **conditional quantum field** [118,119] on $\mathbb{H}$, where $\mathbb{H}$ is a Hilbert space, is an integrable function $\mathbf{f}\,(\,\cdot\,)$

35

from $\mathbb{X}$ into the non-negative definite, compact, self-adjoint operators on $\mathbb{H}$ such that $\int_{\mathbb{X}} \mathbf{f}(x) \, dx = \mathbf{I}$, where the convergence is in the operator norm.

Remark 10. When $\mathbb{H}$ is separable and a fixed basis is chosen, the coefficients of each $\mathbf{f}(x)$ form a non-negative definite, compact, and hermitian matrix $[f_{ij}(x)]_{1 \leqslant i,j \leqslant \mathbf{dim}(\mathbb{H})}$ of integrable complex-valued functions. Moreover, these functions satisfy $\int_{\mathbb{X}} f_{ij}(x) \, dx = \delta_{ij}$, the Kronecker delta.

Definition 10. Hidden Quantum Models: Let $\mathbf{f}(\,\cdot\,)$ be a conditional quantum field on the measure space $\mathbb{X}$ and let $\mathbf{\Psi}(\,\cdot\,)$ be a quantum state process on configuration space $\mathbb{H}$. Then the **formal hidden quantum model** (HQM) generated by prior $\mathbf{\Psi}(\,\cdot\,)$ and conditional $\mathbf{f}(\,\cdot\,)$ is the formal stochastic process with posterior distribution functions

$$p_{t_1,\cdots,t_n}(x_1,\ldots,x_n) = \mathbf{tr}\left(\mathbf{f}(x_1) \otimes \cdots \otimes \mathbf{f}(x_n) \cdot \mathbf{\Psi}(t_1,\cdots,t_n)\right). \tag{3.12}$$

Remark 11. Using the generalized Born relation Eq. 3.2 this can be informally interpreted as stating there is some observable X whose measured values are contained in the space $\mathbb{X}$ and for which

$$\mathsf{Prob}_{\mathbf{\Psi}}\left[X(t_1) = x_1, \ldots, X(t_n) = x_n\right] = \mathsf{E}\left[\mathrm{I}_{x_1}(X(t_1)) \cdots \mathrm{I}_{x_n}(X(t_n)) \mid \mathbf{\Psi}(\,\cdot\,)\right],$$

where $\mathrm{I}_x(\,\cdot\,)$ denotes the indicator functions on $\mathbb{X}$: $\mathrm{I}_x(y) \overset{\text{def}}{=} \delta_{x,y}$.

An important feature of HQM's is that, according to Def. 10, measurements of the manifest X process are entirely classical[5]: they do not disturb the hidden quantum stochastic process in any way. One can view them as macroscopic "readings" such as the global voltage through a patch of neuronal membrane [71, 120].

Example 7. Diagonalizable HQMs: When the state process $\mathbf{\Psi}(t_1,\cdots,t_n)$ is diagonalizable (Sec. 3.1, Def. 4), the posterior distribution Eq. 3.12 reduces to

$$p_{t_1,\cdots,t_n}(x_1,\ldots,x_n) = \sum_{i_1,\cdots,i_n} f_{i_1}(x_1) \cdots f_{i_n}(x_n) \Psi_{i_1,\ldots,i_n}(t_1,\cdots,t_n), \tag{3.13}$$

---

[5]Note, however, we have not formally excluded the non-classical situation $p_{t_1,\cdots,t_n}(x_1,\ldots,x_n) < 0$, for certain values. There are reasonable interpretations of negative probabilities in quantum mechanics [83].

where $\Psi_{i_1,\dots,i_n}(t_1,\cdots,t_n)$ is the $(i_1,\dots,i_n)^{\text{th}}$ main diagonal coefficient of the prior state $\Psi(t_1,\cdots,t_n)$ in the basis $\{|\phi\rangle_i \mid 1 \leqslant i \leqslant \dim(\mathbb{H})\}$.

Remark 12. It is clear that, except for notation, the posterior distribution Eq. 3.13 of a hidden quantum model has precisely the same **form** as a classical discrete-state, continuous-time formal hidden model (Sec. 2.1.2.1, Eq. 2.3). Moreover, there are concrete hidden stochastic processes which **simulate** this posterior. However, there is a vast conceptual difference in terms of **physical** models.

Specifically, the latent process I of a classical discrete-state hidden model takes one and only one of the possible outcomes $i = 1, 2, \dots$ at every instant t of time. In the usual language, the latent process I (Markov or not) is "in state i at time t". However, this is far from the case with a hidden quantum model. For an HQM, the latent quantum process is almost never "in" one of the basic pure states $\Psi_i = |\phi_i\rangle \cdot \langle\phi_i|$. The underlying state always should be regarded as a **simultaneous superposition of all its latent possibilities**, just like Schrödinger's famous cat.

Of course, if all we are studying is the posterior distribution $p_{t_1,\cdots,t_n}(x_1,\dots,x_n)$ then these subtleties are irrelevant. However, as will be seen, if we provisionally accept latent quantum explanations for well-known classical hidden models such as Hodgkin-Huxley ion channels, we may sometimes extract new information (such as the structural-energy operators Sec. 4.4.2) not readily available from the posteriors alone. Moreover, hidden quantum layers allow canonical population models through the formalism of tensor products of configuration spaces which suggest new explanations for phenomena such as $1/f$–type noise).

Definition 11. A hidden quantum model is A–**coherent** if the hidden quantum prior is generated by an A–coherent family for some observable A (Sec. 3.1, Examp. 3).

Theorem 2. *The HQM-HMM Theorem*

(i.) The posterior distribution of a coherent HQM is a classical, formal HMM (Sec. 2.1.2.1).

(ii.) Conversely, every discrete-time, formal HMM has at least one representation as a coherent, discrete-time HQM for an appropriate configuration space and observable.

(iii.) Every continuous time HMM with Poisson rate $\lambda > 0$ has at least one representation as a coherent, continuous-time HQM, with Poisson rate $\lambda > 0$, for an appropriate configuration space and observable.

Proof. (*i.*) Let $\mathcal{P}_{t|s}$ be an A–coherent family on a set T of times and let $\boldsymbol{\Psi}_0 \in \mathcal{S}(A)$ be an initial coherent state. Let $\{\boldsymbol{\Psi}_j \mid j \in J\}$ be a basis for $\mathcal{S}(A)$. Since every $\mathcal{P}_{t|s}$ is coherent and $\{\boldsymbol{\Psi}_j\}$ is a basis for coherent states, we have, for every i, unique mixing coefficients $\pi_{t|s}(j|i) \geqslant 0$ such that

$$\mathcal{P}_{t|s}[\boldsymbol{\Psi}_i] = \sum_j \pi_{t|s}(j|i)\, \boldsymbol{\Psi}_j.$$

Also, $\boldsymbol{\Psi}_0$ is coherent by assumption so there are unique coefficients $\pi_0(i) \geqslant 0$ such that

$$\boldsymbol{\Psi}_0 = \sum_i \pi_0(i)\, \boldsymbol{\Psi}_i.$$

These functions satisfy

$$\begin{cases} \pi_{t|t}(j|i) = \delta(j-i) \\[2mm] \sum_j \pi_{t|s}(k|j)\, \pi_{s|r}(j|i) = \pi_{t|r}(k|i), \quad \text{for } t \geqslant s \geqslant r \\[2mm] \sum_j \pi_{t|s}(j|i) = 1 \\[2mm] \sum_i \pi_0(i) = 1. \end{cases} \tag{3.14}$$

by using uniqueness and the composition rules Eq. 3.5. Moreover, by expanding the definition Def. 3.6 of the state process $\mathcal{P}(t_n, \cdots, t_1)$, the functions $\pi_{t|s}(j|i)$ and $\pi_0(i)$ are seen to satisfy

$$\begin{aligned} \mathcal{P}(t_n, \cdots, t_1) = \\ \sum_{i_n, \cdots, i_0} \pi_{t_n|t_{n-1}}(i_n|i_{n-1}) \cdots \pi_{t_2|t_1}(i_2|i_1) \cdot \pi_{t_1|t_0}(i_1|i_0) \cdot \pi_0(i_0)\, \boldsymbol{\Psi}_n \otimes \cdots \otimes \boldsymbol{\Psi}_1. \end{aligned} \tag{3.15}$$

Let $\mathbf{f}(x)$ be a conditional quantum field (Def. 9) on a measure space $\mathbb{X}$. For $j \in J$, define

$$f_i(x) \overset{\text{def}}{=} \mathbf{tr}\left(\mathbf{f}(x) \cdot \boldsymbol{\Psi}_i\right).$$

The posterior HQM distribution is then, by definition and using Eq. 3.14 and Eq. 3.15,

$$p_{t_n,\cdots,t_1}(x_n,\ldots,x_1) = \mathbf{tr}\left(\mathbf{f}(x_n) \otimes \cdots \otimes \mathbf{f}(x_1) \cdot \boldsymbol{\Psi}(t_n,\cdots,t_1)\right)$$

$$= \sum_{i_n,\cdots,i_1} f_{i_n}(x_n) \cdots f_{i_1}(x_n)\, \pi_{t_n,\cdots,t_1}(i_n,\ldots,i_1),$$

where $\pi_{t_n,\cdots,t_1}(i_n,\ldots,i_1) \overset{\text{def}}{=} \pi_{t_n|t_{n-1}}(i_n|i_{n-1}) \cdots \pi_{t_2|t_1}(i_2|i_1) \cdot \pi_0(i_1)$.

The Markov independence property (Sec. 2.1.2.1, Eq. 2.4) follows from the definition of $\pi_{t_n,\cdots,t_1}(i_n,\ldots,i_1)$ above.

(*ii.*) Let $p_{t_n,\cdots,t_1}(x_n,\ldots,x_1)$ be a formal HMM with hidden M–state Markov matrix $\boldsymbol{\Pi}$ and condtional distributions $f_i(x)$. Define the configuration space to be $\mathbb{H} \overset{\text{def}}{=} \mathbb{C}^M$ and the observable $A \overset{\text{def}}{=} \mathbf{I}_M$. For $1 \leqslant i \leqslant M$, define the basic state $\boldsymbol{\Psi}_i \overset{\text{def}}{=} |e_i\rangle \cdot \langle e_i|$, where $e_i \overset{\text{def}}{=} [0,\cdots,0,1,0,\cdots,0]^{\text{T}}$, with 1 in the ith place. Define the initial state $\boldsymbol{\Psi}_0 \overset{\text{def}}{=} \sum_i \pi_0(i)\,\boldsymbol{\Psi}_i$. Define the coherent transition $\mathcal{P}$ on basic states $\boldsymbol{\Psi}_i$ by $\mathcal{P}(\boldsymbol{\Psi}_i) \overset{\text{def}}{=} \sum_j \boldsymbol{\Pi}(j,i)$ and then extend to all mixtures by linearity. Then the discrete-time state process $\mathcal{P}(i_n,\ldots,i_1)$ generated by $\mathcal{P}$ (Examp. 4) together with the quantum field $\mathbf{f}(x)$ given by the $(M \times M)$ matrix whose diagonal entries are $f_i(x)$ yield an HQM with posterior $p_{t_n,\cdots,t_1}(x_n,\ldots,x_1)$.

(*iii.*) The same as (*ii.*) above except $\mathcal{P}^\lambda(t_n,\ldots,t_1)$ is the continuous-time HQM with Poisson rate λ (Examp. 5) . □

Remark 13. Note that the rules Eq. 3.14 and the expansion Eq. 3.15 imply the marginalization property of $\mathcal{P}(t_n,\cdots,t_1)$, showing that this is a quantum state process as claimed in Sec. 3.1, Examp. 3.

Remark 14. The similarity to classical Markov processes is evident from Eq. 3.15. However, it must be constantly born in mind that the physical system is almost never in one of the Markov "states" labeled i. The actual quantum state $\mathcal{P}(t_n,\cdots,t_1)$ is a superposed **mixture** of the Markov states i; it is best to think of the physical system as being in **all** the i–states simultaneously, at every moment t. The quantum nature of this superposition of Markov states can, at any time, manifest itself by making a measurement of an observable B which is incoherent with the original A. Individual A–labels i will become completely meaningless in the resulting B–coherent state, revealing the non-classical behavior of HQMs.

3.4 Hidden Activated Measurement Models and Formal Markov Processes

In this section, hidden activated measurement models are defined and shown to generate hidden Markov models as posterior distributions.

Definition 12. A **hidden activated measurement model (HAMM)** is a hidden quantum model (Def. 10) whose prior quantum state process (Def. 1) is from an activated family (Def. 8). A hidden activated measurement model is called **diagonalizable** the state process is diagonalizable (Def. 4).

The results of the previous sections now show:

Theorem 3. *Every HAMM has posterior distribution which is a formal hidden Markov model (Sec. 2.1.2.1).*

This theorem demonstrates there are formal hidden Markov models which derive from latent physical processes which are not Markov. There are no Markov states through which the activated measurement process is cycling, not even the eigenstates in the diagonal basis for the observable A. The system is generally in mixed quantum states before activation and incoherent quantum states while activated, almost never in an eigenstate.

Definition 13. Nondegenerate Markov transitions: A square matrix Π is a **nondegenerate Markov transition matrix** if

- Π is nonnegative definite.

- All entries of Π are real and nonnegative: $\Pi \geqslant 0$.

- $\mathbf{1} \cdot \Pi = \mathbf{1}$, where $\mathbf{1} = [1, \ldots, 1]$.

- The eigenvalue 1 has multiplicity 1.

- There is a column vector $\boldsymbol{\pi}_\infty$ (the **equilibrium distribution**) such that $\Pi \cdot \boldsymbol{\pi}_\infty = \boldsymbol{\pi}_\infty$ and all coefficients of $\boldsymbol{\pi}_\infty$ are real and strictly positive: $\boldsymbol{\pi}_\infty > 0$. Without loss of generality, choose the unique $\boldsymbol{\pi}_\infty$ such that $\mathbf{1} \cdot \boldsymbol{\pi}_\infty = 1$.

- $\boldsymbol{\Pi}$ is **reversible**: The matrix $\boldsymbol{\Pi} \cdot \mathbf{D}_\infty$ is symmetric, where $\mathbf{D}_\infty$ is the diagonal matrix with diagonal $\boldsymbol{\pi}_\infty$.

A Markov process is called **nondegenerate** if its Markov transition matrix is nondegerate.

Note that a nondegenerate Markov transition matrix is diagonalizable, with nonnegative eigenvalues in which the eigenvalue 1 occurs precisely once.

For any matrix or vector $\mathbf{B}$, let $\mathbf{B}^{|2|}$ denote the matrix whose entries are the squared absolute values $|b_{ij}|^2$ of the entries b_{ij} of $\mathbf{B}$. The following is the key result linking classical Markov processes with activated measurement HQMs:

Theorem 4. *Let R be an nonnegative definite, hermitian operator with eigenvalue 1 of multiplicity 1. Let A be a compact observable and let $\mathbf{R}$ be the matrix of R in a coherence basis for A. Suppose there is an invertible matrix $\mathbf{J}$ and column vector $\boldsymbol{\kappa}$ such that*

$$
\begin{cases}
\|\boldsymbol{\kappa}\|_2 = 1 \\[4pt]
\mathbf{1} \cdot \mathbf{J} = \boldsymbol{\kappa}^{\mathrm{H}} \\[4pt]
\mathbf{J} \cdot \boldsymbol{\kappa} = \boldsymbol{\kappa}^{|2|} \\[4pt]
\mathbf{J} \cdot \mathbf{R} \cdot \mathbf{J}^{-1} \geqslant 0.
\end{cases}
$$

Then: (i.) $\boldsymbol{\Pi} \overset{\text{def}}{=} \mathbf{J} \cdot \mathbf{R} \cdot \mathbf{J}^{-1}$ is a nondegenerate Markov transition matrix with equilibrium distribution $\boldsymbol{\pi} \overset{\text{def}}{=} \boldsymbol{\kappa}^{|2|}$.

(ii.) There is an activator $\mathbf{Q}$ for A such that the HAMM generated by $\mathbf{Q}$ has posterior distribution identical to a classical HMM with Markov transition matrix $\boldsymbol{\Pi}$.

Proof. Choose any matrix $\mathbf{Q}$ for which $\mathbf{Q}^{|2|} = \mathbf{J} \cdot \mathbf{R} \cdot \mathbf{J}^{-1}$. Since $\mathbf{1} \cdot \mathbf{J} \cdot \mathbf{R} \cdot \mathbf{J}^{-1} = \mathbf{1}$, the columns of $\mathbf{Q}$ are unit vectors in a coherence basis for A so, by Sec. 3.2, Lem. 1, $\mathbf{Q}$ is an activator for A. Simple calculations prove the remaining results. $\qquad\square$

Thm. 3 and Thm. 4 show that, if the only distribution available concerning a physical process is a posterior

formal hidden Markov model (as occurs with Hodgkin-Huxley type ion channels Sec. 4.4.2), then there is no method to distinguish the situation of an hidden classical Markov process from an underlying hidden quantum process. They are scientifically indistiguishable and the decision between them therefore must be made on other grounds.

CHAPTER 4: AN ENERGY-MODULATED QUANTUM ION CHANNEL MODEL

In this section[1] we define a new abstract ion channel model to begin to fill the conceptual and technical gaps discussed in Chap. 1. The design and modeling philosophy is briefly outlined in Sec. 4.1. In Sec. 4.2, the four mathematical components of the model are presented. Applications of the model to ion channel analysis and synthesis are outlined in Sec. 4.4. Finally, in Sec. 4.4, the equations defining the models, in both the discrete- and continuous-time forms, are presented and proven to satisfy the design specifications. In addition, Appendix C contains details of scaling functions needed for the model.

4.1   Modeling Philosophy

While evolving the model, we were guided by four overarching principles:

1. The number of distinct noise mechanisms should be as small as possible.

2. Ion/channel kinetics are governed by probabilities derived from quantum operators.

3. Channels statistics are modulated by energy barriers.

4. Neural noise should be explained in terms of thermodynamic categories.

Principle 1 is a kind of "Ockham's Razor", advocating the use, if at all possible, of known channel mechanisms to explain neural noise generation. In particular, as discussed in Sec. 2.2.5, we believe that researchers starting with Hill & Chen [32] have not used sufficiently sophisticated models as the basis for their rejection of ion channel kinetics as a possible source of $1/f$ noise.

---

[1]Portions of this chapter have appeared in [1, 2, 121].

Principle 2 was discussed briefly in the introduction. Its interpretation is best explained in context (cf. Sec. 4.4).

Principle 3 embodies the important insight from concrete ion channel models [34, 61] and abstract Eyring rate channels (Sec. 2.2.4) that gating (i.e., the **modulation** of the ion permiability characteristics of the channel) is effected by changes in certain activation energies governing internal channel structure. These changes are made in response to external controls such as membrane voltage, ligand density, pressure, light, and so forth.

Principle 4 is meant to restrict attention to biophysical principles rather than **meta**-physical ones such as "scale-similarity" [88, 122] which, although occasionally explaining the formal mathematical structure of noise, adds nothing to our scientific comprehension.

These principles lead us to define four independent, physically-based **components** of our quantum ion channel model whose numerical parameters must be measured from experimental data:

1. The conformation space (Sec. 4.2.1).

2. The ion mobility process (Sec. 4.2.2).

3. The structural-energy operator (Sec. 4.2.3).

4. The Poisson transition rate (Sec. 4.2.4).

Finally, these components were linked by three sets of **axioms and equations** to form the final models:

1. Dissipative quantum Markov processes (Sec. 4.4.1: Eq. 4.2).

2. The energy-modulated discrete-time channel (Sec. 4.4.2: Def. 17).

3. The energy-modulated continuous-time channel (Sec. 4.4.3: Def. 18).

4.2 Model Components

4.2.1 *Conformations and States*

As alluded to previously, we propose to model a single type or **species** of neuronal ion channel as a finite-dimensional quantum system [73–75, 77, 103, 104] whose physical shapes, states, or as we call them, **conformations** determine the flow of ionic charges through the channel.

A channel c with M elementary conformations is associated with an an M-dimensional Hilbert space $\mathbb{H}_c$ [103] as well as a fixed orthonormal basis of **elementary wavefunctions** $\psi_i \in \mathbb{H}_c$, $i = 1, 2, \ldots, M$.

For example, the standard Hodgkin-Huxley Na^+ channel with three open/closed "*m*" subunits and one open/closed "*h*" subunit is classically modeled as an 8-state Markov process (cf. Sec. 2.2.5 and Sec. 4.4.2), each state i corresponding to 0, 1, 2, or 3 *m*–subunits and 0 or 1 *h*–subunits open in a particular physical channel conformation. However, we base our Na^+ model on an 8-dimensional Hilbert space $\mathbb{H}_{Na^+}$ with fixed basis $\psi_1, \ldots, \psi_8$ in order to reflect microscopic non-observability.

Remark 15. Our approach is in radical contrast to the classical model [34, 41] in which the channel was necessarily in one and only one of the elementary conformations $i = 1$ or $i = 2$ or ... or $i = M$ when the ion passed through, although which one may be unknown. Instead, since we do not actually observe an abstract conformation, we must regard the channel as existing in all conformations **simultaneously**, consistent with quantum mechanics [77, 103, 110].

The statistics of the channel at time t is determined by a **conformation**, which is just a **state $\Psi(t)$** [77, 123]. As previously discussed, the **Measurement Axiom** of quantum mechanics is the physical principle that any measurement of an observable A at time t_{meas} will discontinuously drive a mixed channel conformation $\Psi(t_{\mathrm{meas}}^-)$ before the measurement to a pure channel conformation $\Psi(t_{\mathrm{meas}}^+) = |\psi(t_{\mathrm{meas}}^+)\rangle \cdot \langle\psi(t_{\mathrm{meas}}^+)|$ after the measurement. This is also refered to as the **collapse of the wavefunction**. Unless the measurement was a direct observation of an elementary conformation, the resulting collapsed $\psi(t_{\mathrm{meas}}^+)$ will be a non-trivial **superposition** $\psi(t_{\mathrm{meas}}^+) = \sum_i a_i \psi_i$ in which each $|a_i|^2$ is the probability that a subsequent channel

45

conformation observation will yield elementary conformation i. As mentioned in Remark 15, our model is meant to capture indirect conformation measurements by means of net conductance properties. Thus we expect such measurements to leave the channel in non-trivial superposed conformations.

The conformation space of a population of multiple channels in neural membranes will be modeled as a direct sum $\bigoplus_c \mathbb{H}_c$ with appropriately-dimensioned conformation matrices $\boldsymbol{\Psi}_c(t)$, where c runs over all channels in the tissue, possibly of distinct species.

Remark 16. The direct sum formulation models the observer's inability to determine not only the channel through which a single charge passed or the elementary conformation of that channel but even the ion species to which the charge was associated. This makes good sense for large-scale conductance noise models which are meant to aggregate total current variations across membranes rather than account for species-specific noise components.

4.2.2 The Ion Mobility Process

We further assume that the channel in elementary conformation i determines an ion's **mobility** [41] $U_i \geqslant 0$ through the channel. This is a random variable with known distribution function $f_i(u)$, $u \geqslant 0$, $\int_0^\infty f_i(u)\,du = 1$.

In general, mobility is a local attribute with physical dimension velocity/force which measures the velocity of an ion as a result of a given driving force at a particular location [41]. However, we will regard the mobility variable U_i as an aggregate characteristic of the entire channel in elementary conformation i which gives the terminal velocity of an ion when it experiences a constant external electric force along the channel.

Thus an ion species with valence z will emerge from the channel with velocity $v_{\text{out}} = -U_i \cdot qz \cdot \Delta V$, where $q > 0$ is the unit of charge and ΔV is the voltage across the channel. This represents a current increment $\Delta I = qz \cdot v_{\text{out}} = -U_i \cdot q^2 z^2 \cdot \Delta V$ and incremental conductance $g = U_i \cdot q^2 z^2$.

For example, when $f_i(u) \equiv \delta(u)$, the ion mobility U_i is almost surely 0, so i represents a **closed** conformation. Similarly, $f_i(u) \equiv \delta(u - u_{\max})$ represents an (almost surely) **open** conformation with maximum

mobility $u_{\max}$ while $f_i(u) \equiv \delta(u - u_0)$, $0 < u_0 < u_{\max}$, is a conformation which passes a fixed interme-diate fraction $u_0/u_{\max}$ of ions from the ensemble, perhaps by means of a tunneling mechanism. This latter corresponds to a **leaky** conformation (cf. Sec. 2.2.5) with a constant rate of drip.

We will often explore mobilities $U(t)$ of the channel in mixed conformation $\boldsymbol{\Psi}(t)$ at time t which are random processes with distribution functions

$$f_U(t, u) = \Psi_{11}(t)f_1(u) + \cdots + \Psi_{MM}(t)f_M(u),\tag{4.1}$$

where $\Psi_{ii}(t)$ are the diagonal entries of $\boldsymbol{\Psi}(t)$.

Hence in our model, the dynamics of the conformation matrix $\boldsymbol{\Psi}(t)$ determines the statistics of the ionic mobility process $U(t)$ and, ultimately, the net membrane conductance noise characteristics.

Remark 17. When some $f_i(u)$ has non-zero variance, the channel may be termed **sputtering**: even in the presence of a smooth spatial distribution of ions at the channel entrance, the fraction which pass through the channel varies randomly. We will show in Appendix E that sputtering gives rise to a delta component, $R_0(t, s) = \bar{\sigma}_g^2(t)\delta(t - s)$, in the non-stationary autocorrelation of channel conductance, where $\bar{\sigma}_g^2(t) \stackrel{\text{def}}{=} \sigma_{g1}^2 \cdot \Psi_{11}(t) + \cdots + \sigma_{gM}^2 \cdot \Psi_{MM}(t)$ and $\sigma_{gi}^2 \stackrel{\text{def}}{=} q^4 z^4 \cdot \mathsf{Var}[U_i]$.

Remark 18. There is nothing in the formalism that would prevent negative mobilities $U_i < 0$; i.e., certain conformations for which there is a non-zero probability of an ion passing backwards through the channel against a membrane voltage in the opposite direction. This is physically possible because the ion is exposed to many non-membrane fields inside the channel. However, for the purpose of this article, we will not investigate this situation which could even give rise to negative conductances.

4.2.3   *The Structural Energy Operator*

As mentioned in Sec. 2.2.4, we will adopt a modified form of Eyring rate theory based on energy barriers. However, we generalize the theory in several ways:

- The energy barriers are not associated with geometric stations along the ion channel but, instead, with the channel conformations discussed above.

- To account for non-steady-state kinetics, we associate the energy barriers with an activated measurement process (Sec. 3.4, Def. 12). This is discussed in detail in Sec. 4.4.2.

Our model thus assumes the existence of a nonnegative-definite hermitian [103, 111] **structural-energy operator** $\mathcal{E} = \mathcal{E}(V)$ on $\mathbb{H}$ which is a function of the gating variable V.

We further require there to be a wavefunction $\phi_{\mathcal{E}}(V) \in \mathbb{H}$ of norm 1, associated with the **resting conformation** at gating value V, such that $\langle \phi_{\mathcal{E}} | \mathcal{E} \phi_{\mathcal{E}} \rangle$ is minimized over the sphere $\|\phi\| = 1$. The interpretation is that, when the channel is in the mixed distribution associated with some conformation matrix $\mathbf{\Phi}$, the value $\mathbf{tr}(\mathcal{E}(V) \cdot \mathbf{\Phi}) \geqslant 0$, is the expected structural energy stored the channel. This expected energy is thus minimized in the resting conformation $\mathbf{\Phi}_{\mathcal{E}}(V) \overset{\text{def}}{=} |\phi_{\mathcal{E}}(V)\rangle \cdot \langle \phi_{\mathcal{E}}(V)|$.

Remark 19. Appropriate restrictions on structural energy operators $\mathcal{E}$ are presented in Sec. 4.4.2, Def. 15. The form of typical functional dependence $\mathcal{E}(V)$ will be derived from standard ion channel kinetic equations in Sec. 4.4.1.

4.2.4   The Poisson Rate Function

Any discrete-time, time-homogeneous Markov process $X(n)$ with transition matrix $\mathbf{\Pi}_X$ can be transformed into a continuous-time process $X_\lambda(t)$ with the same steady-state distribution by executing the discrete Markov transitions according to a Poisson process with mean rate $\lambda > 0$ per unit time [79]; that is, the probability of executing precisely k state transitions of the X process during the time interval $[s, t]$ is $e^{-\lambda(t-s)} \cdot (\lambda(t-s))^k \big/ k!$.

For neuronal channels, we expect that the mean transition rate $\lambda(T)$ to depend mainly on the available thermal energy as measured by the absolute temperature T. Requirements for $\lambda(T)$ are presented in Sec. 4.4.3 and sample $\lambda(T)$ functions are presented in Appendix C.

4.3   Model Axioms and Equations

In Sec. 4.4.1 – Sec. 4.4.3, the components of Sec. 4.2 are assembled to form the new model using appropriate axioms, definitions, and lemmas.

4.3.1   Dissipative Quantum Processes

As pointed out in Sec. 2.2.4, the standard Eyring rate approach [34, 60] does not provide mechanisms which account for random deviations from its predicted mean flux values or the transition from transient to steady-state behavior [105, 106] required to fit Hodgkin-Huxley-type conductance curves [25]. Even a channel model based on quantum conformations (Sec. 4.2) cannot, by itself, explain the transition to steady-state since Schrödinger's Equation conserves energy ([77]).

To account for dissipative behavior, we posit that the channel's processing of single ions at discrete times $t = 0, 1, 2, \cdots$ constitute **measurements of the channel** but **not of its conformations**. For instance, we may register a voltage spike in our recording equipment because an ion has passed from one side of the membrane to the other but we have no way of determining the particular elementary conformation of the channel which allowed it to pass.

In such a situation, the channel's time-dependent wave function (cf. Sec. 4.2.1) $\psi(t)$ will collapse successively at $t = n \in \mathbb{N}$ to a sequence

$$\psi(0) = a_1(0)\,\psi_1 + a_2(0)\,\psi_2 + \cdots$$

$$\psi(1) = a_1(1)\,\psi_1 + a_2(1)\,\psi_2 + \cdots$$

$$\cdots$$

of pure superposed conformations. At intermediate times $n < t < n + 1$, the channel will generally be characterized by a mixed conformation $\Psi(t)$ of which nothing will be known.

Recalling that the amplitudes $|a_i(n)|^2$ of a pure conformation distribution represent the probabilities of

finding the channel in the various elementary conformations when an observation is made, we require the probability amplitude vectors

$$\left[|a_1(n)|^2, |a_2(n)|^2, \cdots \right]^{\mathrm{T}},$$

$n = 0, 1, \ldots$, of a channel's pure conformations are also the distributions of a discrete-time, time-homogeneous Markov process governed by some transition matrix $\mathbf{\Pi}(\mathcal{E}, T)$ which depends on the structural-energy operator $\mathcal{E}$ and the ambient temperature T. That is, $\mathbf{\Pi}(\mathcal{E}, T)$ satisfies the conditions for a stochastic matrix [82] and, for all discrete times $n \geqslant 0$,

$$\left[|a_1(n)|^2, |a_2(n)|^2, \cdots \right]^{\mathrm{T}} = \mathbf{\Pi}(\mathcal{E}, T)^n \cdot \left[|a_1(0)|^2, |a_2(0)|^2, \cdots \right]^{\mathrm{T}}, \tag{4.2}$$

which is consistent with all known kinetic behavior of ion channels

Remark 20. Recall that a Markov process $X(n)$ is **time-homogeneous** if the transition probability matrices $\mathbf{\Pi}_X(n|m)$, where $\Pi_{Xji}(n|m) \overset{\mathrm{def}}{=} \mathsf{Prob}(X(n) = j \mid X(m) = i)$ for $m \leqslant n$, depend only on the difference $(n - m)$. This holds just in case $\mathbf{\Pi}_X(n|m) = \mathbf{\Pi}_X^{(n-m)}$ for some matrix $\mathbf{\Pi}_X \geqslant 0$ for which $[1, \ldots, 1]$ is a left eigenvector of eigenvalue 1.

In the next section we examine the functional dependence of the matrix $\mathbf{\Pi}(\mathcal{E}, T)$ on the structural-energy operator $\mathcal{E}$ and temperature T.

4.3.2 The Energy-Modulated Discrete-Time Channel

There are several reasonable constraints on the functional dependence of the discrete Markov transition matrix $\mathbf{\Pi}(\mathcal{E}, T)$ on the structural-energy operator $\mathcal{E}$ and ambient temperature T:

1. For sufficiently large temperatures T, $\mathbf{\Pi}(\mathcal{E}, T)$ must be a valid Markov transition matrix [79]; that is, $\mathbf{\Pi}(\mathcal{E}, T)$ has real, non-negative entries and left eigenvector $\mathbf{1} \overset{\mathrm{def}}{=} [1, \ldots, 1]$ of eigenvalue 1.

2. If $\boldsymbol{\phi}_{\mathcal{E}} = \phi_{\mathcal{E}1} \cdot \boldsymbol{\psi}_1 + \phi_{\mathcal{E}2} \cdot \boldsymbol{\psi}_1 + \cdots$ is the decomposition of the resting conformation in the elementary basis (the **resting coefficients** of $\mathcal{E}$) then $\boldsymbol{\phi}_{\mathcal{E}} \overset{\mathrm{def}}{=} \left[|\phi_{\mathcal{E}1}|^2, |\phi_{\mathcal{E}2}|^2, \ldots \right]^{\mathrm{T}}$ must be an equilibrium distribution

50

of $\mathbf{\Pi}\left(\mathcal{E}, T\right)$; that is, $\phi_{\mathcal{E}}$ must be a right eigenvector of $\mathbf{\Pi}\left(\mathcal{E}, T\right)$ of eigenvalue 1.

3. Detailed balance [82] must hold at the resting distribution. In terms of the transition matrix $\mathbf{\Pi}\left(\mathcal{E}, T\right)$ this is reversibility or the **Kolmogoroff condition** for Markov processes which requires the product of transition probabilities over any closed cycle of conformations be the same in both directions [34].

The following **irreducibility** constraint ([123], Chap. 8) is not strictly necessary but it is technically useful because it excludes certain degenerate situations:

4. For all i, we require $\langle \phi_{\mathcal{E}} | \psi_i \rangle \neq 0$; that is, the resting conformation $\phi_{\mathcal{E}}$ has a non-trivial projection onto every elementary conformation $\psi_1, \psi_2, \cdots$. If this were to fail, then certain channel conformations would be inaccessible at equilibrium.

With these constraints in mind, we define structural energy operators in the simplest manner consistent with them:

Definition 14. Let $\mathcal{E}$ be an nonnegative-definite hermitian operator [103] $\mathbb{H} \xrightarrow{\mathcal{E}} \mathbb{H}$, where $\mathbb{H}$ is the M-dimensional channel conformation space (Sec. 4.2.1). The operator $\mathcal{E}$ will be called **irreducible** if it is of rank $(M-1)$ and has an eigenvector $\phi_{\mathcal{E}} \in \mathbb{H}$, of minimum eigenvalue, such that $\langle \phi_{\mathcal{E}} | \psi_i \rangle \neq 0$ for all basic conformations $\psi_1, \ldots, \psi_M$.

Definition 15. An operator $\mathcal{E}$ is a **structural-energy operator** if it is irreducible and, further, $\mathcal{E}$ and $\phi_{\mathcal{E}}$ satisfy the **energy detailed balance** requirement:

$$E_{ij} \cdot \left(\frac{\phi_{\mathcal{E}i}}{\phi_{\mathcal{E}i}^*} \right) = E_{ji} \cdot \left(\frac{\phi_{\mathcal{E}j}}{\phi_{\mathcal{E}j}^*} \right) \tag{4.3}$$

for $1 \leqslant i, j \leqslant M$, where the coefficients $E_{ij} \overset{\text{def}}{=} \langle \psi_i | \mathcal{E} \psi_j \rangle$ and $\phi_{\mathcal{E}i} \overset{\text{def}}{=} \langle \phi_{\mathcal{E}} | \psi_i \rangle$ are calculated with respect to the elementary conformations.

Remark 21. Since $\mathcal{E}$ is of rank $(M-1)$, if the conditions of irreducibility and detailed balance hold for any minimum-value eigenstate ϕ then they hold for all such. So, without loss of generality, we can fix one such resting conformation $\phi_{\mathcal{E}}$ of norm 1.

Definition 16. Let $\mathcal{E}$ be a fixed structural-energy operator. For any absolute temperature $T > 0$, define the **transition observable**

$$\mathcal{R}_{\mathcal{E}}(T) \stackrel{\text{def}}{=} \mathbf{I} + \boldsymbol{\Phi}_{\mathcal{E}} - e^{-(\mathcal{E} - E_0 \mathbf{I})/k_B T},$$

where E_0 is the minimum eigenvalue of $\mathcal{E}$, k_B is Boltzman's constant, and $\boldsymbol{\Psi}_{\mathcal{E}} \stackrel{\text{def}}{=} |\phi_{\mathcal{E}}\rangle \cdot \langle\phi_{\mathcal{E}}|$ is the projection onto the E_0 eigenspace (which is independent of the phase of $\phi_{\mathcal{E}}$).

Definition 17. Discrete-time, Energy-Modulated Channels: A **discrete-time energy-modulated ion channel model** is the discrete-time HAMM with transition matrix

$$\boldsymbol{\Pi}(\mathcal{E}, T) \stackrel{\text{def}}{=} \mathbf{J}_{\mathcal{E}} \cdot \mathbf{R}_{\mathcal{E}}(T) \cdot \mathbf{J}_{\mathcal{E}}^{-1} \tag{4.4}$$

where $\mathcal{E}(T)$ is the matrix of the transition observable $\mathcal{R}_{\mathcal{E}}(T)$ in a coherence basis for $\mathcal{E}$ and $\mathbf{J}_{\mathcal{E}}$ is any invertible matrix such that the equations

$$\begin{cases} \mathbf{1} \cdot \mathbf{J}_{\mathcal{E}} = \phi_{\mathcal{E}}^{\text{H}} \\ \mathbf{J}_{\mathcal{E}} \cdot \phi_{\mathcal{E}} = \phi_{\mathcal{E}}^{|2|} \end{cases} \tag{4.5}$$

hold in that basis.

Remark 22. The irreducibility requirement 4 insures that such $\mathbf{J}_{\mathcal{E}}$'s exist; e.g., the diagonal matrix with diagonal $\phi_{\mathcal{E}}^{\text{H}}$

The existence of the underlying activated measurement model mentioned in Def. 17 is the following:

Theorem 5. *Let $\mathcal{E}$ be a structural energy operator (Def. 15) and let $\boldsymbol{\Pi}(\mathcal{E}, T)$ be the matrix defined in Def. 17 for some appropriate $\mathbf{J}_{\mathcal{E}}$.*

Then there exists a constant $T_{\mathcal{E}} \geqslant 0$ such that, for all $T \geqslant T_{\mathcal{E}}$, $\boldsymbol{\Pi}(\mathcal{E}, T)$ satisfies constraints 1– 4 and, moreover, is the Markov transition matrix of an HAMM generated by some activator $Q(T)$ of $\mathcal{E}$.

Proof. Since $\phi_{\mathcal{E}}$ is an eigenvector of $\mathcal{E}$ of eigenvalue 1, we can choose a coherence basis for $\mathcal{E}$ such that

$$\mathbf{\Pi}\left(\mathcal{E}, T\right) = \mathbf{I} + \phi_{\mathcal{E}} \cdot \mathbf{1} - \mathbf{J}_{\mathcal{E}} \cdot \mathbf{D}\left(T\right) \cdot \mathbf{J}_{\mathcal{E}}^{-1},$$

where $\phi_{\mathcal{E}} \stackrel{\text{def}}{=} \phi_{\mathcal{E}}^{|2|}$ and $\mathbf{D}\left(T\right)$ is the diagonal matrix with diagonal

$$\left[e^{-(E_1 - E_0)/k_B T}, \cdots, e^{-(E_{M-1} - E_0)/k_B T}, 1\right].$$

So $\mathbf{\Pi}\left(\mathcal{E}, T\right) \to \phi_{\mathcal{E}} \cdot \mathbf{1}$ as $T \to \infty$. But every entry of $\phi_{\mathcal{E}} \cdot \mathbf{1}$ is strictly positive by definition of a structural energy operator hence

$$\liminf_{T \to \infty} \min_{i,j} \left\{ \mathbf{\Pi}\left(\mathcal{E}, T\right)_{i,j} \right\} > 0.$$

As a result, there is a $T_{\mathcal{E}} \geqslant 0$ such that, for all $T \geqslant T_{\mathcal{E}}$, $\mathbf{\Pi}\left(\mathcal{E}, T\right) > 0$, which implies constraint 1. The other constraints are straightforward.

The equivalence to a HAMM then follows from Thm. 4. $\qquad \square$

4.3.3   The Energy-Modulated Continuous-Time Channel

Recall the discussion in Sec. 4.2.4 of the temperature-dependent Poisson rate function $\lambda\left(T\right)$. As with the discrete-time channel (Sec. 4.4.2), there are reasonable constraints which may be placed on the temperature dependence of the evolution rate function $\lambda\left(T\right)$:

1. The actual transition rate $\lambda\left(T\right)$ should be a small fraction of some maximum possible transition rate $\overline{\lambda}$, itself determined by the thermal energy available to the channel.

2. For small variations $T \approx T_0$ around a standard temperature, the rate change should follow the well-known "Q_{10}" dependence for biological kinetics; that is $\lambda\left(T\right) \approx \lambda\left(T_0\right) \cdot Q_{10}^{(T - T_0)/10°\text{K}}$, for some constant Q_{10}. Note that Hodgkin and Huxley used $Q_{10} \approx 3$ in their original papers [25, 26] which seems typical for neurological tissue.

3. As $T \to 0$, we require $\mathbf{\Pi}\left(\mathcal{E}, T\right) \to \mathbf{I}$, the identity, which is the transition matrix which never leaves its initial distribution $\boldsymbol{\pi}\left(0\right)$. The channel is **frozen** into its initial distribution.

4. As $T \to \infty$, we require $\mathbf{\Pi}\left(\mathcal{E}, T\right) \to \left[1, \ldots, 1\right] \cdot \boldsymbol{\phi}_{\mathcal{E}}$, which makes a transition from any initial distribution $\boldsymbol{\pi}\left(0\right)$ to the equilibrium $\boldsymbol{\phi}_{\mathcal{E}}$ in precisely one step. This means there is sufficient thermal energy to immediately jump over any finite energy barrier.

To make a crude estimate of $\overline{\lambda}$, we reason as follows: At the standard temperature T_0, each degree of freedom of the channel should have roughly $k_B T_0$ Joules of thermal energy available which, for the M-dimensional configuration space of a channel, corresponds to a total $M k_B T_0$ Joules. In quantum mechanical terms, this corresponds to a maximum "phonon" frequency $\overline{\lambda} \overset{\text{def}}{=} M k_B T_0 / h$, where h is Planck's constant. By the Uncertainty Principle [104], this seems to be a rational absolute upper bound on the rate at which a quantum channel could change its conformation. For example, at the Hodgkin-Huxley base temperature of $T_0 = 6°\text{C}$ [25] and the standard 5-state Markov model [33, 41] of the K^+ channel, this yields $\overline{\lambda} \approx 30$ THz, by no means unreasonable for a nanoscale process.

Remark 23. The condition $\mathbf{\Pi}\left(\mathcal{E}, T\right) \to \mathbf{I}$ as $T \to 0$ may require $\mathbf{\Pi}\left(\mathcal{E}, T\right)$ to pass through regions for which it is not a valid Markov matrix (cf. Thm. 5). Obviously we cannot expect any biological model to remain valid down to absolute zero or above the boiling point of water. Nevertheless, these asymptotic conditions are important for determining the mathematical behavior at all temperatures.

See Appendix C for various forms of Poisson rate functions $\lambda\left(T\right)$ which satisfy constraints $1 - 4$.

Definition 18. Continuous-time, Energy-Modulated Channels: A **continuous-time energy-modulated ion channel model** is the continuous-time HAMM derived from the discrete-time $\mathbf{\Pi}\left(\mathcal{E}, T\right)$ (Def. 17) via the one of the Poisson rate functions $\lambda\left(T\right)$ defined in Appendix C.

4.4   The Synthesis and Analysis of Quantum Ion Channel Models

In this section, we present several applications of the ion channel concepts developed in the previous sections. Sec. 4.4.1 and Sec. 4.4.2 show how structural-energy operators can be extracted from Hodgkin-Huxley

rate matrices. This may lead to important new insights in neuroscience. Finally, Sec. 4.4.3 introduces techniques for the design of virtual ion channels which could have an impact on biomimetic computation.

The key to these applications is exploiting the relationship between the structural-energy operator and the gating variable. Since the operator $\mathcal{E}(V)$ depends on the gating variable V, Eq. 4.4 shows how the transition matrix $\mathbf{\Pi}(\mathcal{E}(V), T)$ is indirectly gated by V. Since $\mathbf{\Pi}(\mathcal{E}(V), T)$ determines the dynamic probability amplitude vectors through Eq. 4.2 which, in turn, determines the state matrix $\mathbf{\Psi}$ and the mobility distributions $f_i(u)$ through Eq. 4.1, we can explore the dynamics of this interlinked system which is ultimately controlled by the gating variable and the ambient temperature.

4.4.1 Activation Energy from Reaction Rate Matrices

As we have discussed several times, ion channel kinetics are typically well-modeled as continuous-time, 1st-order Markov processes [33, 41] i.e., the conformation distribution vector $\phi(t) = [\pi_1(t), \ldots, \pi_M(t)]^{\mathrm{T}}$ satisfies a kinetic equation

$$\frac{d\boldsymbol{\pi}}{dt} + \mathbf{K} \cdot \boldsymbol{\pi} = \mathbf{0}, \tag{4.6}$$

where $\mathbf{K}$ is a real, constant $(M \times M)$ matrix of reaction rates which has rank at most $(M-1)$.

If the reaction rate matrix $\mathbf{K}$ and ambient temperature T are known then, using Def. 16 and Def. 18, we could solve the structural-energy channel Eq. 4.4 for the structural-energy matrix $\mathbf{E}$:

$$\mathbf{E}(\mathbf{K}, T) = -k_B T \log \left[|\phi\rangle \cdot \langle\phi| + \frac{1}{\lambda(T)} \mathbf{J}^{-1} \mathbf{K} \mathbf{J} \right], \tag{4.7}$$

where ϕ is a vector such that $\left[|\phi_1|^2, \ldots, |\phi_M|^2 \right]^{\mathrm{T}} = \boldsymbol{\pi}_\infty$, with $\boldsymbol{\pi}_\infty$ a left 0-eigenvector of $\mathbf{K}$, and $\mathbf{J}$ is some choice of matrix defined by Eq. 4.5. (E.g., $\mathbf{J}$ is a diagonal matrix with diagonal ϕ.)

Remark 24. Note that Eq. 4.7 generalizes [60], Eq. (4).

4.4.2 Hodgkin-Huxley Activation Energies

The most important use of the formula Eq. 4.7 of the previous section is to derive structural-energy operators for the standard Hodgkin-Huxley K^+/Na^+ channels.

Voltage-gated Hodgkin-Huxley K^+ channels [25, 34, 62] are composed of four identical independent 2-state subunits (refered to as "n-subunits"), all of which must be in the "permissive" conformation for the channel to be open.

Letting $i = 0, 1, 2, 3, 4$ be the number of permissive subunits, the standard continuous 5-state Markov model of this channel [33, 41, 70] uses rate matrix

$$\mathbf{K}_{K^+}(V) = \begin{bmatrix} 4\alpha_n & -\beta_n & 0 & 0 & 0 \\ -4\alpha_n & 3\alpha_n + \beta_n & -2\beta_n & 0 & 0 \\ 0 & -3\alpha_n & 2\alpha_n + 2\beta_n & -3\beta_n & 0 \\ 0 & 0 & -2\alpha_n & \alpha_n + 3\beta_n & -4\beta_n \\ 0 & 0 & 0 & -\alpha_n & 4\beta_n \end{bmatrix} \tag{4.8}$$

where $V \stackrel{\text{def}}{=} E_{\text{mem}} - E_{\text{rest}}$ is the voltage across the membrane in excess of its resting potential and $\alpha_n(V), \beta_n(V)$ are the Hodgkin-Huxley n–subunit gating functions (at the standard ambient temperature $T_0 = 6°C$)

$$\begin{cases} \alpha_n(V) = 0.01(V + 10) / \left(e^{(V+10)/10} - 1 \right) \\ \beta_n(V) = 0.125 \, e^{(V/80)}, \end{cases} \tag{4.9}$$

with V measured in mV, which were fitted to the conductance data empirically [25].

Letting $p_n(V, T) \stackrel{\text{def}}{=} \alpha_n/(\alpha_n + \beta_n)$ and $q_n(V, T) \stackrel{\text{def}}{=} \beta_n/(\alpha_n + \beta_n)$, the equilibrium distribution is the right 0-eigenvector $\mathbf{p}_{K^+} \stackrel{\text{def}}{=} \left[q_n^4, \, 4q_n^3 p_n, \, 6q_n^2 p_n^2, \, 4q_n p_n^3, \, p_n^4 \right]^{\mathrm{T}}$ given by the binomial probabilities.

Using $\mathbf{p}_{K^+}$ as the last vector of a basis of eigenvectors of $\mathbf{K}_{K^+}$, Eq. 4.7 shows the activation-energy matrix

diagonalizes to

$$\mathbf{E}_{K^+}(V, T) \propto k_B T \cdot (\log(\tau_n(V, T)) \cdot \mathbf{I}_5 + \mathbf{diag}[0, \log 1, \log 1/2, \log 1/3, \log 1/4]), \qquad (4.10)$$

where $\mathbf{I}_5$ is the (5×5) identity matrix and, $\tau_n(V, T) \stackrel{\text{def}}{=} (\alpha_n(V, T) + \beta_n(V, T))^{-1}$ is the mean time for an n-subunit to switch between permissive and non-permissive configurations [41].

A similar analysis can be performed to find the activation energy matrix $\mathbf{E}_{Na^+}$ of the standard 8–state Markov model [33] of Hodgkin-Huxley Na^+ channels. It is one of the most important features of our new ion channel model that important, additional biophysical information can be extracted from the classic 1952 Hodgkin-Huxley research [25].

4.4.3   Examples of Synthetic Channels

The simplest way to engineer energy-modulated channels is to observe that when the resting conformation vector $\pi_{\mathcal{E}}$ has real components then the detailed balanced constraint Eq. 4.3 implies the energy matrix $\mathbf{E}$ also has real components; i.e., $\mathbf{E}$ is a real symmetric matrix. The converse also holds :

Definition 19. An $(M \times M)$ matrix $\mathbf{G}$ is an **structural metric** if it is a nonnegative-definite real symmetric matrix of rank $(M - 1)$ whose 0-eigenvector $\mathbf{u_G}$ has non-zero components. It is called **standard** if $\mathbf{G}$ has strictly positive components.

Lemma 2. *Let $\mathbf{E}$ be a square matrix. Then $\mathbf{E}$ is the matrix of a structural energy matrix (Def. 15) if and only if there is a structural metric $\mathbf{G}$ and a complex vector $\mathbf{u}$ whose components satisfy $|u_i| = 1$ such that $\mathbf{E} = \mathbf{D_u} \mathbf{G} \mathbf{D_u^H}$, where $\mathbf{D_u}$ is the matrix whose diagonal is $\mathbf{u}$. If $\mathbf{G}$ is required to be a standard structural metric then both $\mathbf{G}$ and $\mathbf{u}$ are unique.*

Remark 25. The standard structural metric $\mathbf{G_E}$ and its associated vector $\mathbf{u_E}$ are thus comparable to the **magnitude** and **phase** of the energy matrix $\mathbf{E}$.

Lem. 2 shows that gated structural-energy operators $\mathcal{E}(V)$ can be designed by specifying their eigenvector

$\boldsymbol{\pi}\left(V\right)$ in a real space of dimension M together with the singular metric ellipsoid $\mathbf{G}\left(V\right)$ of dimension $M-1$ which is perpendicular to $\boldsymbol{\pi}\left(V\right)$. The metric specifies the squared structural "distance" from an arbitrary vector $\boldsymbol{\xi}$ in the space to $\boldsymbol{\pi}\left(V\right)$ and can be designed to achieve particular goals. Although the function $\mathcal{E}\left(\cdot\right)$ is not required to be continuous, it is a physically plausible extra condition. In that case, the graph of $\boldsymbol{\pi}\left(\cdot\right)$ should be contained in a single orthant so that the direction cosines with the ψ_i axes never vanish.

Fig. 4.1 depicts the arrangement for distinct values V_1, V_2 of the gating variable in which the metric ellipsoids have been translated from the origin to the ends of the vectors for clarity.
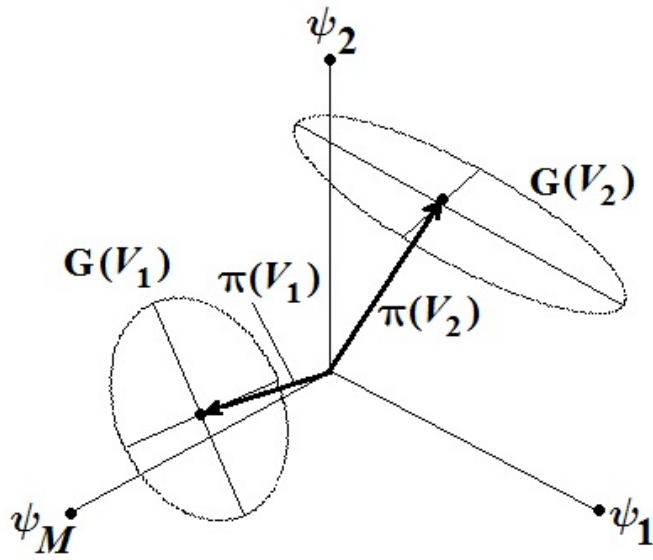
Figure 4.1: Metric ellipses for the synthesis of quantum ion channels.

CHAPTER 5: NOISY TISSUE AND THE VAN DER ZIEL - MCWHORTER PARADIGM

We have been investigating more plausible models of neurological noise specifically for real-time EEG applications but potentially useful all the way down to the channel level. In previous works [121, 124] we focused on the spectral structure of our noise models. In this chapter[1], we present new noise modeling concepts and methods we developed for the time domain. We also present initial findings concerning time domain optimal causal filtering of this noise.

5.1   Noise from Ion Channel Populations in Thermal Equilibrium

In this section we will discuss how constained entropy maximization applied to populations of energy-modulated quantum channels provides the missing optimization principle alluded to in Sec. 2.2 and can explain the ubiquitous $1/f$-type noise present in neurological measurements. The detailed proofs are presented in Appendix E.

We have isolated an important class of random processes we call **multiple-species generalized van der Ziel - McWhorter noise** (or **multi-GVZM noise**).

Definition 20. A **multiple-species GVZM** process is any stationary random process $\{\nu(t)\}_{t=-\infty}^{\infty}$ whose autocovariance function is of the form

$$R_\nu(\tau) \propto \int_X \frac{1}{v_1(x)^{2-\theta_1}} \cdots \frac{1}{v_C(x)^{2-\theta_C}} \left(\sigma_1^2 e^{-|\tau|/v_1(x)v_1(x)} + \cdots + \sigma_C^2 e^{-|\tau|/v_1(x)v_1(x)} \right) d\mu(x), \quad (5.1)$$

where $v_1(x) > 0, \cdots, v_C(x) > 0$ are **time-constant functions**, one for each of C species of chan-

---

[1]Portions of this chapter have appeared in [1–3, 121, 124].

nel, $\theta_1, \cdots, \theta_C$ are the constant **spectral exponents**, $\sigma_1^2, \cdots, \sigma_C^2$ are weighting constants, and (X, μ) is a "**neurologically relevant**" **measure space** [78].

The simplest examples of GVZM noise uses our generalization of van der Ziel and McWhorter's original autocorrelation [95, 96],

$$R_{\mathrm{GVZM}(\theta)}(\tau) \propto \int_{\upsilon_1}^{\upsilon_2} \frac{1}{\upsilon^\theta} e^{-|\tau|/\upsilon} d\upsilon, \tag{5.2}$$

which has power spectra

$$S_{\mathrm{GVZM}(\theta)}(f) \approx \frac{1}{f^\theta} \quad \text{for} \quad \frac{1}{2\pi\upsilon_2} < f < \frac{1}{2\pi\upsilon_1}. \tag{5.3}$$

In these cases, the neurological measure space is the closed interval $X = [\upsilon_1, \upsilon_2]$ with the ordinary Riemann-Lebesgue measure [78] and the time constant function is the identity $\upsilon(x) \equiv x$.

Fig. 5.1 shows a simple example of a fit of a $\mathrm{GVZM}(\theta)$ spectrum which is seen to approximate closely the experimental EEG data Fig. 1.2. However, all GVZM noises have family similarities.

The connection of GVZM to ion channel noise is most easily seen by analyzing Hill and Chen's well-known formula [33, 70] for the conductance autocorrelation of the Hodgkin-Huxley K^+ channel with a single open conformation:

$$R_{K^+}(t) \propto \left(p_n + q_n e^{-|t|/\upsilon_n}\right)^4 - p_n^4 = \sum_{k=1}^{4} \binom{4}{k} p_n^{4-k} q_n^k e^{-k|t|/\upsilon_n}, \tag{5.4}$$

where p_n, q_n, υ_n are defined in Sec. 4.4.2.

Note that the expressions $e^{-k|t|/\upsilon_n}$ are reminiscent of McWhorter's decay rates $1/\upsilon = e^{-E/k_B T}$ (Eq. 2.8) and that the coefficients υ_n/k are precisely the **reciprocal eigenvalues** of the Hodgkin-Huxley reaction rate matrix (e.g.; see Eq. 4.8 below). In turn, this matrix is directly related to the activation-energy operator by Eq. 2.8.
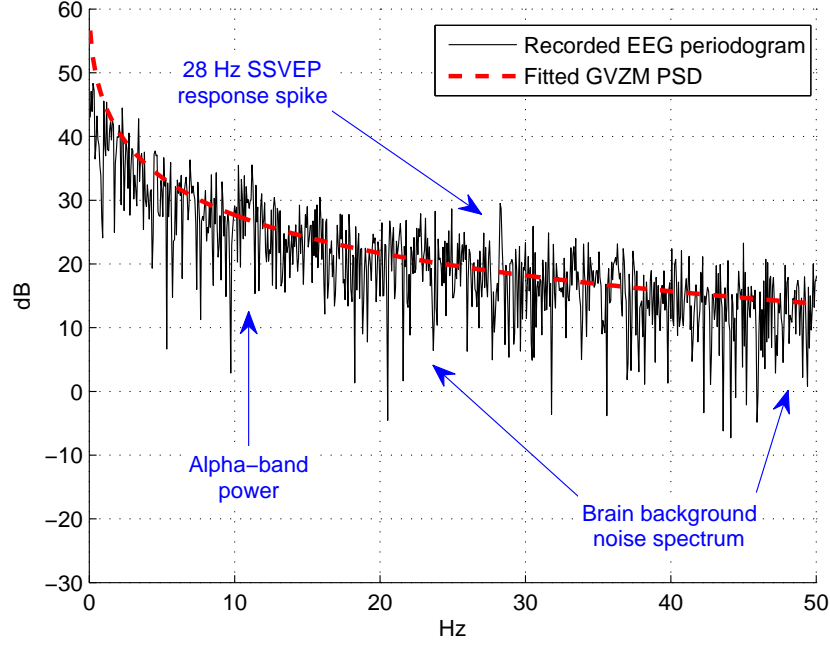
Figure 5.1: GVZM (θ) power spectral density $\theta = 1.1219$ fitted to 28 Hz stimulus raw EEG periodogram.

These links form the basis of Thm. 6 below.

Theorem 6. *Let $\mathbb{X} \subseteq \{0, 1, \ldots\} \times X$ be a "neurological measure space" with probability ρ, interpreted as the population density of ion channel conformations $i \in \{0, 1, \ldots\}$ for channels $x \in X$. Let $\mathcal{E}(x)$, $x \in X$, be structural-energy operators with minimum energies $E_0(x)$ as discussed in Sec. 4.4.3, derived from C distinct ion channel species. Let $g\left(\overline{\Delta E}, i, x\right)$ be the maximum entropy probability distribution [105, 106] under the energy constraints*

$$\int_{\mathbb{X}} \left(E_i(x) - E_0(x)\right) g\left(\overline{\Delta E}, i, x\right) d\rho(i, x) = \overline{\Delta E},$$

Then there are unique spectral exponent functions

$$\theta_1\left(\overline{\Delta E}\right), \cdots, \theta_C\left(\overline{\Delta E}\right)$$

and activators (Def. 6) $\mathbf{Q}(x)$ for $\mathcal{E}(x)$, $x \in X$, for which the population conductance noise is of the multi-GVZM form Eq. 5.1.

61

Proof of Thm. 6. See Appendix E.

5.2 A Model of Noisy Tissue

This section[2] presents our model of noisy biological tissue.

In Sec. 5.2.1, we describe the stochastic process background theory we developed for our noise models. In Section 5.2.2 we review our schematic models of noisy neurological tissue. In the following Sec. 5.2.7 and Sec. 5.2.4, we specialize to the simplest case, yielding the GVZM noise process. Sec. 5.2.5 presents some preliminary results towards developing real-time detection algorithms based on optimal filtering of GVZM noise.

5.2.1 Hidden Autoregressive Processes

Example 8. Define a pth–order **autoregressive (AR) simplicial process** [56] to be a continuous-time, stationary, K–component simplicial process $\mathbf{X}(t)$ for which there are $p - 1$ constant $(K \times K)$ matrices $\mathbf{A}_1, \ldots, \mathbf{A}_{p-1}$ such that the stochastic differential equation [125]

$$\frac{d^p \mathbf{X}}{dt^p} + \mathbf{A}_1 \frac{d^{p-1} \mathbf{X}}{dt^{p-1}} + \cdots + \mathbf{A}_{p-1} \mathbf{X} = \nu$$

holds for all t, where $\nu(t)$ is an independent and identically distributed K–component, $\mathbf{0}$–mean Gaussian process (the **innovation** process). (The existence of such processes is a consequence of Thm. 7 below.)

Remark 26. As with $\mathbf{X}(t)$ itself, the components of $\nu(t)$ cannot be independent Gaussians; i.e., the covariance matrix $\mathbf{\Sigma}_\nu$ is singular. Thus we could simultaneously rotate $\mathbf{X}(t)$ and $\nu(t)$ to have at least one component equal to the constant 0. (Transients are excluded by stationarity.) We define the **dimension** of an AR simplicial process with innovation ν to be the rank of $\mathbf{\Sigma}_\mathbf{X}$.

Example 9. By analogy, when $G(t)$ is an AR process, we say that $G(t)$ is **hidden autoregressive model**

---

[2]Portions of this section have appeared in [3].

(HARM).

Finally, we define a a **mixed HARM** to be a (finite or infinite) summation $G(t) = \int G_E(t)\,dE$ of an indexed family $\{G_E(t)\}_{E \in \mathcal{E}}$ of hidden AR models.

5.2.2 Noisy Biological Tissue

Our abstraction of noisy tissue consists of a large collection of schematic "channels", of various "energies" $E_1, E_2, \ldots$, embedded in a membrane. (See Fig. 5.2.) The spatial density of channels with energy E is given by a function $\rho(E)$.
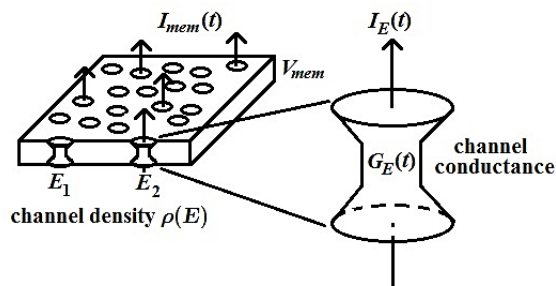
Figure 5.2: Hidden simplicial noisy tissue

Each channel is characterized by an abstract stochastic conductance process $G_E(t)$ which determines the flow of current $I_E(t)$ through the channel via a common membrane voltage. The accumulated current $I_{\mathrm{mem}}(t)$ through the membrane at time t is the model noise signal.

Abstract channels could be Hodgkin-Huxley-type K^+ and Na^+ channels [34] if we are at the level of individual neuron membranes in which case conductances and currents correspond to the actual physical entities. However, channels could be as large as cortical microcolumns [36] for EEG applications in which case conductances and currents represent abstractions. But we always make three critical modeling assumptions:

- All channels in the membrane are statistically independent at equilibrium.
- Channels with the same energy E have identically-distributed conductance processes $G_E(t)$.
- Every $G_E(t)$ is a hidden simplicial model.

63

Thus noisy tissue is a mixed hidden simplicial model and so we immediately infer:

Corollary 1. *the autocovariance $C_I(t, s)$ of the membrane noise current is determined by*

$$C_I(t, s) \propto \int \rho(E)\, C_{G_E}(t, s)\, dE, \tag{5.5}$$

where $C_{G_E}(t, s)$ is given by (2.7) and $\propto$ denotes "is proportional to."

Example 10. It is well-known [34] that the dynamic behavior of Hodgkin-Huxley-type channels can be accurately modeled by continuous-time HMMs with forward equation

$$\frac{\partial \mathbf{\Pi}(t, s)}{\partial t} + \frac{1}{\tau} \mathbf{A} \cdot \mathbf{\Pi}(t, s)$$

for $t \geqslant s$, where $\mathbf{\Pi}(t, s)$ is the state probability matrix at times t, s, the parameter τ is the mean waiting time between Poisson jumps from state-to-state, and $\mathbf{A}$ is an ion channel **rate matrix**. Thus if the waiting time $\tau(E)$ depends in some fashion on the available energy E, then neuron membranes containing a large number of such ion channels are hidden simplicial membranes.

Example 11. An example of such energy-dependence is the classic **Eyring rate** model [34] of ion channel equilbrium in which

$$\tau(E) \propto e^{-(E - E_{\min})/kT}, \tag{5.6}$$

where E is an activation energy, $E_{\min}$ is some baseline energy, T is the ambient temperature, and k is Boltzmann's constant. We shall return to the Eyring rate formula in the next section.

A rate matrix $\mathbf{A}$ is called **reversible** or satisfies the **detailed balance** condition [34] if the equation $\mathbf{A} \cdot \mathbf{P}_\infty = \mathbf{P}_\infty \cdot \mathbf{A}^{\mathrm{T}}$ holds, where $\mathbf{P}_\infty$ is the diagonal matrix whose diagonal is the equilibrium probability of the Markov process. For instance, it can be checked that the standard Hodgkin-Huxley rate matrices $\mathbf{A}_{\mathrm{K}+}$ and $\mathbf{A}_{\mathrm{Na}+}$ [34] are reversible. We have proved the following important result:

Theorem 7. *Let a noisy tissue be made of identically distributed, K–state, reversible HMMs. Then as the*

number of channels becomes large, the conductance process $G\left(t\right)$ becomes asymptotic to a single 1st–order HARM of dimension $K - 1$.

Corollary 2. *Noisy reversible mixed HMM tissue is asymptotic to mixed HARM tissue.*

Remark 27. Note that the innovations of all AR processes (simplicial or not) are Gaussian by definition. The significance of Thm. 7 is that it implies the hidden $\mathbf{X}\left(t\right)$ process of noisy tissue is itself asymptotically Gaussian. For example, the 1st–order AR process $d\mathbf{X}/dt + \mathbf{A}\mathbf{X} = \nu$ has formal solutions

$$\mathbf{X}\left(t\right) = e^{-\mathbf{A}t} \int_{-\infty}^{t} e^{\mathbf{A}s} \nu\left(s\right) ds + \mathbf{P}_0, \tag{5.7}$$

where $\mathbf{P}_0$ is any (non-random) vector satisfying $\mathbf{A}\mathbf{P}_0 = 0$, showing how $\mathbf{X}\left(t\right)$ can be expressed as a linear combination of Gaussians.

5.2.3 Tissue and GVZM Noise

In order to explore the results of the previous sections, we considered a highly simplified version of hidden simplicial tissue which is adapted to EEG applications.

Define a hidden Markov channel with rate matrix $\left(1/\tau\right)\mathbf{A}$ to be **secular** if the conductance value $G\left(t\right)$ returned from the mixed distribution $x_1 f_1\left(g\right) + \cdots + x_K f_K\left(g\right)$, where $x_1 = X_1\left(t\right), \ldots, x_K = X_K\left(t\right)$, is actually the average value of a large random sample taken at a rate much faster than the state transition rate $1/\tau$. For secular hidden Markov channels, we can reasonably replace the processes $G\left(t\right)$ and $G\left(t\right)^2$ by $\hat{G}\left(t\right) = \boldsymbol{\mu}_{\mathbf{f}} \cdot \mathbf{X}\left(t\right)$ and $\hat{G^2}\left(t\right) = \boldsymbol{\mu}_{2,\mathbf{f}} \cdot \mathbf{X}\left(t\right)$ respectively, where $\boldsymbol{\mu}_{2,\mathbf{f}}$ is the vector of second moments of the conditionals $\mathbf{f}$. We then investigated noisy membranes of the following highly restricted form:

- All channels are 2-state, secular HMMs which are identical except for the time constants $\tau\left(E\right)$ of their rate matrices $\left(1/\tau\left(E\right)\right)\mathbf{A}$.
- The number of channels is large.
- The time constant function $\tau\left(E\right)$ is given by the Eyring rate formula (5.6).

65

• The channel density function $\rho(E)$ is such that entropy is maximized under an energy constraint

$$\int_{E_1}^{E_2} E \rho(E) \, dE = \hat{E},$$

where $\hat{E}$ is some fixed value, $\hat{E} > E_{\min}$.

We can readily establish the following result:

Theorem 8. *(i) The noise process $G(t)$ is stationary and asymptotically Gaussian.*

(ii) The autocovariance of $G(t)$ can be written in the GVZM form [124]

$$C_G(t) = P_0 \int_{\tau_1}^{\tau_2} \tau^{\theta-2} e^{-|t|/\tau} d\tau + P_1 \delta(t), \tag{5.8}$$

*where $P_0, P_1 \geqslant 0$ have units of power, $\tau_2 > \tau_1 > 0$ have units of time, and $\theta > 0$ is a dimensionless constant (the **spectral exponent**).*

(iii) The process $G(t)$ is uniquely defined by (i) and (ii).

(iv) $G(t)$ can be realized as a 1-dimensional mixed AR process.

As discussed in [124], when $\theta \leqslant 2$, the frequency spectrum of GVZM noise falls off as $1/f^0$ near $f = 0$, as $1/f^\theta$ for middle frequencies, and as $1/f^2$ for large frequencies. Thus it is a $1/f^\theta$–type noise which avoids the singularity at low frequency and the infinite total power which plagues less sophisticated neurological $1/f^\theta$ noise models.

Not only do the real and synthetic spectra have the same shape and general variability, we showed in [2] that the statistical match is sufficient to improve the performance of standard periodogram-based SSVEP estimation algorithms.

5.2.4 Properties of GVZM Noise

.

Definition 21. The **GVZM PSD** $S_{\text{GVZM}}(f)$ is the family of functions[3] with five parameters $0 < \theta < 2$, $0 < \upsilon_1 < \upsilon_2$, $P_0 \geqslant 0$, $P_{\text{s}} \geqslant 0$ and defined by

$$S_{\text{GVZM}}(f) \overset{\text{def}}{=} P_0 |f|^{-\theta} \left(\tan_\theta^{-1}(2\pi\upsilon_2 |f|) \right.$$
$$\left. -\tan_\theta^{-1}(2\pi\upsilon_1 |f|) \right) + P_{\text{s}}, \tag{5.9}$$

where

$$\tan_\theta^{-1}(x) \overset{\text{def}}{=} \text{sgn}(x) \int_0^{|x|} \frac{u^{\theta-1}}{1+u^2} du. \tag{5.10}$$

Note that for $\theta = 1$, Eq. (5.10) is the ordinary $\arctan(x)$. The dimension of υ_1, υ_2 is time while that of P_0, P_{s} is amplitude^2/frequency (i.e., noise power). The spectral exponent θ is dimensionless.

The importance of this definition is that, so far as the author is aware, this is the first simple model of the average EEG background noise spectrum proposed in the literature which can match recorded EEG periodograms from near 0 Hz to over 30 Hz, with a fixed number of parameters. Moreover, the GVZM PSD function approximates a power law $1/f^\theta$ in the mid-frequencies without requiring infinite power. In fact, $S_{\text{GVZM}}(f)$ always has finite amplitude and finite total power.

The properties of $\tan_\theta^{-1}(x)$ show that, once the noise floor P_{s} is subtracted, we have the approximate proportionalities $S_{\text{GVZM}}(f) \propto 1/f^0$ (i.e., a constant) for $f < 1/(2\pi\upsilon_2)$, $S_{\text{GVZM}}(f) \propto 1/f^\theta$ for $1/(2\pi\upsilon_2) < f < 1/(2\pi\upsilon_1)$, and $S_{\text{GVZM}}(f) \propto 1/f^2$ for $f > 1/(2\pi\upsilon_1)$. Thus its roll-off transitions smoothly through the $1/f^\theta$ regime, without any of the so-called "catastrophes" [88] of apparent infinite power density when $f \to 0$ and infinite integrals as $f \to \infty$ which plague true $1/f$–type noises. In particular, $S_{\text{GVZM}}(f)$ approaches the finite limiting value $P_0 \left((2\pi\upsilon_2)^\theta - (2\pi\upsilon_1)^\theta \right)/\theta + P_{\text{s}}$ as $f \to 0$.

---

[3]Portions of this section have appeared in [2]

GVZM PSD function fitted to the periodogram of recorded EEG data from an SSVEP session. The GVZM curve follows the periodogram closely except for the α-band power [36] and the SSVEP response spike.

Eq. (5.9) has it origin in investigations dating to the 1930's [90] on apparent $1/f$-type noise in vacuum tubes and semiconductors. In 1957, A.L. McWhorter proposed [95] a simple explanation for $1/f$–type semiconductor noise at thermal equilibrium, based on the assumption that the logarithm of the rate at which electrons drop from an activated state was proportional to the energy of that state. Subsequently A. van der Ziel and others [126] abstracted the McWhorter mechanism to general noise processes. Our formula (5.9) reduces to the original van der Ziel-McWhorter PSD function for $\theta = 1$.

5.2.5 *Causal Filtering of GVZM Noise*

.

The Gaussian conclusion[4] of Thm. 7 allows the application of standard detection and estimation procedures [127] to hidden simplicial noisy tissue.

Specifically we can find a least-squares-optimal causal filter $a(t)$, $t \geqslant 0$, which transforms a GVZM noise signal $\nu_{\mathrm{GVZM}}(t)$ with known or estimated parameters into an independent and identically distributed Gaussian noise process $\nu_{\mathrm{Gauss}}(t)$ by means of a running time-domain convolution on past values

$$\nu_{\mathrm{Gauss}}(t) = \int_0^\infty a(s)\,\nu_{\mathrm{GVZM}}(t - s)\,ds.$$

Fig. 5.3 shows such a procedure applied to an SSVEP dataset. As we demonstrated in [2], a standard SSVEP detection procedure was unable to separate the 28Hz response peak from the noise peaks surrounding it. But, as the lower graph shows, after optimal causal filtering, not only does the spectrum flatten (i.e., become "whiter"), the SSVEP peak is enhanced and stands out clearly above the residual background noise.

---

[4]Portions of this section have appeared in [3]
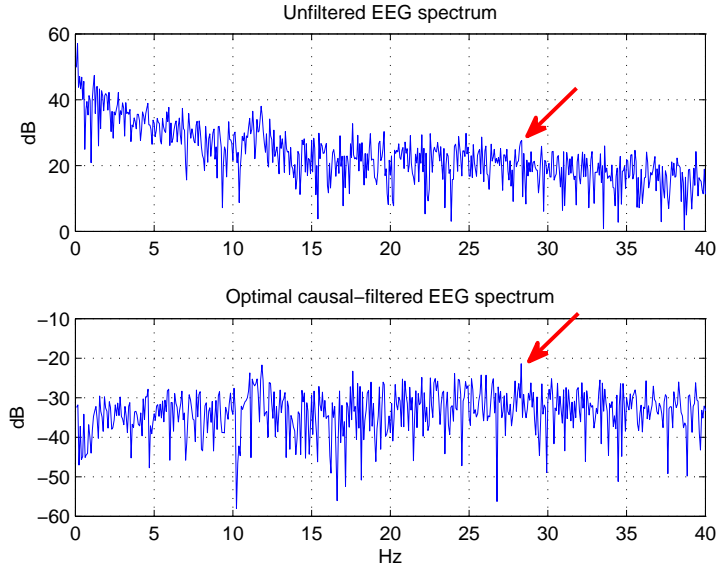
Figure 5.3: A 28Hz SSVEP response nearly lost in background noise compared to the enhanced response optained by causal filtering based on GVZM noise.

5.2.6 Autoregressive Approximations to GVZM Noise

.

Let $0 < \upsilon_1 < \upsilon_2$ be fixed parameters with the dimension of time, $0 < \theta < 2$ be dimensionless, and $P_0, P_{\mathrm{s}} \geqslant 0$ have dimension amplitude^2/frequency. Let $K > 0$ be an integer and define $\Delta\upsilon = (\upsilon_2 - \upsilon_1)/(K-1)$. Let $\Delta t > 0$ be a time step.

For $0 \leqslant k \leqslant K-1$, define the AR coefficients a_k, b_k and weights w_k by

$$
\begin{cases}
a_k \stackrel{\mathrm{def}}{=} e^{-\Delta t/(\upsilon_1 + k\Delta\upsilon)}, & b_k \stackrel{\mathrm{def}}{=} \sqrt{1 - a_k^2}, \\[2mm]
w_k \stackrel{\mathrm{def}}{=} \sqrt{\dfrac{1}{(\upsilon_1 + k\Delta\upsilon)^{2-\theta}}\,\Delta\upsilon\Delta t}.
\end{cases}
\tag{5.11}
$$

69

Let $x_k(n)$ be the 1st–order, stationary AR process [56]

$$x_k(n) = a_k\, x_k(n-1) + b_k\, \sqrt{P_0}\, \varepsilon_k(n)\,,$$

where the error processes $\varepsilon_k(n)$ are iid standard normal ($N(0,1)$) random variables.

Then EEG background processes can be modeled by the discrete-time, mixed AR simulations

$$x_K(n) \stackrel{\text{def}}{=} \sum_{k=0}^{K-1} w_k{\cdot}x_k(n) + \sqrt{P_{\text{s}}} \cdot \varsigma_{\text{s}}(n)\,, \tag{5.12}$$

where the error process $\varsigma_{\text{s}}(n)$ is an $N(0,1)$ random variable which is independent of all the $\varepsilon_k(n)$'s. We call such processes AR-GVZM, simulations of EEG noise.
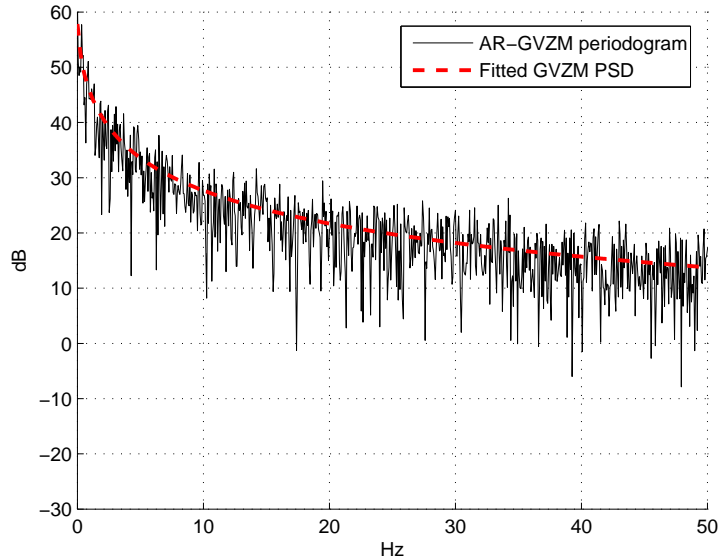
Figure 5.4: Periodogram of AR-GVZM simulation of EEG noise, with $K = 300$, using the Fig. 5.1 parameters.

Fig. 5.4 shows the periodogram of such a simulation $x_K(n)$, with $K = 300$ AR subprocesses $x_k(n)$, using the GVZM parameters that optimally fit the data. It can be seen how accurately the periodogram of $x_K(n)$ matches the characteristics of the recorded data, except for the SSVEP response spike and the excess α-band power. Note that Fig. 5.4 is the periodogram of a simulated EEG time series, in contrast to Fig. 5.5 which

shows the direct simulation of an EEG periodogram, with no underlying time series.
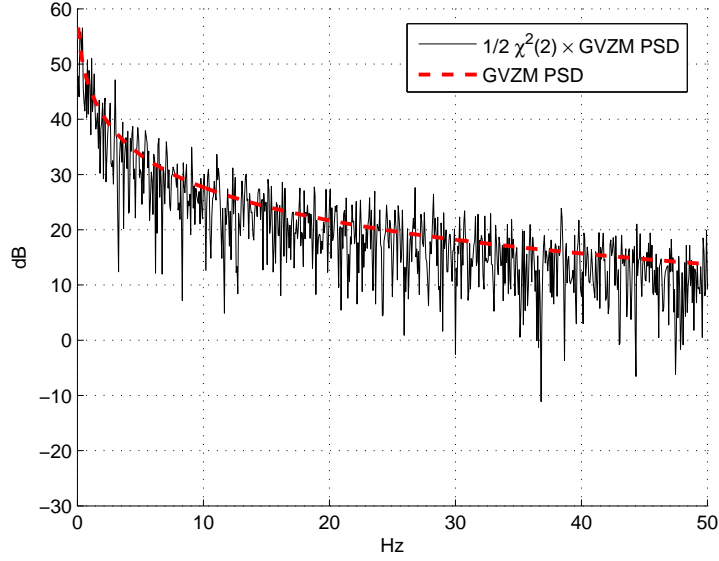
Figure 5.5: $\text{GVZM}\left(\theta\right) \cdot \left(1/2\right)\chi^2\left(2\right)$ simulated EEG periodogram using the parameters derived from the Fig. 5.1 data.

We choose some $0 \leqslant k \leqslant K - 1$ and let $\upsilon = \upsilon_1 + k\Delta\upsilon$ in (5.11). For small Δt, we find $a_k = 1 - \Delta t/\upsilon$ and $b_k = \sqrt{2\Delta t/\upsilon}$, where we have ignored terms of order higher than Δt. Defining $\Delta x_k\left(n\right) \overset{\text{def}}{=} x_k\left(n\right) - x_k\left(n - 1\right)$, we easily calculate

$$\frac{\Delta x_k\left(n\right)}{\Delta t} + \frac{1}{\upsilon} \cdot x_k\left(n - 1\right) = \sqrt{\frac{2P_0}{\upsilon\Delta t}} \cdot \varepsilon_k\left(n\right). \tag{5.13}$$

Let $y_k\left(n\right) \overset{\text{def}}{=} w_k \cdot x_k\left(n\right)$. Using the definition of w_k in (5.11), (5.13) becomes

$$\frac{\Delta y_k\left(n\right)}{\Delta t} + \frac{1}{\upsilon} \cdot y_k\left(n - 1\right) = \sqrt{\frac{2P_0}{\upsilon \cdot \upsilon^{2-\theta}}\Delta\upsilon} \cdot \varepsilon_k\left(n\right).$$

Now suppose the values $\varepsilon_k\left(n\right)$ are samples $\varepsilon_k\left(n\Delta t\right)$ of a continuous-time, iid $N\left(0, 1\right)$ process $\varepsilon_k\left(t\right)$. Then, as $\Delta t \to 0$, $y_k\left(n\right)$ will approach a continuous-time, stationary, Gaussian AR process $y_k\left(t\right)$ satisfying the stochastic differential equation

$$\frac{dy_k}{dt} + \frac{1}{\upsilon} \cdot y_k\left(t\right) = \sqrt{\frac{2P_0}{\upsilon \cdot \upsilon^{2-\theta}}\Delta\upsilon} \cdot \varepsilon_k\left(t\right). \tag{5.14}$$

71

It is well-known [38] that the autocovariance function of $y_k(t)$ satisfying (5.14) is

$$R_k(\tau) = P_0 \frac{1}{v^{2-\theta}} e^{-|\tau|/v} \Delta v.$$

Using (5.12), suppose the values $\varsigma_s(n)$ are also samples $\varsigma_s(n\Delta t)$ of a continuous-time, iid $N(0,1)$ process $\varsigma_s(t)$ which is independent of all the $\varepsilon_k(t)$'s. Then the AR-GVZM, processes $x_K(n)$ in (5.12) will approach a continuous-time, stationary, Gaussian, mixed AR process with autocovariance function

$$R_K(\tau) = P_0 \sum_{k=0}^{K-1} \frac{1}{v^{2-\theta}} e^{-|\tau|/v} \Delta v + P_s \cdot \delta(t).$$

Therefore, as $K \to \infty$, the $x_K(t)$'s themselves will approach a Gaussian process $x_*(t)$ with autocovariance

$$R_*(\tau) = P_0 \int_{v_1}^{v_2} \frac{1}{v^{2-\theta}} e^{-|\tau|/v} dv + P_s \cdot \delta(\tau). \tag{5.15}$$

It is now easy to check that the PSD function of $x_*(t)$, which is the Fourier transform of $R_*(\tau)$ [16], is given precisely by the formula of Eq. (5.9); i.e., the GVZM PSD function.

This is a significant result since zero-mean, Gaussian processes are uniquely defined by their autocovariance [56]. Noting that the GVZM periodogram model implies the autocovariance must be given by (5.15), if we make the additional assumption that a particular EEG noise time series $x_{\mathrm{EEG}}(t)$ is zero-mean and Gaussian, then we **must** have $x_{\mathrm{EEG}}(t) \sim x_*(t)$. Hence AR-GVZM, simulations can be made to approximate EEG background noise with arbitrary precision by means of the double limiting process $\Delta t, \Delta v \to 0$ described above.

Note also that the converse can be proven using methods of [56]; i.e., if the EEG noise process $x_{\mathrm{EEG}}(t)$ is given by limits of AR-GVZM processes, then $x_{\mathrm{EEG}}(t)$ is zero-mean, Gaussian, and the GVZM periodogram model must apply to it. This is important for practical applications because it defines the correct statistical model of the periodogram when AR-GVZM approximations are used to simulate EEG noise.

.

Definition 22. Let $x(n)$, $0 \leqslant n \leqslant N-1$ be samples[5], at sample rate f_{samp}, of an actual or virtual EEG electrode of a naturally-occuring ensemble of brain background noise processes, of a single subject, over a time interval short enough for $x(n)$ to be considered stationary. Then the **GVZM noise model** of the periodogram values $S_x(k)$, $0 \leqslant k \leqslant N-1$ is the random process

$$S_x(k) = S_{\mathrm{GVZM}}(k\Delta f) \cdot (1/2)\,\Xi(k), \tag{5.16}$$

where $\Xi(k)$ is a sequence of $\chi^2(2)$ distributed [93] random variables, such that $\Xi(k), \Xi(l)$ are independent for $0 \leqslant k, l < N/2$ when $k \neq l$, $\Delta f \stackrel{\mathrm{def}}{=} f_{\mathrm{samp}}/N$, and $S_{\mathrm{GVZM}}(f)$ is an appropriate GVZM PSD defined by (5.9).

Note that the reason for the restriction of independence to $0 \leqslant k, l < N/2$ is that $S_x(N-k) = S_x(k)$ since $x(\cdot)$ is real. Also note that the half-interval definition $0 \leqslant k, l < N/2$ applies whether N is even or odd.

We can write (5.16) informally as

$$S_x(k) \sim S_{\mathrm{GVZM}}(k\Delta f) \cdot (1/2)\,\chi^2(2),$$

where $\sim$ denotes "is distributed as."

The $(1/2)\,\chi^2(2)$ periodogram distribution holds exactly for special processes such as N-periodic ARMA defined in Appendix F. When conditions for the Central Limit Theorem hold, the $(1/2)\,\chi^2(2)$ distribution holds asymptotically as the data length $N \to \infty$ [56]. Both N-periodic ARMA and the large-N approximations are appropriate for EEG noise.

---

[5]Portions of this section have appeared in [2]

Note that Eq. (5.16) implies that the expected value $\mathsf{E}\left[S_x\left(k\right)\right]$ is equal to $S_{\text{GVZM}}\left(k\Delta f\right)$. The previous paragraph implies that the converse holds asymptotically; i.e., if $\mathsf{E}\left[S_x\left(k\right)\right] = S_{\text{GVZM}}\left(k\Delta f\right)$, then $S_x\left(k\right)$ converges uniformly in distribution to $S_{\text{GVZM}}\left(k\Delta f\right) \cdot (1/2)\,\Xi\left(k\right)$ as $N \to \infty$ (cf. [56], Chapter 10 for details).

Def. 22 is consistent with the single-epoch approach of [56, 92] but multi-epoch averages of such single-epoch spectra can be used as well. Our methods will apply to such general periodograms merely by replacing "$\chi^2\left(2\right)$" with "$1/M\ \chi^2\left(2M\right)$," where M is the number of (statistically independent) epochs.

Fig. 5.1 should be compared to Fig. 5.5 which shows a **simulated** periodogram based on the fitted GVZM PSD function and (5.16); that is, samples of an independent and identically distributed (iid) $\chi^2\left(2\right)$ pseudo–random process $\Xi\left(k\right)$, for $0 \leqslant k < N/2$, were generated and each sample was multiplied by the factor $(1/2) \cdot S_{\text{GVZM}}\left(k\Delta f\right)$. The results were then plotted against frequency on a log-linear scale. Clearly the simulated periodogram has the same general visual characterstics as the recorded periodogram.

CHAPTER 6: METRICS FOR SSVEP ALGORITHM COMPARISONS
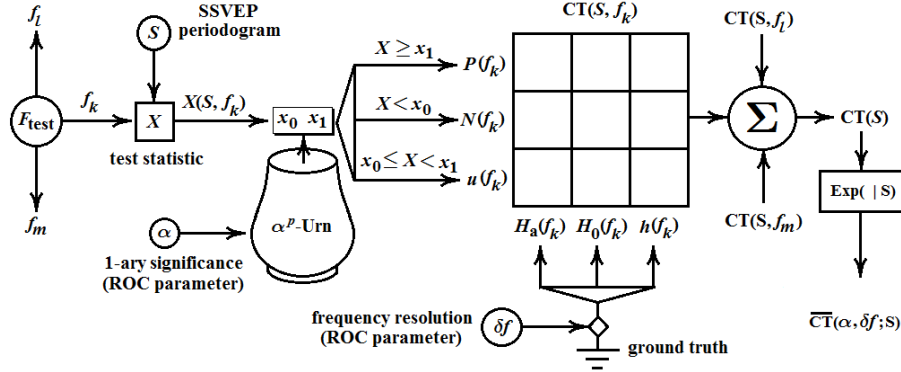
Figure 6.1: Flow chart for the calculation of $\overline{\mathrm{CT}}\left(\alpha, \Delta f; S\right)$: the minimum variance, unbiased, single-trial estimator of the 3×3 contingency table of the input periodogram S, with ROC control parameters $\alpha, \Delta f$.

This chapter[1] presents an innovative, statististically sound, and extremely flexible methodology developed specifically for the comparison and validation of SSVEP algorithms. It forms the foundation for the single-trial **receiver operating characteristics (ROC) graphs** of Fig. 7.3 and Fig. 7.6 and the summary statistics of Table 7.1 and Table 7.2.

See Fig. 6.1 for a flow chart of the protocol.

6.1 SSVEP Estimation Protocol

Let $\mathbf{S}\left(\tau\right)$ be the signal from a randomly-selected instance τ of an SSVEP experiment. We refer to τ as a "trial." The signal may be the actual raw EEG time series, a processed EEG spectrum, or even an arbitrary index into a table of signal exemplars. What is important is that $\mathbf{S}\left(\tau\right)$ must be an **observable** random variable of the **unobservable** trial instance τ which ranges over the underlying probability space $(\mathrm{T}, \mathrm{Prob})$ of the experiment. That is, each trial $\tau \in \mathrm{T}$, whose occurrences governed by the probability measure [128] $\mathrm{Prob}\left[\,\cdot\,\right]$, encapsulates all the uncertainties of the SSVEP experiment:

---

[1]Portions of this chapter have appeared in [2].

- Variations between subjects chosen at random.

- Variations within the same subject on different days, different times of the same day, or different moods.

- Impedence variations caused by non-uniform application of electrode gel.

- Artifacts.

- Stray electromagnetic fields.

- The particular stimulus frequencies used for this trial.

- The stimulus frequency to which the subject attends as well as the time interval of attention.

- The dice-rolls or coin-tosses we may use for randomized decision rules.

- The vast number of other unnamed lurking variables in any SSVEP/EEG experiment.

Let $F_{\text{ssvep}}(\tau)$ be the (random) set of **stimulus frequencies** we are trying to estimate from $\mathbf{S}(\tau)$ during trial τ. Note that $F_{\text{ssvep}}(\tau)$ should include all possible fundamental stimulus frequencies which were flashing when $\mathbf{S}(\tau)$ was observed. It may also include some harmonics and subharmonics [9] of these fundamental SSVEP frequencies.

Let $F_{\text{test}\star}$ be an initial set of **test frequencies**. When given any single-trial signal $\mathbf{S}$, our estimation protocol is to succesively test every $f \in F_{\text{test}\star}$ for its presence or absence in $F_{\text{ssvep}}(\tau)$. Thus we are performing **frequency estimation by *m*-ary testing** [127], where *m* is the size of $F_{\text{test}\star}$. A given testing procedure may or may not have access to $F_{\text{ssvep}}(\tau)$; that is, it may or may not be **blind**.

An essential aspect of SSVEP estimation, especially for BCI applications, is that every trial partitions $F_{\text{test}\star}$ into three subsets:

1. Those f satisfying $f \in F_{\text{test}\star} \cap F_{\text{ssvep}}(\tau)$.

2. Those $f \in F_{\text{test}\star} \setminus F_{\text{ssvep}}(\tau)$ which thus were not present during this trial but **might have been**. These could be, for example, frequencies of non-selected fields during a BCI test.

3. All other $f \in F_{\text{test}\star}$.

In typical blind SSVEP frequency estimation, case (3) vastly outnumbers (1) and (2). For example, the data used in Chap. 7 contained 614 initial test frequencies while there were only 19 possible distinct stimulus frequencies and harmonics. In such a situation, simple m-ary control procedures such as Bonferroni correction (see [129] for a survey) are out of the question because they yield impractically small corrected significance levels. Even less conservative procedures such as those used to control the false discovery rate (FDR) [130] yield overall significance levels which often produce no discoveries at all. This because the signal-to-noise ratio of SSVEP signals is usually too low for estimation statistics to yield sufficiently small P-values even at fundamental stimulus frequencies.

Moreover, non-stimulus frequencies that we particularly want to reject may slip into the signal, the most important example being the frequencies of non-selected but still visible fields during BCI experiments. The assessment of any algorithm must test its ability to positively exclude these potential contaminants even when blind.

It is therefore essential to develop estimation and validation procedures which can distinguish the combined situation $(1) \cup (2)$ from (3).

A solution to all the problems of the preceeding paragraphs is to assume a second randomly-varying set $F_{\text{null}}(\tau)$ of **null frequencies** such that $F_{\text{null}}(\tau) \cap F_{\text{ssvep}}(\tau) = \emptyset$. Once the signal $\mathbf{S}(\tau)$ is observed, the hypotheses we decide at each test frequency $f \in F_{\text{test}\star}$ are

$\mathrm{H}_0(f)$: $f \in F_{\text{null}}(\tau)$

$\mathrm{H}_{\text{alt}}(f)$: $f \in F_{\text{ssvep}}(\tau)$

but we **do not assume** that the testing procedure always makes a decision between $\mathrm{H}_0(f)$ and $\mathrm{H}_{\text{alt}}(f)$; that

is, we must allow **undetermined** as a possibility.

We require a **ground truth frequency estimation algorithm** for SSVEP experiments as a baseline. This may be:

- A look-up table from a laboratory notebook.

- An electronic spectral analyzer or oscilloscope.

- Gold-standard spectral estimation software.

- A synthetic ground truth algorithm which simulates real SSVEP results. This can be used for validating a new algorithm. It is the ground truth used to produce the tables and figures of Chap. 7.

The ground truth may or may not be blind. We want to measure the performance of a **comparison algorithm** (which is usually assumed to be blind) against this ground truth.

Both the ground truth and comparison algorithms may involve randomized decision rules [127]. However we make the assumption that the randomization procedures of the two algorithms are **independent given S**. That is, once the signal outcome $\mathbf{S} = \mathbf{S}(\tau)$ is known, whatever τ-dependent dice-rolls or coin-tosses each uses to make its decisions about $\mathrm{H}_0(f)$ and $\mathrm{H}_{\mathrm{alt}}(f)$ are statistically independent of one another. We also assume that any randomized rules of each individual algorithm are independent at distinct test frequencies, given $\mathbf{S}$. (This latter assumption actually excludes some interesting potential algorithms but is required for the calculation of the parametrized contingency tables discussed below. However it is sufficiently general to hold for most practical algorithms including those from Chap. 7.)

6.2 Example: Synthetic SSVEP Algorithms

$$\begin{cases} \mathrm{P_{ssvep}}\,[f \mid \mathrm{S}] = \mathrm{p_{ssvep}}\,(f) \cdot \mathrm{s}\,(f) \\ \mathrm{P_{null}}\,[f \mid \mathrm{S}] \;\; = \mathrm{p_{null}}\,(f) \cdot \mathrm{s}\,(f)\,, \end{cases}$$

where, for all f,

$$\begin{cases} \mathrm{p_{ssvep}}\,(f) \geqslant 0 \\ \mathrm{p_{null}}\,(f) \geqslant 0 \\ \mathrm{p_{ssvep}}\,(f) + \mathrm{p_{null}}\,(f) \leqslant 1 \\ \mathrm{s}\,(f) \overset{\mathrm{def}}{=} \mathrm{S}\,(f) \; / \; \underset{g}{\max}\,\mathrm{S}\,(g)\,. \end{cases}$$

6.3 The Contingency Table Statistic

Since we do not assume that the algorithm always determines the truth values of the two hypotheses, there are 9 possible outcomes for a test at $f \in F_{\mathrm{test}\star}$. The full 3×3 contingency table at f is defined by Table 6.1:

Table 6.1

The 3×3 contingency table at each test frequency f showing the primary indicator terms and the null hypothesis bias $\mathrm{b_0}$. (©2016 IEEE)

Ground Truth

		$\mathbf{H_{alt}}$ **True**	$\mathbf{H_0}$ **True**	$1 - \mathrm{b_0}$	$\mathrm{b_0}$	
				$\mathbf{H_\star}$ **(undetermined)**	
	Accept $\mathbf{H_{alt}}$ (Positive)	$\mathrm{TP_\star}\,(f)$	$\mathrm{FP_\star}\,(f)$	$\mathrm{tP}\,(f)$	$\mathrm{fP}\,(f)$	$\mathbf{P_\star}\,(f)$
Comparison Algorithm	**Accept** $\mathbf{H_0}$ (Negative)	$\mathrm{FN_\star}\,(f)$	$\mathrm{TN_\star}\,(f)$	$\mathrm{fN}\,(f)$	$\mathrm{tN}\,(f)$	$\mathbf{N_\star}\,(f)$
	Accept $\star$ (Neither)	$\mathrm{Fn}\,(f)$	$\mathrm{Fp}\,(f)$			
		$\mathbf{m_{alt\star}}\,(f)$	$\mathbf{m_{0\star}}\,(f)$			$\mathbf{m}\,(f)$

The 4 core cells are $0, 1$-valued indicator functions given by:

$$
\begin{cases}
\mathrm{TP}_\star(f) = \mathbf{I}_\mathrm{P}(f) \cdot \mathbf{I}_\mathrm{alt}(f) \\[4pt]
\mathrm{FP}_\star(f) = \mathbf{I}_\mathrm{P}(f) \cdot \mathbf{I}_0(f) \\[4pt]
\mathrm{FN}_\star(f) = \mathbf{I}_\mathrm{N}(f) \cdot \mathbf{I}_\mathrm{alt}(f) \\[4pt]
\mathrm{TN}_\star(f) = \mathbf{I}_\mathrm{N}(f) \cdot \mathbf{I}_0(f),
\end{cases}
\tag{6.1}
$$

where $\mathbf{I}_\mathrm{P}(f)$, $\mathbf{I}_\mathrm{N}(f)$ are the indicators for accepting $\mathrm{H}_\mathrm{alt}(f)$, $\mathrm{H}_0(f)$ and $\mathbf{I}_\mathrm{alt}(f)$, $\mathbf{I}_0(f)$ are the indicators for ground truth.

The remaining labeled cells are fractional indicators whose values are in the interval $[0, 1]$. They are used to compress the 3×3 table into a 2×2 table by allocating the indeterminate cells as described below:

If no decision was reached by the comparison algorithm on a test frequency but its ground truth was determinable then we should regard that test as false. The logic is that sufficient information was available to the ground truth procedure but the comparison algorithm failed to extract it. These are the cells labeled $\mathrm{Fn}(f)$ and $\mathrm{Fp}(f)$ in Table 6.1.

If both the comparison and the ground truth algorithms were unable to determine the status of a frequency, then it should be excluded from both the initial set $F_{\mathrm{test}\star}$ of test frequencies and any further analysis since neither algorithm is able to make any definitive statement about it. This is the blank cell in Table 6.1. The resulting set of frequencies, at which at least one algorithm was determined, is denoted F_{test}. In practice, F_{test} is usually much smaller than than $F_{\mathrm{test}\star}$. For example, in Sec. 7.3, the 614 initial test frequencies are usually reduced to a few 10's. This balances the contingency counts, eliminating most of the problems discussed above in regards to Bonferroni and the FDR.

The ambiguous situation is that in which the comparison algorithm arrived at a decision but no ground truth was available. We resolve this ambiguity by selecting a **null hypothesis bias** b_0, $0 \leqslant b_0 \leqslant 1$, which specifies how much the protocol favors H_0 when ground truth is unknown. Using a legal metaphor, $b_0 = 1$ means that uncertain evidence always favors the defendant while $b_0 = 0$ means evidence of uncertain merit

is nevertheless considered incriminating. This allows the unambigous assigment of the $H_\star$ cells as follows:

$$\begin{cases} \text{tP}(f) = (1 - b_0) \cdot \mathbf{H}_\star \mathbf{P}(f) \\ \text{fP}(f) = b_0 \cdot \mathbf{H}_\star \mathbf{P}(f) \\ \text{tN}(f) = (1 - b_0) \cdot \mathbf{H}_\star \mathbf{N}(f) \\ \text{fN}(f) = b_0 \cdot \mathbf{H}_\star \mathbf{N}(f), \end{cases} \tag{6.2}$$

where $\mathbf{H}_\star \mathbf{P}(f)$, $\mathbf{H}_\star \mathbf{N}(f)$ are the indicators for positive and negative decisions respectively under the condition that the ground truth for the test frequency f is undetermined:

$$\begin{cases} \mathbf{H}_\star \mathbf{P}(f) = \mathbf{I}_\mathrm{P}(f) \cdot \mathbf{I}_{\mathrm{H}\star}(f) \\ \mathbf{H}_\star \mathbf{N}(f) = \mathbf{I}_\mathrm{P}(f) \cdot \mathbf{I}_{\mathrm{H}\star}(f). \end{cases} \tag{6.3}$$

Note that these are typically fractional indicators.

The marginal cells $\mathrm{P}_\star(f)$, $\mathrm{N}_\star(f)$, $\mathrm{m}_{\mathrm{alt}\star}(f)$, $\mathrm{m}_{0\star}(f)$, and $\mathrm{m}(f)$ are the sums of the associated columns and rows.

The derived 2×2 table now is given by Table 6.2 with cells

$$\begin{cases} \text{TP}(f) = \text{TP}_\star(f) + \text{tP}(f) \\ \text{FP}(f) = \text{FP}_\star(f) + \text{fP}(f) + \text{Fp}(f) \\ \text{FN}(f) = \text{FN}_\star(f) + \text{Fn}(f) + \text{fN}(f) \\ \text{TN}(f) = \text{TN}_\star(f) + \text{tN}(f) \end{cases} \tag{6.4}$$

and marginals as shown.

Definition 23. The (unparameterized) **contingency table statistic** is defined to be

$$\mathbf{CT}(\tau) \overset{\text{def}}{=} \sum_{f \in F_{\text{test}}} \mathbf{CT}(\tau, f),$$

Table 6.2

The derived 2×2 minimum variance, unbiased, single-trial contingency table. (©2016 IEEE)

Ground Truth

		$\mathbf{H}_{\text{alt}}$ **True**	$\mathbf{H_0}$ **True**	
	Accept $\mathbf{H}_{\text{alt}}$ (Positive)	$\overline{\text{TP}}$	$\overline{\text{FP}}$	$\overline{\mathbf{P}}$
Comparison Algorithm	**Accept $\mathbf{H_0}$** (Negative)	$\overline{\text{FN}}$	$\overline{\text{TN}}$	$\overline{\mathbf{N}}$
		$\overline{\mathbf{m}}_{\text{a}}$	$\overline{\mathbf{m}_{\mathbf{0}}}$	$\overline{\mathbf{m}}$

where $\mathbf{CT}\left(\tau, f\right)$ denotes the derived 2×2 table at f given by Table 6.2 when processing signal $\mathbf{S}\left(\tau\right)$.

Note that because we have allowed randomized decision rules, $\mathbf{CT}\left(\tau\right)$ is actually a multi-dimensional random variable, not merely a function of $\mathbf{S}\left(\tau\right)$. It is this statistic which we use to make inferences about the the relative performance of a comparison algorithm to ground truth.

The algorithms we consider are usually parameterized by a significance level α as the basis for comparison to the *P*-value, computed at each $f \in F_{\text{test}}$, of some spectral statistic (but see the following section which analyzes this process in detail). Examples include the SNR (Sec. 7.3) or the Liavas, et al. spectral *F*-ratio (Sec. 7.4), with or without the GVZM baseline.

It is also extremely helpful to be able to parameterize the frequency precision of each algorithm's decisions. Let $\Delta_F > 0$ be a frequency radius in Hz. Define the **parameterized hypotheses** at $f \in F_{\text{test}}$ to be

$\text{H}_0\left(\alpha, \Delta_F; f\right)$: $\quad \left(\forall g\right)\left[|g - f| < \Delta_F \text{ implies } g \in F_{\text{null}}\left(\tau\right)\right]$

$\text{H}_{\text{alt}}\left(\alpha, \Delta_F; f\right)$: $\left(\exists g\right)\left[|g - f| < \Delta_F \text{ and } g \in F_{\text{stim}}\left(\tau\right)\right]$,

where the membership of g is determined at significance level α.

Definition 24. The (parameterized) **contingency table statistic** is defined to be

$$\mathbf{CT}\left(\alpha, \Delta_F; \tau\right) \overset{\text{def}}{=} \sum_{f \in F_{\text{test}}} \mathbf{CT}\left(\alpha, \Delta_F; \tau, f\right),$$

where the table at f is determined by testing $\mathrm{H}_0\left(\alpha, \Delta_F; f\right)$ against $\mathrm{H}_{\text{alt}}\left(\alpha, \Delta_F; f\right)$.

Again, $\mathbf{CT}\left(\alpha, \Delta_F; \tau\right)$ is a multi-dimensional random variable. The parameters α, Δ_F can be systematically varied to examine the relative performance of the comparison algorithm at various **operating points** [131].

6.4   Whitening by (β, α)-Urn Testing

Let $\mathbf{X}\left(\mathbf{S}, \tau, f\right)$ be whatever numerical measure is extracted by the comparison algorithm from the signal $\mathbf{S} = \mathbf{S}\left(\tau\right)$ at frequency $f \in F_{\text{test}}$ during trial $\tau \in \mathbf{T}$ whose P-values determine the truth of the hypotheses. For example, $\mathbf{X}\left(\mathbf{S}, \tau, f\right)$ could be the SNR of Sec. 7.3 or the F-test ratio of Sec. 7.4. Regard $\mathbf{X}$ as a sequence $\{\mathbf{X}\left(\mathbf{S}\left(\cdot\right), \cdot, f\right) \mid f \in F_{\text{test}}\}$ of random variables on the trial space $\left(\mathbf{T}, P\right)$. We consider the issues of independence and identical distribution (iid).

It often makes sense to assume $\mathbf{X}\left(f\right)$ and $\mathbf{X}\left(g\right)$ are independent for $f \neq g$. For example, the GVZM model of the background EEG periodogram (Sec. 5.2.7) includes this as an hypothesis. In other cases, it may make more sense to assume some dependency among distinct test frequencies such as frequencies which are harmonically related.

However, the typical spectral measures used by estimators are almost never identically distributed between distinct frequencies unless special processing takes place. Even the GVZM model, which assumes a $(1/2) \cdot \chi^2\left(2\right)$-shaped distribution at each f, nevertheless requires frequency-dependent means. This makes good sense for the human brain: we cannot expect naive spectral-based measures of EEG power to be the same in the α-band, for instance, as in the γ-band.

Yet there is considerable conceptual, algorithmic, and even graphical advantage to "whitening" $\mathbf{X}\left(f\right)$ across

the test frequencies; that is, deriving a new process $\{\mathbf{U_X}(f) \mid f \in F_{\text{test}}\}$ which contains the same statistical information as $\mathbf{X}$ but for which all $\mathbf{U_X}(f)$ have identical, or at least very similar, distributions.

This section presents a whitening methodology which our empirical work has shown is very appropriate for SSVEP data.

For every $f \in F_{\text{test}}$, let $Q_{\mathbf{X}}(x, f)$ be the cumulative distribution function (cdf) of $\mathbf{X}(f)$; that is

$$Q_{\mathbf{X}}(x, f) = \mathsf{Prob}\left[\tau \in \mathbf{T} \mid \mathbf{X}(\mathbf{S}(\tau), \tau, f) \leqslant x\right]$$
$$\stackrel{\text{def}}{=} \mathsf{Prob}\left[\mathbf{X}(f) \leqslant x\right].$$

and let $P_{\mathbf{X}}(x, f) \stackrel{\text{def}}{=} 1 - Q_{\mathbf{X}}(x, f)$ be the complementary cdf; i.e., the **P-value function** of $\mathbf{X}$;

Definition 25. The **likelihood function** derived from $\mathbf{X}$, with significance $0 \leqslant \beta \leqslant \alpha \leqslant 1$, is the conditional probability

$$L_{\mathbf{X}}(\beta, \alpha; x, f) \stackrel{\text{def}}{=}$$
$$\mathsf{Prob}\left[\mathbf{X}(f) \leqslant x \mid \beta < P_{\mathbf{X}}(\mathbf{X}, f) \leqslant \alpha\right]. \tag{6.5}$$

For any P-value-based algorithm, one can think of $L_{\mathbf{X}}(\beta, \alpha; x, f)$ as the likelihood that the alternative hypothesis $\mathrm{H_{alt}}(f)$ is true, given that $\mathbf{X}(f) = x$ and that P-value of $\mathbf{X}(f)$ lies in the interval $(\beta, \alpha]$.

Supressing the argument f we can prove:

Lemma 3.

$$L_{\mathbf{X}}(\beta, \alpha; x) = \begin{cases} 0 & \text{if } x < P_{\mathbf{X}}^{-1}(\alpha) \\ 1 & \text{if } x \geqslant P_{\mathbf{X}}^{-1}(\beta) \\ \frac{\alpha_+ - P_{\mathbf{X}}(x)}{\alpha_+ - \beta_+} & \text{otherwise,} \end{cases}$$

where, for any $0 \leqslant \gamma \leqslant 1$,

$$\begin{cases} P_{\mathbf{X}}^{-1}(\gamma) \stackrel{\text{def}}{=} \inf\{x \mid P_{\mathbf{X}}(x) \leqslant \gamma\} \\ \gamma_+ \stackrel{\text{def}}{=} \inf\{P_{\mathbf{X}}(x) \mid P_{\mathbf{X}}(x) > \gamma\}. \end{cases}$$

84

This formula is very easy to calculate or estimate, even for cdf's found empirically.

Remark 28. Note that we have not excluded the possibility that $\beta = \alpha$ in (6.5), in which case the restricted probability space is empty. This is necessary to insure $L_{\mathbf{X}}(\beta, \alpha; x, f) \to 1$ as $\alpha \to 1$, thus guaranteeing the almost-surely-truth of $\mathrm{H}_{\mathrm{alt}}(f)$ in this boundary case (see Def. 27 below). By choosing a fixed functional relation such as $\beta = \alpha^p$, for some $p > 1$, the boundary conditions are attained smoothly. Our empirical work has shown $p \approx 3$ to be a reasonable choice for SSVEP BCIs.

Definition 26. The **uniformizing statistic** derived from $\mathbf{X}$, with parameters $0 \leqslant \beta \leqslant \alpha \leqslant 1$, is the random variable

$$\mathbf{U}_{\mathbf{X}}(\beta, \alpha; f) \overset{\text{def}}{=} L_{\mathbf{X}}(\beta, \alpha; \mathbf{X}(f), f), \tag{6.6}$$

where the dependence on the random trial $\tau \in \mathbf{T}$ is implicit.

Clearly every $\mathbf{U}_{\mathbf{X}}(\beta, \alpha; f)$ satisfies $0 \leqslant \mathbf{U}_{\mathbf{X}} \leqslant 1$. It somewhat surprising that, in fact, $\mathbf{U}_{\mathbf{X}}(\beta, \alpha; f)$ is "almost" uniformly distributed at every $f \in F_{\text{test}}$ for which we know $0 < \mathbf{U}_{\mathbf{X}}(\beta, \alpha; f) < 1$. The divergence from $\mathbf{U}_{\mathbf{X}} \sim \text{unif}(0, 1)$ occur at the jump discontinuities of $Q_{\mathbf{X}}(x, f)$ since $\mathbf{U}_{\mathbf{X}}(\beta, \alpha; f)$ cannot take on the probability values over which $Q_{\mathbf{X}}$ jumps. The cdf of $\mathbf{U}_{\mathbf{X}}(\beta, \alpha; f)$ is flat over these intervals. But if $\mathbf{X}(f)$ has a continuous cdf, then $\mathbf{U}_{\mathbf{X}} \sim \text{unif}(0, 1)$ precisely (given that $\mathbf{U}_{\mathbf{X}} \neq 0, 1$); in particular this holds for the GVZM model Sec. 5.2.7 and asymptotically for periodograms of white Gaussian noise [56]. In practice, we have found it an excellent approximation even for empirically-estimated cdf's which are necessarily discontinous.

$\mathbf{U}_{\mathbf{X}}$ is our whitened statistic. Not least of its merits is that its values at the test frequencies can be plotted on the same axes so that direct comparisons of frequency-to-frequency variations in $\mathbf{X}(f)$ are easily detected by eye.

Definition 27. The (β, α)-**Urn Test** are the decision rules:

$$
\begin{cases}
\text{Accept } H_0 & \text{if } \mathbf{U_X}\,(\beta, \alpha; f) = 0 \\[2mm]
\text{Accept } H_{\text{alt}} & \text{if } \mathbf{U_X}\,(\beta, \alpha; f) = 1 \\[2mm]
\text{Undetermined} & \text{otherwise.}
\end{cases}
$$

All of the SSVEP procedures of Chap. 7, including models of ground truth, can be recast in this uniformized, whitened form. Furthermore, such procedures can be parameterized by frequency resolution Δ_F as defined by Def. 28.

When β is a function of α as discussed in Remark 28, we can vary α, Δ_F independently over some intervals to obtain random, single-trial contingency tables $\mathbf{CT}\,(\alpha, \Delta_F)$ at different operating points. As will be seen, each such pair (α, Δ_F) will yield one point on our optimal, single-trial ROC graphs.

Remark 29. The terminology "(β, α)-urn test" derives from the following randomized decision procedure which can be shown to yield the same overall statistics as the $\mathbf{U_X}$-test Def. 27 (although individual outcomes may differ):

A (β, α)-**urn for** $\mathbf{X}\,(f)$ consists of a conceptual jar containing slips of paper, on each of which is written a pair (x_0, x_{alt}) of values from the range of $\mathbf{X}\,(f)$. Specifically, the pairs must satisfy $x_0 \leqslant x_{\text{alt}}$ and both $\beta < P_{\mathbf{X}}\,(x_0) \leqslant \alpha$ and $\beta < P_{\mathbf{X}}\,(x_{\text{alt}}) \leqslant \alpha$.

Moreover, the slips must be distributed precisely as would be pairs of actual $\mathbf{X}\,(f)$'s. Specifically,

$$
\text{Prob}\left[(x_0, x_{\text{alt}}) \mid y \leqslant x_0 \text{ and } x_{\text{alt}} < x\right] =
$$
$$
\frac{P_{\mathbf{X}}\,(y, f)_+ - P_{\mathbf{X}}\,(x, f)_+}{\alpha_+ - \beta_+}
$$

and must be statistically independent of $\mathbf{X}\,(f)$.

Letting $\mathbf{X}\,(f)$ be an actual value of the test statistic the decision rule is:

Randomly choose a slip (x_0, x_{alt}) from the (β, α)-urn and then

$$\begin{cases} \text{Accept H}_0 & \text{if } \mathbf{X}(f) < x_0 \\[2mm] \text{Accept H}_{\text{alt}} & \text{if } \mathbf{X}(f) \geqslant x_{\text{alt}} \\[2mm] \text{Undetermined} & \text{otherwise.} \end{cases}$$

6.5   The Optimal Estimator Metric

The contingency table statistic $\mathbf{CT}(\tau)$ is a function of the unobservable value $\tau \in \mathrm{T}$ and is thus a purely theoretical construct. By assumption, all we are able to observe is the signal $\mathbf{S}(\tau)$ which contains far less information than the actual trial τ. The best we can do is **estimate $\mathbf{CT}(\tau)$** based on knowledge of $\mathbf{S}(\tau)$. This problem has a well-known solution; namely the **regression** of $\mathbf{CT}(\tau)$ onto $\mathbf{S}(\tau)$:

Definition 28. Define the function $\overline{\mathbf{CT}}(s)$ on the set of all possible signals by the conditional expected value

$$\overline{\mathbf{CT}}(s) \overset{\text{def}}{=} \mathsf{E}\left[\mathbf{CT} \mid \mathbf{S} = s\right].$$

Then $\overline{\mathbf{CT}}(s)$ is known to be the minimum mean-squared-error (MSE), unbiased estimator of $\mathbf{CT}(\tau)$ from $\mathbf{S}(\tau)$ [93]; that is, the composite random variable $\overline{\mathbf{CT}}(\mathbf{S}(\tau))$ satisfies $\mathsf{E}\left[\overline{\mathbf{CT}}(\mathbf{S}(\tau))\right] = \mathsf{E}\left[\mathbf{CT}(\tau)\right]$ and has the smallest MSE of any unbiased estimate of the form $K(\mathbf{S}(\tau))$, for functions $K(s)$ over the space of signals.

For this reason, we regard the estimated contingency table $\overline{\mathbf{CT}}(\mathbf{S})$ as the best metric of performance of a comparison algorithm against ground truth when we know the input signal $\mathbf{S}$.

To calculate the estimate $\overline{\mathbf{CT}}(\mathbf{S})$ we note that all the formulas in (6.4) reduce to sums of products of pairs of indicator functions. Using the independence assumptions of the protocol, this will allow the optimal estimator function $\mathsf{E}\left[\mathbf{CT} \mid \mathbf{S} = s\right]$ to push through all formulas of (6.4), **turning indicators into probabilities**. We will do a typical calculation where we supress most occurences of the signal portion " $\mid \mathbf{S}$" for

simplicity:

$$E\left[\mathrm{FP}\left(f\right)\right] = E\left[\mathrm{FP}_\star\left(f\right)\right] + E\left[\mathrm{fP}\left(f\right)\right] + E\left[\mathrm{Fp}\left(f\right)\right].$$

$$E\left[\mathrm{FP}_\star\left(f\right)\right] = E\left[\mathbf{I}_\mathrm{P}\left(f\right) \cdot \mathbf{I}_0\left(f\right) \mid \mathbf{S}\right]$$

$$= E\left[\mathbf{I}_\mathrm{P}\left(f\right) \mid \mathbf{S}\right] \cdot E\left[\mathbf{I}_0\left(f\right) \mid \mathbf{S}\right].$$

This critical step is the result of the assumption that the comparison algorithm and the ground truth algorithm are independent, given the signal $\mathbf{S}$.

We next note that the expected value of any indicator function is the probability of the underlying event [80] so that

$$E\left[\mathbf{I}_\mathrm{P}\left(f\right) \mid \mathbf{S}\right] = \mathrm{Prob}\left[\mathrm{P}\left(f\right) \mid \mathbf{S}\right]$$

$$E\left[\mathbf{I}_0\left(f\right) \mid \mathbf{S}\right] = \mathrm{Prob}\left[\mathrm{H}_0\left(f\right) \mid \mathbf{S}\right]$$

so that

$$E\left[\mathrm{FP}_\star\left(f\right)\right] = \mathrm{Prob}\left[\mathrm{P}\left(f\right) \mid \mathbf{S}\right] \cdot \mathrm{Prob}\left[\mathrm{H}_0\left(f\right) \mid \mathbf{S}\right].$$

In a similar way

$$E\left[\mathrm{fP}\left(f\right)\right] = \mathrm{b}_0 \cdot E\left[\mathrm{H}_\star\mathrm{P}\left(f\right)\right]$$

$$= \mathrm{b}_0 \cdot E\left[\mathbf{I}_\mathrm{P}\left(f\right) \cdot \left(1 - \mathbf{I}_0\left(f\right) - \mathbf{I}_\mathrm{alt}\left(f\right)\right)\right]$$

$$= \mathrm{b}_0 \cdot \mathrm{Prob}\left[\mathrm{P}\left(f\right) \mid \mathbf{S}\right] \cdot$$

$$\left(1 - \mathrm{Prob}\left[\mathrm{H}_0\left(f\right) \mid \mathbf{S}\right] - \mathrm{Prob}\left[\mathrm{H}_\mathrm{alt}\left(f\right) \mid \mathbf{S}\right]\right),$$

$$E\left[\mathrm{Fp}\left(f\right)\right] = E\left[\mathrm{H}_0 \star \left(f\right)\right]$$

$$= E\left[\mathbf{I}_0\left(f\right) \cdot \left(1 - \mathbf{I}_\mathrm{P}\left(f\right) - \mathbf{I}_\mathrm{N}\left(f\right)\right)\right]$$

$$= \mathrm{Prob}\left[\mathrm{H}_0\left(f\right) \mid \mathbf{S}\right] \cdot$$

$$\left(1 - \mathrm{Prob}\left[\mathrm{P}\left(f\right) \mid \mathbf{S}\right] - \mathrm{Prob}\left[\mathrm{N}\left(f\right) \mid \mathbf{S}\right]\right).$$

Therefore, from knowledge of the condtional probabilities we can obtain the optimal estimator $\overline{\mathbf{CT}}\left(f, \mathbf{S}\right)$

at each test frequency $f \in F_{\text{test}}$ and then the full estimator by simply adding these results

$$\overline{\mathbf{CT}}(\mathbf{S}) \overset{\text{def}}{=} \sum_{f \in F_{\text{test}}} \overline{\mathbf{CT}}(\mathbf{S}, f).$$

These same formulas may be combined, using standard probability arguments [80], to form the parameterized (Def. 28) estimator

$$\overline{\mathbf{CT}}(\alpha, \Delta_F; \mathbf{S}) \overset{\text{def}}{=} \mathsf{E}[\mathbf{CT}(\alpha, \Delta_F) \mid \mathbf{S}]$$

from which ROC graphs can be created.

The conditional probabilities involving the comparison algorithm such as $\mathsf{Prob}[\mathrm{P}(f) \mid \mathbf{S}]$ are known through an analysis of the behavior of the $\mathbf{X}(f)$ statistic on the signal on $\mathbf{S}$ and the (β, α)-urn test. This requires knowledge of cdf's which are found either from distributions given by formulas, such as with F ratio (7.3), or empirically derived by bootstrap resampling [132] or other procedure.

On the other hand, the ground truth probabilites such as $\mathsf{Prob}[\mathrm{H}_{\text{alt}}(f) \mid \mathbf{S}]$ are really laboratory issues and should be approached via the Bayesian formula

$$\mathsf{Prob}[\mathrm{H}_{\text{alt}}(f) \mid \mathbf{S}] = \frac{\mathsf{Prob}[\mathbf{S} \mid \mathrm{H}_{\text{alt}}(f)] \cdot \mathsf{Prob}[\mathrm{H}_{\text{alt}}(f)]}{\mathsf{Prob}[\mathrm{S}]};$$

that is, we need to know, based on our experimental protocol, the probability of a subject's being shown stimulus frequency f. More importantly, we need to estimate, based on our equipment, experience, stimulus methodology, and many other factors, what is the probability that the signal $\mathbf{S}$ will be generated when a subject is stimulated by frequency f. This latter is difficult yet interesting question [5].

For synthetic ground truth algorithms, these conditional probabilities must be modeled based on reasonable assumptions about the dependence of certain signal characteristics, such as spectral spikes in the periodogram, on SSVEP stimuli. Synthetic spectra which are sums of Gaussians translated to the stimulus frequencies work quite well.

6.6 Single-trial ROC Graphs and Derived Metrics

Let $\mathbf{S}$ be a fixed signal. Every pair (α, Δ_F) over some range of values $\alpha_{\min} \leqslant \alpha \leqslant \alpha_{\max}$ and $\Delta_{F,\min} \leqslant \Delta_F \leqslant \Delta_{F,\max}$ will yield an estimated contigency table $\overline{\mathbf{CT}}\,(\alpha, \Delta_F; \mathbf{S})$ as defined by Def. 28.

From this we can derive the single-trial rate metrics (the **operating point**):

Definition 29. The **true positive rate** (TPR) and **false positive rate** (FPR) at (α, Δ_F) are given by [131]

$$
\begin{cases}
\mathrm{TPR}\,(\alpha, \Delta_F; \mathbf{S}) \stackrel{\text{def}}{=} \dfrac{\overline{\mathrm{TP}}\,(\alpha, \Delta_F; \mathbf{S})}{\overline{\mathrm{m}}_{\mathrm{alt}}\,(\alpha, \Delta_F; \mathbf{S})} \\[3mm]
\mathrm{FPR}\,(\alpha, \Delta_F; \mathbf{S}) \stackrel{\text{def}}{=} \dfrac{\overline{\mathrm{FP}}\,(\alpha, \Delta_F; \mathbf{S})}{\overline{\mathrm{m}}_0\,(\alpha, \Delta_F; \mathbf{S})},
\end{cases}
$$

where the right-hand side factors are taken from $\overline{\mathbf{CT}}\,(\alpha, \Delta_F; \mathbf{S})$ according to the scheme in Table 6.2.

For example, every one of the 256 solid circles shows the $\mathrm{TPR}\,(\alpha, \Delta_F; \mathbf{S})$ and $\mathrm{FPR}\,(\alpha, \Delta_F; \mathbf{S})$ for 16 values $.005 \leqslant \alpha \leqslant .25$ and 16 values $0 \leqslant \Delta_F \leqslant .25$ of the GZVM-based algorithms compared to a synthetic ground truth for a particular 28 Hz stimulus signal $\mathbf{S}$. Similarly, the open circles show the standard, non-GVZM algorithms.

The fact that almost all operating points of the GVZM algorithms are closer to the ideal operating point $(0, 1)$ is clear evidence [131] that the GVZM-based algorithms outperform their rivals.

There are numerous possible measures of optimality that can be applied to a single-trial ROC graph. One is the previously-mentioned relationship to the ideal point $(0, 1)$. We refer to the relative distance from this point the **confusion** of an operating point:

$$
\mathrm{confusion} \stackrel{\text{def}}{=} \frac{1}{\sqrt{2}} \sqrt{(1 - \mathrm{TPR})^2 + \mathrm{FPR}^2},
$$

with smaller confusion indicating better performance. In the figures, a line segment is drawn from $(0, 1)$ to least confused operating points of the two rivals.

A measure closer to the usual concept of accuracy is what we define to be the **truth rate**

$$\text{truth rate} \overset{\text{def}}{=} (1 - \text{p}_0) \cdot \text{TPR} + \text{p}_0 \cdot (1 - \text{FPR}),$$

where $0 \leqslant \text{p}_0 \leqslant 1$. In a Bayesian formulation with binary hypotheses, if $\text{p}_0 = \text{Prob}[\text{H}_0]$ then the truth rate would be the probability of a correct decision by the algorithm.

Similar to cost functions [131], points in the TPR-FPR plane which have the same truth rates lie on parallel lines. The optimal operating point of an algorithm is where these lines are tangent to its **convex hull**.

In the figures, the value $\text{p}_0 = 1/2$ is used and the optimal parallels are drawn in solid (GVZM) and broken (rivals) lines tangent to the optimal points. It is obvious from the figures that the GVZM-based algorithms have substantially higher optimal truth rates, once again clearly demonstrating the superiority of the GVZM-based algorithms.

Remark 30. In most cases we have analyzed, when the algorithm has a good operating point in the confusion measure, it also has a good optimal in truth rate. Moreover, more often than not, these optimal operating points are the same as it true for the GVZM graphs in the figures.

For multiple-trial summary statistics, we have found it best to separate into groups consisting of all trials of a single subject and a single stimulus condition because the variation between subjects and stimuli is too extreme for a single pool.

We have also found it valuable, when comparing rival algorithms, to exclude trials in which both rivals are confused above some maximum level. The logic is that when both rivals are very confused, comparing them for performance can reveal nothing useful and will actually contaminate the summary statistics. In practice, we have found that 35% is a reasonable maximum confusion for both rivals.

A paired *t*-test for the difference of means can then be performed on both confusion and truth rate, with the number of pairs equal to the number of subject-stimulus groups.

Table 7.1 and Table 7.2 show the results of such *t*-tests. The dataset contained SSVEP EEG signals for 4

subjects with 5 trials each of 3 different stimulus conditions yielding a total of 60 trials.

For Table 7.1, the rivals were mutually confused on 26 of the trials leaving 34 unconfused trials. However, there were still enough trials remaining to get $4 \times 3 = 12$ subject-stimulus groups and thus $12 - 1 = 11$ degrees of freedom for the t-tests.

The standard error (SE) for each test was the pooled value

$$\text{SE} = \sqrt{\frac{1}{12}\left(s_{\text{GVZM}}^2 + s_{\text{SNR}}^2\right)},$$

where s_{GVZM} and s_{SNR} are the sample standard deviations of the 12 groups.

From this information, the two differences of means could be tested for significance. Table 7.1 shows that the GVZM-based algorithm outperformed its SNR rival in both confusion and truth rate with significance $\leqslant .005$.

Table 7.2 is the comparable test for GVZM against a smoothed periodogram rival. The only difference in calculation is that just 4 confused trials needed to be excluded due to the stability of the F-ratio statistic (7.3). Once again, the GVZM-based algorithm outperformed its rival in both measures with excellent significance.

CHAPTER 7: GVZM-BASED SSVEP ALGORITHMS

In this section[1], we explore two new SSVEP frequency estimation algorithms we have designed, based on the GVZM noise model, which we refer to as **GVZM-χ^2** and **GVZM-F**. We evaluate the performance of the new algorithms by comparing each with an existing, commonly-used procedure (to be be described later). Our statistical analysis demonstates that the GVZM-based algorithms outperform both their rivals.

In Sec. 7.2 we examine the GVZM-χ^2 algorithm, which is based on GVZM-χ^2-**critical levels** for the EEG periodogram. These critical levels are curves drawn on the graph of the periodogram, which are parallel to the GVZM spectrum $S_{\mathrm{GVZM}}(f)$ defined in Sec. 5.2.7. Each represents the PSD level beneath which a random $S_{\mathrm{GVZM}}(f) \cdot (1/2)\,\chi^2(2)$ variable should remain, with specified probability(see Fig. 7.1 and Fig. 7.2 for examples of GVZM-χ^2-critical levels).

In Sec. 7.3, we perform a statistical performance comparison of GVZM-χ^2 against a commonly-used BCI algorithm [5, 133, 134] we refer to as **BCI-SNR**. Note that BCI-SNR is based on forming certain ratios of periodogram values around the frequencies that are being tested as SSVEP stimuli (see Sec. 7.3 Def. 30).

Sec. 7.4 examines two versions of the well-known periodogram F-test frequency estimation method used in [37, 92]. The first version, which we call the **smoothed-F** algorithm, implements [92] directly. The second version, which we call the **GVZM-F** algorithm, replaces a key data-estimated periodogram with the optimally-fitting GVZM PSD while making no other alterations. We compare the performance of the GVZM-F and the smoothed-F algorithms statistically.

All four algorithms are used as SSVEP frequency estimators according to the protocol described in Chap. 6. This chapter also describes the procedures we used to create the summary data statistics in Table 7.1 and Table 7.2.

---

[1]Portions of this chapter have appeared in [2].

7.1   Set-up and Preprocessing

As our data, we used the publicly-available EEG recordings [37] of four subjects undergoing a series of SSVEP experiments, using a 128-channel Biosemi active-electrode EEG system (`http://www.biosemi.com`) sampled at 256 Hz. Each subject experienced 15 25-second trials divided into five trials each of approximately 8 Hz, 16 Hz, and 28 Hz stimulation frequencies. Each 25-second trial consisted of a 5-second pre-stimulation epoch, a 15-second visual stimulation epoch, and a 5-second post-stimulation epoch. Further experimental conditions are presented in [37].

Using recommended treatments for Biosemi recordings [37], the central Cz channel (in 10/20-nomenclature) was subtracted from all other electrodes. For each epoch, quadratic trends in each channel were removed and a virtual electrode over the visual cortex was created by averaging the Biosemi-nomenclature electrodes A14, A15, A16, A21, A22, A23, A25, A27, A28, and A29. A virtual electrode close to the eye muscles was created by averaging the frontal 10/20 Fp2, Fpz, and Fp1 electrodes. The visual electrode was linearly regressed onto the eye electrode and the residual was used as the SSVEP response signal. This simple method of removing eyeblink artifacts worked well for our subjects.

We excluded the mid-α (9.5 Hz–13.5 Hz) and high β (23.5 Hz–26.5 Hz) bands, the main sources of non-stationarity, [92] from all PSD functions, as well as frequencies below 6 Hz and above 50 Hz. This left 614 frequencies per periodogram for testing against the known stimuli.

The cumulative distribution functions (CDFs) of the BCI-SNR statistic, required in Sec. 7.3, were calculated by bootstrap resampling [132]. For every one of the four subjects, each of their 15 pre-stimulation epochs was independently concatenated to their 15 post-stimulation epochs, yielding 225 sample baseline datasets which were then multiplied by a Tukey window with parameter 0.1 (to match [134]). For each baseline, the BCI-SNR statistic was computed using equation Eq. (7.1) at each of the 614 test frequencies resulting in 614 "urns", each urn containing the approximately 225 distinct SNR values which occured at that frequency. For each test frequency, 1000 samples (with replacement) of size 225 were then selected from its urn. Each of these 1000 samples generated its own CDF. Then these 1000 CDFs were averaged to obtain a representative

CDF at that frequency. Repeating this procedure at every one of the 614 test frequencies yielded 614 empirical CDFs for each of the four subjects.

The smoothed-F algorithm [92] of Sec. 7.4 estimated the expected PSD of the pre-stimulation epoch $x_{\text{pre}}(n)$ by the smoothed periodogram approach of [135]. The circular autocorrelation [16] $R_{\text{pre}}(m)$ of $x_{\text{pre}}(n)$ was computed and then the DFT $S_{\text{pre}}(k)$ of the windowed autocorrelation $h(m) \cdot R_{\text{pre}}(m)$ was regarded as the expected PSD. The window $h(m)$ was a symmetric Hamming window of length $2M + 1$, where M is approximately 10% of the data length of $x_{\text{pre}}(n)$. In [92], the pre-stimulation data length was specifically chosen to be same as the stimulated epoch $x_{\text{stim}}(n)$ so that their respective DFTs $S_{\text{pre}}(k)$ and $S_{\text{stim}}(k)$ could be compared easily at equal frequency indices k. Since our pre-stimulation epochs are shorter than the stimulation epochs, spline interperpolation of $S_{\text{pre}}(k)$ was performed to resample it to the larger length. We found that the 10% smoothed periodogram was sufficiently smooth that such resampling was very accurate.

The authors of [92] time-averaged multiple epochs to improve the signal-to-noise ratio prior to detection. This required about 2 minutes of trial data, a very long duration for practical real-time BCIs. For example, the longest epoch used by the well-known and successful SSVEP BCI of [5] was only 8 seconds, which was then continuously processed to yield average inter-selection intervals between 3.40 and 5.68 seconds. We tested the GVZM-F and smoothed-F algorithms on the generous, single-trial, unaveraged epochs of 15 seconds.

We performed the paired algorithm comparisons of GVZM-χ^2 vs. BCI-SNR in Sec. 7.3 and GVZM-F vs. smoothed-F in Sec. 7.4 by procedures detailed in Chap. 6. (See Fig. 7.3, Fig. 7.6, Table 7.1, and Table 7.2.)

All fits of GVZM PSDs in Def. 21 to actual EEG periodograms, used by both the GVZM-χ^2 and GVZM-F algorithms, were obtained by weighted least-squares optimization using weights proportional to f^κ, for $\kappa \approx 1.5$, where the f are the frequencies over which we are optimizing (which must exclude non-stationary bands). This weighting increased the accuracy in the higher frequencies where the signal power is inherently small.

Figures displaying spectra and the results of spectral tests show power density S in dB relative to 1; that

is $10 \log_{10}(S/1)$. However, all actual critical values have been determined and hypothesis tests were performed in the original units of (amplitude unit)^2/Hz.

7.2   Real-time Estimation of SSVEP Responses using the GVZM-χ^2 Algorithm

The most direct way to utilize the GVZM noise model in an estimation algorithm is by optimally fitting a GVZM PSD to a recorded periodogram and calculating $(1/2) \chi^2(2)$ critical levels parallel to it. A GVZM-χ^2-critical level at particular P-value is a curve, parallel to $S_{\mathrm{GVZM}}(f)$, showing the power below which periodogram values are confined with probability $1 - P$, assuming the GVZM noise model to be correct. Then the frequencies of any spikes extending above the level associated to a pre-assigned P-value are regarded as positives; i.e., frequencies at which the GVZM-χ^2 algorithm will report the EEG as having true power, not merely random noise. All others are reported as negatives. In this way, stimulus frequency estimation is implemented by a collection of hypothesis tests [93, 130], one at every frequency we intend to examine.
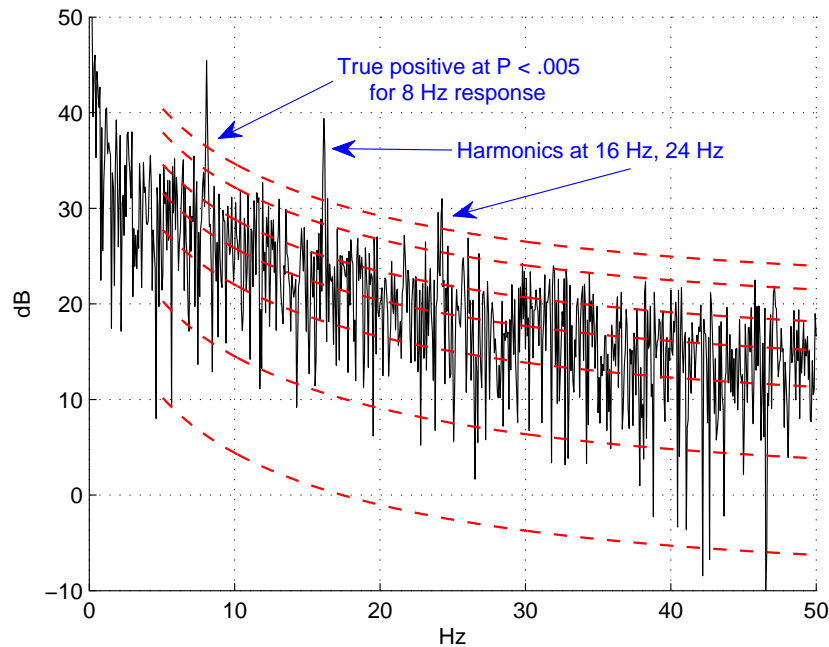
Figure 7.1: 8 Hz stimulus: $\mathrm{GVZM}(\theta) \cdot (1/2) \chi^2(2)$ critical levels corresponding to $P = 0.005, 0.05, 0.25, 0.5, 0.75, 0.95, 0.995$ (top to bottom).

96
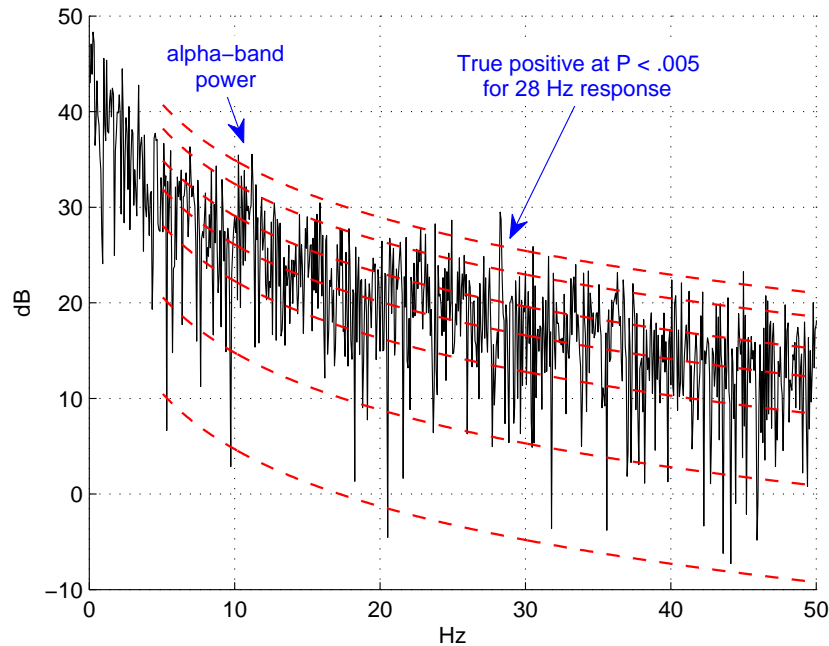
Figure 7.2: 28 Hz stimulus: GVZM $(\theta) \cdot (1/2) \, \chi^2 (2)$ critical levels corresponding to $P = 0.005, 0.05, 0.25$, $0.5, 0.75, 0.95, 0.995$ (top to bottom).

Fig. 7.1 and Fig. 7.2 show the results of the GVZM-χ^2 algorithm for SSVEP experiments at 8 Hz and 28 Hz respectively (subject 3, trial 2). In particular, according to the GVZM noise model, it is 99.5% probable that a spectral spike will lie below the upper dashed critical level. These critical levels also display how closely the GVZM noise model fits the distribution of recorded EEG background processes.

It is clear from Fig. 7.1 that the GVZM-χ^2 algorithm accurately estimated the 8Hz fundamental SSVEP response and its two harmonics at significance level $P = 0.005$, thus generating no false negatives (also called) Type II errors [93]). Moreover, it has correctly excluded all other spikes as simply random noise and thus avoided all false positives. (Also called Type I errors [93] or false discoveries [130]).

In Fig. 7.2 the 28 Hz response was estimated accurately also. However there are several false positives arising because of non-stationary power in the α-band. As discussed in Sec. 7.1, non-stationary bands need to be pre-excluded from all procedures.

7.3 SSVEP Frequency Estimation Using the GVZM-χ^2 and BCI-SNR Algorithms

In this section, we describe the BCI-SNR algorithm and compare it to the GVZM-χ^2 algorithm.

The BCI-SNR statistic for SSVEP procedures was first defined in [5], where it was used as a simple measure of signal strength for determining optimal stimulus frequencies. It subsequently became a popular frequency estimator for SSVEP BCIs [134] and more general applications [101]. The phrase "power spectral density analysis" (PSDA) also has been used [133] for methods based on the BCI-SNR.

Definition 30. The BCI-SNR statistic [5] of a signal x at the kth test frequency f_k is the ratio

$$SNR_x\left(f_k\right) = \frac{n \cdot \hat{S}_x\left(f_k\right)}{\sum\limits_{\substack{j=-n/2 \\ j \neq 0}}^{n/2} \hat{S}_x\left(f_k + j \cdot \Delta f\right)}, \tag{7.1}$$

where $\hat{S}_x$ is an estimator of the sample spectrum, Δf is the spectral resolution of the estimated frequency domain, and n is a small integer. To be consistent with [134], we use $n = 6$.

The BCI-SNR statistic is sometimes used as a non-blind detector for a short list $f_1, \ldots, f_K$ of known SSVEP BCI selection frequencies. The subject's selection is considered to be that frequency f_k which has the largest SNR_x value; i.e., $f_{\text{selected}} = \text{argmax}_{f_k} SNR_x\left(f_k\right)$. (For example, [133, 134].)

To use the BCI-SNR algorithm as a blind SSVEP frequency estimator, as described in Chap. 6, we require each individual probability distribution function of $SNR_x\left(f_k\right)$ for every test frequency f_k. These were estimated by bootstrap resampling as described in Sec. 7.1.

Fig. 7.3 shows an example of a minimum-variance, unbiased, single-trial estimate of the comparison **receiver operating characteristics (ROC)** graph [131] as described in Sec. 6.6. The dataset is that of Fig. 7.4 (subject 3, trial 1, 28 Hz stimulus).

In Fig. 7.3, TPR and FPR denote the true and false positive rates, calculated at 256 operating points as
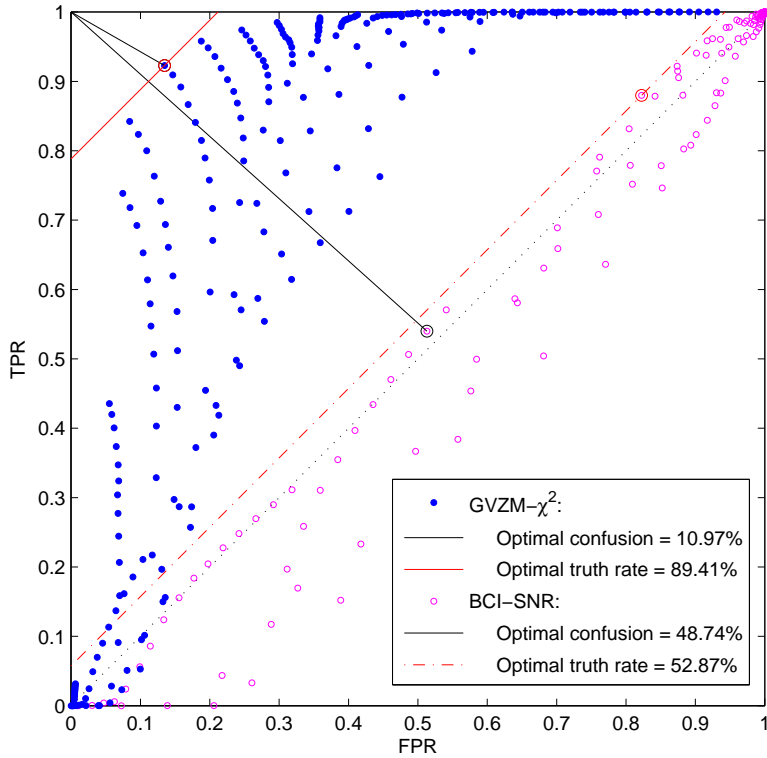
Figure 7.3: GVZM-χ^2 vs. BCI-SNR example: the minimum-variance, unbiased, single-trial ROC estimator, showing optimal operating points, using the 28 Hz data of Fig. 1. (©2016 IEEE)

detailed in the Appendix. Confusion measures the relative distance of an operating point from the ideal (TPR, FPR) = (1, 0), while the truth rate is a weighted average of the TPR and the true negative rate TNR = (1 - FPR):

$$
\begin{cases}
\text{Confusion} = \sqrt{(1 - \text{TPR})^2 + \text{FPR}^2}/\sqrt{2} \\
\text{Truth Rate} = (1 - p_0) \cdot \text{TPR} + p_0 \cdot (1 - \text{FPR}),
\end{cases}
$$

where $0 \leqslant p_0 \leqslant 1$. Both are intended as measures of accuracy. In a Bayesian situation, with p_0 the probability of the null hypothesis [93], the truth rate is the probability of a true decision. We use $p_0 = 1/2$.

We observe that the GVZM-χ^2 algorithm outperforms the BCI-SNR algorithm at nearly every operating point. Moreover, even on this very difficult 28 Hz stimulus, the optimal operating point for GVZM-χ^2 identifies the true stimulus frequency with probability above 90% and FPR below 20%.

Table 7.1
Performance improvement of GVZM-χ^2 over BCI-SNR. (©2016 IEEE)

Combined Optimal Results	%	Unconfused Trials	Pooled SE	t-score	df	P-value
Confusion Decrease	29.77	34	0.0371	3.253	11	0.004
TruthRate Increase	17.92	34	0.0356	3.133	11	0.005

Table 7.1 summarizes the pooled ROC results for the $N = 34$ trials in which at least one of the algorithms had confusion below 35% ("unconfused" trials by definition). Pooled SE denotes the standard error

$$\text{Pooled SE} = \sqrt{\left(\sigma_{\text{GVZM}}^2 + \sigma_{\text{SNR}}^2\right)/N}$$

appropriate to the t-test for the difference of means.

Table 7.1 shows that the GVZM-χ^2 algorithm outperforms the BCI-SNR algorithm on both the confusion and truth rate measures with statistical significance above 99%.

7.4 SSVEP Frequency Estimation Using the GVZM-F and Smoothed-F Algorithms

In [92], the authors assume, based on the theory of periodograms developed in detail in [56], that the periodogram random process $S_x(k)$, $0 \leqslant k \leqslant N-1$ of the EEG background time series $x(n)$ is given asymptotically by

$$S_x(k) = \mathsf{E}\left[S_x(k)\right] \cdot (1/2)\, \Xi(k), \tag{7.2}$$

where $\Xi(k)$, $0 \leqslant k \leqslant N-1$ is a process with $\Xi(k) \sim \chi^2(2)$ and which are independent for $0 \leqslant k, l < N/2$ with $k \neq l$.

When the function $\mathsf{E}\left[S_x(k)\right]$ is known, (7.2) implies that the test statistics

$$s_x(k) \stackrel{\text{def}}{=} 2 \cdot S_x(k)\,/\,\mathsf{E}\left[S_x(k)\right],$$

for $0 \leqslant k < N/2$, are iid $\chi^2(2)$ random variables.

A fixed set of indices $\Omega \subseteq \{0, 1, \cdots, N-1\}$ is selected to represent what we regard as stationary frequencies; e.g., α-band frequencies are excluded (cf. Sec. 7.1). Then, under the null hypothesis that there is no SSVEP spike at frequency index k_{test}, we must have

$$\frac{\sum_{k \in \Omega_{\text{test}}} s_x(k) \, / \, N_{\text{test}}}{\sum_{k' \in \Omega \backslash \Omega_{\text{test}}} s_x(k') \, / \, (N_\Omega - N_{\text{test}})} \tag{7.3}$$
$$\sim F(N_{\text{test}}, N_\Omega - N_{\text{test}}),$$

where Ω_{test} is the set of indices k_{test} and its harmonics in Ω, N_{test} is the size of Ω_{test}, N_Ω the size of Ω, and $F(d_1, d_2)$ is the F–distribution with degrees of freedom d_1, d_2 [93].

The key issue then is how to obtain the function $\mathsf{E}\left[S_x(k)\right]$. In [92], the authors estimated this function by computing a "smoothed periodogram" $S_{\text{smooth}}(k)$ of a pre-stimulation epoch as described in Sec. 7.1 and used $S_{\text{smooth}}(k)$ as a substitute for $\mathsf{E}\left[S_x(k)\right]$. This was their smoothed-F algorithm.
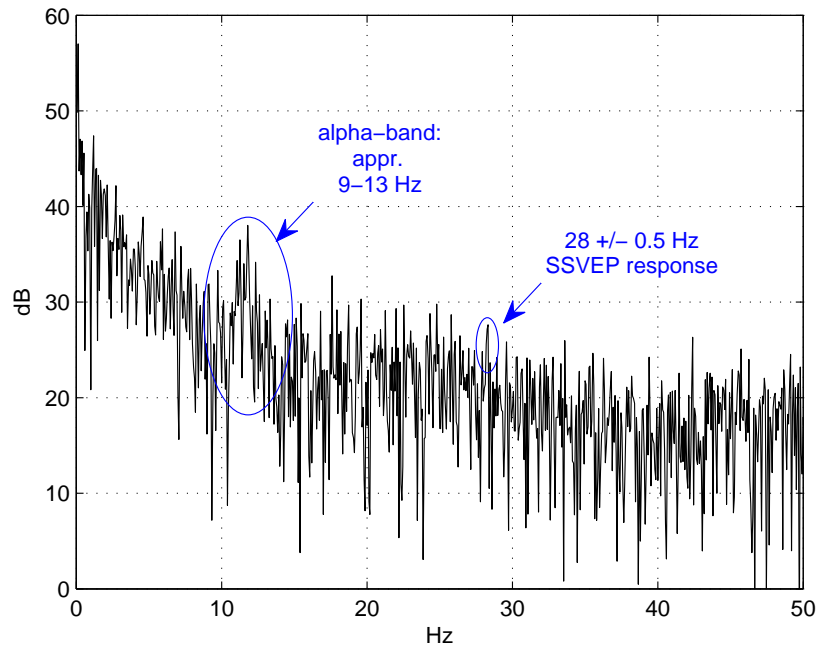
Figure 7.4: Recorded EEG periodogram from a 15-second, SSVEP experiment showing α-band power. The target 28 Hz response peak is nearly lost in the background noise. (©2016 IEEE)

However, according to the GVZM noise model, we expect to obtain a more accurate baseline estimate by using the GVZM PSD which optimally fits the same pre-stimulus epoch as a substitute for $\mathsf{E}\left[S_x\left(k\right)\right]$. This is our GZVM-*F* algorithm. Fig. 7.5 shows the periodogram from the pre-stimulus epoch of the data of Fig. 7.4 (subject 3, trial 1, 28Hz stimulus) with both the smoothed periodogram and the fitted GVZM PSD displayed. The two algorithms are compared as described in Chap. 6. Fig. 7.6 shows an example of a minimum-variance, unbiased, single-trial estimate of the comparison ROC graph.
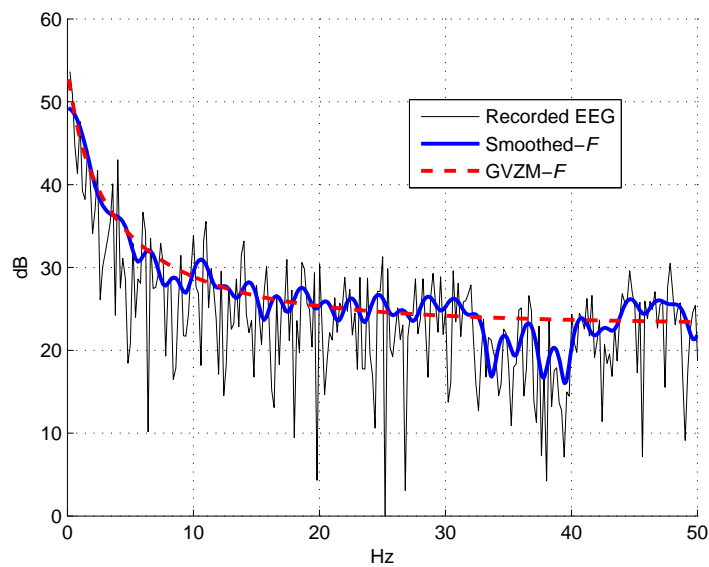
Figure 7.5: Baseline (non-stimulus) PSDs used as the 28 Hz, χ^2 references for the smoothed-*F* and GVZM-*F* algorithms. (©2016 IEEE)

The dataset is that of Fig. 7.4 (subject 3, trial 1, 28 Hz stimulus). As in Sec. 7.3, the GVZM-*F* algorithm outperforms the smoothed-*F* algorithm at nearly every operating point, achieving an optimal performance of over 95% probability of true identification with FPR just above 20%.

Table 7.2 summarizes the pooled ROC results as described in Sec. 6.6 for the 56 trials in which at least one of the algorithms had confusion below 35%. The large number of unconfused trials of these algorithms is a result of the inherent stability of the carefully-designed underlying statistic (7.3).

Table 7.2 shows that GVZM-*F* algorithm outperforms the smoothed-*F* algorithm on both the confusion and accuracy measures with statistical significance above 99%.

Table 7.2

Performance improvement of GVZM-*F* over Smoothed-*F*. (©2016 IEEE)

Combined Optimal Results	%	Unconfused Trials	Pooled SE	t-score	df	P-value
Confusion Decrease	30.57	56	0.0322	2.901	11	0.007
TruthRate Increase	12.67	56	0.0278	3.234	11	0.004
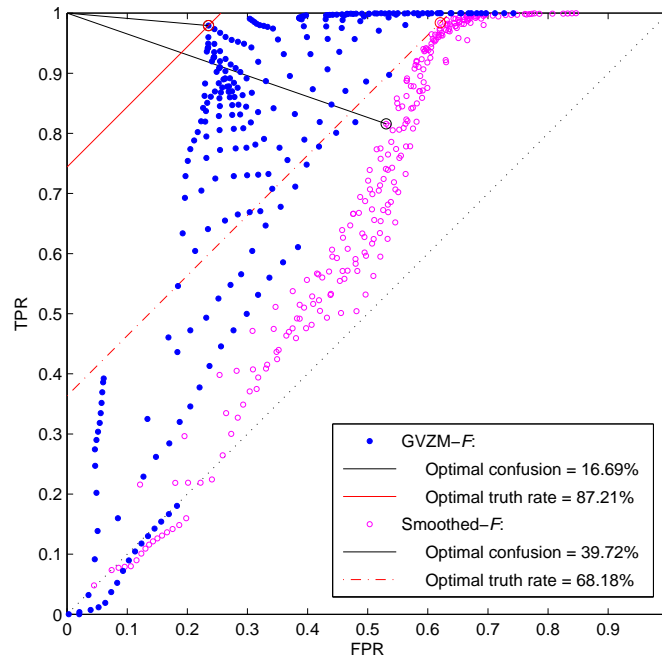
Figure 7.6: GVZM-*F* vs. Smoothed-*F* example: the minimum-variance, unbiased, single-trial ROC estimator, showing optimal operating points, using the 28 Hz data of Fig. 7.4. (©2016 IEEE)

APPENDIX A: A PRECIS OF NON-RELATIVISTIC QUANTUM

MECHANICS

A.1 Conventions and Definitions

The theories of general quantum [77, 103, 104] and statistical mechanics [105, 106], as well as stochastic processes [79, 82], have a vast and accessible literature. The following is a minimalist quantum theory compatible with any detailed quantum model of ion channels.[1]

Let $\mathbb{H}$ be a fixed separable complex Hilbert space with inner product $\langle \cdot | \cdot \rangle$ [109]. The space $\mathbb{H}$ is the **configuration space** of the quantum system. Vectors $|\psi\rangle \in \mathbb{H}$ are sometimes called **wavefunctions**, **pure states**, or "**kets**" in Dirac's terminology [110].

In order to simplify the presentation of quantum-based reasoning, in this Appendix we fix a particular orthonormal basis for $\mathbb{H}$ so that all vectors are (possibly infinite) columns of complex numbers, dual vectors (Dirac's "bras" [110]) are rows, and continuous linear operators are (possibly infinite) square matrices. In this way, operators act by matrix multiplication, the inner product $\langle \psi | \phi \rangle$ is just $\psi^{\mathrm{H}} \cdot \phi$ where $(\cdot)^{\mathrm{H}}$ denotes the hermitian transpose (i.e., the adjoint [111]), and the projection operator $\mathbf{P}_\psi$ onto a unit vector ψ is the rank-1 matrix $\mathbf{P}_\psi = |\psi\rangle \cdot \langle\psi|$. Moreover, we will generally consider only bounded, normal operators which are **compact** [109, 111] (so that orthonormal bases of eigenvectors and countable spectral decomposition exist) and even **non-degenerate** (so eigenspaces are 1-dimensional) when convenient. We will often treat $\mathbb{H}$ as finite-dimensional to simplify formulas. These simplifications are replaceable by appropriate functional analysis generalizations [103, 109, 111, 112].

An **operator A** is a linear function $\mathbf{A} : \mathbb{H} \to \mathbb{H}$ which is **normal**: $\mathbf{A} \cdot \mathbf{A}^{\mathrm{H}} = \mathbf{A}^{\mathrm{H}} \cdot \mathbf{A}$. Real-valued **observables** A of the system are associated in a 1-1 manner with (not necessarily bounded) self-adjoint operators $\mathbf{A}$ whose spectrum

$$\mathbf{Sp}\,(\mathbf{A}) \overset{\text{def}}{=} \{\alpha \in \mathbb{R} \mid (\alpha \cdot \mathbf{I}_{\mathbb{H}} - \mathbf{A}) \text{ has no inverse}\},$$

---

[1] Since protein macromolecules are very large systems, it may be advantageous to base quantum ion channel models on Bohm & Hiley's alternative foundation for quantum mechanics which uses non-local **quantum potentials** [102]. In fact, David Bohm and his colleagues have speculated for decades on the relation between non-locality, quantum potentials, and mind (e.g.; [102], pg. 381 and [107]). The highly controversial [29, 31] theories of Penrose [27, 108] and Penrose & Hameroff [28] must be mentioned in this regard as well. We shall, however, avoid these fascinating excursions in favor of more standard quantum "metaphysics."

where $\mathbf{I}_{\mathbb{H}}$ is the identity operator [103, 109, 112], is precisely the set of possible measured values of A.

An operator $\mathbf{A}$ is of **trace class** [111] if

$$\sum_i \langle \phi_i | \left(\mathbf{A}^H \mathbf{A} \right)^{1/2} \phi_i \rangle < \infty$$

for some orthonormal basis $\phi_1, \phi_2, \cdots$. Trace class operators are always compact [111], hence continuous. The **trace** of a trace class operator $\mathbf{A}$ is the (absolutely convergent) series

$$\mathbf{tr}(\mathbf{A}) \overset{\text{def}}{=} \sum_i \langle \phi_i | \mathbf{A} \phi_i \rangle.$$

This value is independent of the orthonormal basis chosen [111]. With our fixed-basis simplifications, the trace becomes just the sum of the diagonal entries of the matrix $\mathbf{A}$. Note that the set $\mathcal{T}(\mathbb{H})$ of trace class operators is closed under convergence in the operator norm and also left- and right-multiplication by bounded operators $\mathcal{B}(\mathbb{H})$ [111]. Thus, for $\mathbf{A} \in \mathcal{T}(\mathbb{H})$ and $\mathbf{B} \in \mathcal{B}(\mathbb{H})$, we have both $\mathbf{AB}, \mathbf{BA} \in \mathcal{T}(\mathbb{H})$ and $\mathbf{tr}(\mathbf{AB}) = \mathbf{tr}(\mathbf{BA})$. (In Appendix B, the definition of trace is generalized. See Def. 36.)

A **state**[2] of the system [77, 103] is then a non-negative definite, self-adjoint operator $\boldsymbol{\Psi}$ on $\mathbb{H}$ of trace class such that $\mathbf{tr}(\boldsymbol{\Psi}) = 1$. The set $\mathcal{S}(\mathbb{H})$ of all states is a convex subset of the set of bounded operators; that is, if $\boldsymbol{\Psi}_x \in \mathcal{S}(\mathbb{H})$, for $x \in X$, where X is an index set, and $p(x)$ is a probability measure on X, then $\int \boldsymbol{\Psi}_x \, dp(x) \in \mathcal{S}(\mathbb{H})$. The state $\int \boldsymbol{\Psi}_x \, dp(x)$ is called a **mixture** of the states $\boldsymbol{\Psi}_x$, with **mixture coefficients** $p(x)$. The boundary $\partial \mathcal{S}(\mathbb{H})$ of $\mathcal{S}(\mathbb{H})$ consists of the **pure** states: those which cannot be expressed as a non-trivial mixture of other states [103]. The state $\boldsymbol{\Psi}$ is pure if and only if it is a projection onto a 1-dimensional subspace [112]; i.e., $\boldsymbol{\Psi} = \mathbf{P}_\psi = |\psi\rangle \cdot \langle \psi|$ for some unit vector ψ, which is unique up to multiplication by a complex number of modulus 1. The pure states form a compact Hausdorff space in

---

[2]An equivalent and more useful definition of a state is a positive linear functional Ψ on the $*$–algebra $\mathcal{B}(\mathbb{H})$ of bounded linear operators for which $\Psi(\mathbf{I}_{\mathbb{H}}) = 1$ [77, 103].

the weak–∗ topology[3] [112] and every state Ψ can be expressed as a weak–∗ mixture

$$\Psi = \int\limits_{\psi \in \partial \mathcal{S}(\mathbb{H})} \mathbf{P}_\psi \, dp(\psi)$$

of pure states, for some set of mixture coefficients $p(\psi)$ on $\partial \mathcal{S}(\mathbb{H})$.

Definition 31. If A is an observable with associated operator $\mathbf{A}$, then a state Ψ is **coherent** with A (or, more simply, A–coherent) if $\mathbf{A} \cdot \Psi = \Psi \cdot \mathbf{A}$.

A state is coherent with A if and only it diagonalizes in any basis in which $\mathbf{A}$ diagonalizes [111, 112]. If $\{\mathbf{P}_\alpha \mid \alpha \in \mathbf{Sp}(A)\}$ are the projections onto the eigenspace of A then Ψ is A–coherent just in case[4] it is a mixture of the **eigenstates** $\Psi_\alpha \overset{\text{def}}{=} \mathbf{P}_\alpha / \dim(\mathbf{P}_\alpha)$, where $\dim(\mathbf{P}_\alpha) = \mathbf{tr}(\mathbf{P}_\alpha)$ is the dimension of the α eigenspace. In this case, and **in this case only**, it is consistent to interpret Ψ by saying that, for all $\alpha \in \mathbf{Sp}(A)$, the observable A has probability $p(\alpha)$ of having the value α, where $\{p(\alpha) \mid \alpha \in \mathbf{Sp}(A)\}$ are the mixture coefficients of Ψ. However it is critical to interpret these probabilities in a **frequentist**[5] [136] sense because the absence of so-called "hidden variables" excludes the possibility of an underlying Kolmogoroff probability space [80].

The following is easily proved but very significant:

Lemma 4. *Let Ψ be any state and $\mathbf{P}_\alpha$ be a projection operator onto an eigenstate of observable A. Then $\mathbf{P}_\alpha \cdot \Psi \cdot \mathbf{P}_\alpha / \mathbf{tr}(\mathbf{P}_\alpha \cdot \Psi)$ is a state which is coherent with A.*

The term "measurable" always means "Borel measurable" [78] unless otherwise stated.

---

[3]i.e.; as linear functionals on $\mathcal{B}(\mathbb{H})$. See the previous footnote.

[4]Shown using an appropriate form of the Gel'fand-Neumark Theorem [112].

[5]or Bohmian [102]

A.2 Born's Axiom

Let $g(\alpha)$ be a bounded measurable function [78] whose domain includes the possible values $\alpha \in \mathbb{R}$ of the real observable A. It can be shown[6] that if the associated self-adjoint operator is $\mathbf{A}$ then there must be an operator $g(\mathbf{A})$ corresponding to the composite observable $g(A)$. We have [103]:

Theorem 9. *Let $\Psi \in \mathbb{H}$ be a state and A a real observable associated with the self-adjoint operator $\mathbf{A}$. Then there is a unique Borel probability measure $\pi_{\Psi,A}$ on $\mathbf{Sp}(\mathbf{A})$ such that, for all bounded measurable functions $g(\alpha)$ whose domain includes the possible values α of A,*

$$\mathbf{tr}\left(g(\mathbf{A}) \cdot \Psi\right) = \int\limits_{\alpha \in \mathbf{Sp}(\mathbf{A})} g(\alpha)\, d\pi_{\Psi,A}(\alpha).$$

The central postulate of quantum theory may now be expressed as:

Definition 32. Born's Law (probability form) Let Ψ, A, $\mathbf{A}$, and $\pi_{\Psi,A}$ be as in Thm. 9. Let $\mathrm{Prob}\left[\cdot \,|\, \Psi\right]$ denote relative frequencies for an ensemble [136] of identical systems in prepared in state Ψ. Then, for every measurable set $E \subseteq \mathbf{Sp}(\mathbf{A})$,

$$\mathrm{Prob}\left[A \in E \,|\, \Psi\right] = \pi_{\Psi,A}(E).$$

(But cf. Sec. A.3 below for the quantum mechanical interpretation of the expression "$A \in E$".)

Born's Law, in probability form, combined with Thm. 9 immediately implies

Corollary 3. *Born's Law (expectation form)*

Let $\Psi \in \mathbb{H}$ be a state, let A be a real observable associated with the self-adjoint operator $\mathbf{A}$, and let $g(\alpha)$ be a bounded measurable function whose domain includes the possible values of A. Then an ensemble of

---

[6]Using the GNS representaion [112] and an appropriate form of the Reisz Representation Theorem [78].

identical systems prepared in state $\boldsymbol{\Psi}$ will produce a frequency average value for $g(A)$ given by

$$\mathsf{E}\left[g\left(A\right)\mid\boldsymbol{\Psi}\right]=\mathbf{tr}\left(g\left(\mathbf{A}\right)\cdot\boldsymbol{\Psi}\right).$$

A.3 Measurements and the Wavefunction Collapse

Terminology concerning the interaction of measuring apparatus (including human observers) with quantum systems is not standardized but we will adopt the following conventions:

Definition 33. (Experiments, Measurements, and Observations)

- An **experiment** specifies an observable A with its associated operator $\mathbf{A}$ together with a measurable function $g:\mathbf{Sp}\left(\mathbf{A}\right)\to\mathbb{C}$ on the space of possible values of A. The experiment itself consists of the determination of one and only one value of $g(A)$. It is conceptually important that no information other than this value be produced by the experiment. It is also important, however, that some value for $g(A)$ be obtained even though the experiment disregards all information about the particular outcome $\alpha\in\mathbf{Sp}\left(\mathbf{A}\right)$ which lead to the determination of $g(\alpha)$. An standard example of an experiment is $g\left(\alpha\right)\overset{\text{def}}{=}\sum_i i\cdot\chi_{E_i}\left(\alpha\right)$, where $\mathbf{Sp}\left(\mathbf{A}\right)=\bigcup_i E_i$, $E_i\cap E_j=\emptyset$ for $i\neq j$ is a measurable partition and $\chi_{(\cdot)}$ denotes characteristic (or indicator) functions. The determination $g(A)=i$ indicates that $A\in E_i$, with no other information about the value of A available. (Of course, additonal experiments may extract some of this missing information.)

- An experiment is **reductive** (or of the **first kind** [77]) if, after a determination $g(A)=\gamma$ is made, then future repetitions of the experiment on the system will always produce the same result. The experiment **reduces** all states to the subset of $\mathcal{S}\left(\mathbb{H}\right)$ for which $g(A)$ is certain to take the value γ.

- An experiment is **nonreductive** (or of the **second kind** [77]) if is it not reductive. An example of a nonreductive experiment is the determination of a particle's momentum by bombarding it with other particles.

- A **measurement** is an experiment in which $g\left(\alpha\right)\overset{\text{def}}{=}1$ identically; i.e., some value for A is obtained

but no information about its particular value is available. A measurement is trivially reductive. Note that measurement is **not** a meaningless experiment: because of the **Measurement Law** Def. 34 discussed subsequently, the act of obtaining some value for A, observed or not, may change the state.

- An **observation** is an experiment using the identity function $g(\alpha) \stackrel{\text{def}}{=} \alpha$; i.e., the value of the observable A is determined precisely. A reductive observation of a non-degenerate observable reduces (or **collapses**) any state Ψ to a wavefunction (pure state, ket, eigenstate, etc.) of $\mathbf{A}$; i.e., $\Psi \mapsto |\psi_\alpha\rangle \cdot \langle\psi_\alpha|$, with $\mathbf{A}\psi_\alpha = \alpha\,\psi_\alpha$.

Recall Def. 31 of A–coherent states. It is only in A–coherent states that we can regard A as having some definite but unknown value. Otherwise there is "quantum interference" between the possible values for A and we have to regard the observable as having **all** values simultaneously. The classic example of quantum interference is the two-slit photon experiment in which the wavefunction $\psi(x, y)$ describing the probability of a photon hitting a point (x, y) on the target screen is not coherent with the observable corresponding to the slit though which a photon passed. As a result, each photon particle must be regarded as passing through both slits simultaneously.

Every reductive experiment on A collapses the prior state to a coherent state. In fact, we have the following

Definition 34. Measurement (or Observation or Projection or ...) Law

Let (A, g) be a reductive experiment and $g^{-1}[\gamma] \stackrel{\text{def}}{=} \{\alpha \in \mathbf{Sp}(\mathbf{A}) \mid g(\alpha) = \gamma\}$. If the experiment produces the result $g(A) = \gamma$ in the prior state Ψ, then the posterior Ψ_γ is the A-coherent state (cf. Lem. 4)

$$\Psi_\gamma \stackrel{\text{def}}{=} \frac{1}{\pi_{\Psi,A}(g^{-1}[\gamma])} \int\limits_{\alpha \in g^{-1}[\gamma]} (\mathbf{P}_\alpha \cdot \mathbf{\Psi} \cdot \mathbf{P}_\alpha)\, d\pi_{\Psi,A}(\alpha). \tag{A.1}$$

Corollary 4. *(i.) If a measurement is made of the observable A in state Ψ (so that the value of A is unknown after the experiment), the state will reduce to the A–coherent state*

$$\Psi_A \stackrel{\text{def}}{=} \int\limits_{\alpha \in \mathbf{Sp}(\mathbf{A})} (\mathbf{P}_\alpha \cdot \mathbf{\Psi} \cdot \mathbf{P}_\alpha)\, d\pi_{\Psi,A}(\alpha).$$

(ii.) If A is non-degenerate and the experiment is reductive, the observation $A = \alpha$ made in state $\mathbf{\Psi}$ will reduce the system to the pure A–coherent state

$$\mathbf{\Psi}_\alpha = \frac{1}{\|\boldsymbol{\psi}_\alpha\|^2} |\boldsymbol{\psi}_\alpha\rangle \cdot \langle \boldsymbol{\psi}_\alpha|$$

The latter example is referred to as **wavefunction collapse**. The Measurement Law and its consequences cause enormous philosophical difficulties for the foundation of quantum mechanics because of the apparent physical role of the observer: the final physical state of the system seems to depend upon what the observer "knows". We can ask what observer? How does he know? How does the system "know" he knows? [27] The famous **Schrödinger's Cat** paradox [77] in which a cat inside a closed box seems neither alive nor dead until we look at it is the classic example of the still unresolved issues of this **Measurement Problem**.

A.4   Quantum Dynamics

Dynamics is modeled as a unitary representation $\mathbf{U}(t)$ of the additive group of $\mathbb{R}$. In the typical case, $\mathbf{U}(t) = e^{-\frac{2\pi}{h}\sqrt{-1}\mathbf{H}t}$, where $\mathbf{H}$ is the time-independent Hamiltonian of the system [77, 103, 104, 110].

If no disturbance by an experiment is made on the system between its initial state $\mathbf{\Psi}_0$ and time t, the system then will be in state $\mathbf{\Psi}(t) = \mathbf{U}(t) \cdot \mathbf{\Psi}_0 \cdot \mathbf{U}(t)^{\mathrm{H}}$, which is the integrated form of **Schrödinger's Equation**.

The function $\mathbf{\Psi}(\,\cdot\,)$ characterizes all stochastic properties of the system as long as there is no disturbance. Thus, in some sense, every observable A defines a physical stochastic process $\{A(t)\}_{-\infty < t < \infty}$ for which we have

$$\mu_A(t) \stackrel{\text{def}}{=} \mathsf{E}[A(t) \mid \mathbf{\Psi}] = \mathbf{tr}(\mathbf{A} \cdot \mathbf{\Psi}(t)).$$

However, even if $\mathbf{\Psi}_0$ is an A–coherent state, generally $\mathbf{U}(t) \cdot \mathbf{\Psi}_0 \cdot \mathbf{U}(t)^{\mathrm{H}}$ will not be one (unless A is a **conserved quantity** which means it commutes with every $\mathbf{U}(t)$). So we have the paradoxical situation that the undisturbed process $A(t)$ always has an *average* value but may not exhibit any *particular* values.

APPENDIX B: A REVIEW OF TENSOR PRODUCTS AND TRACES

The **tensor product** $\mathbb{H}_1 \otimes \cdots \otimes \mathbb{H}_n$ of separable Hilbert spaces $\mathbb{H}_1$, $\mathbb{H}_2$, $\cdots$, $\mathbb{H}_n$ can be defined[1] [111] as the complex Hilbert space with basis consisting of the formal expressions $\phi_{i_1}^1 \otimes \phi_{i_2}^2 \otimes \cdots \otimes \phi_{i_n}^n$, where $1 \leqslant i_1 \leqslant \mathbf{dim}(\mathbb{H}_1)$, ..., $1 \leqslant i_n \leqslant \mathbf{dim}(\mathbb{H}_n)$, and every $\left\{\phi_i^k\right\}_{1 \leqslant i \leqslant \mathbf{dim}(\mathbb{H}_k)}$ is a fixed basis for $\mathbb{H}_k$. Thus $\mathbf{dim}(\mathbb{H}_1 \otimes \cdots \otimes \mathbb{H}_n) = \mathbf{dim}(\mathbb{H}_1) \times \cdots \times \mathbf{dim}(\mathbb{H}_n)$.

The inner product on $\mathbb{H}_1 \otimes \cdots \otimes \mathbb{H}_n$ is defined on basis elements by

$$\left\langle \phi_{i_1}^1 \otimes \cdots \otimes \phi_{i_n}^n, \phi_{j_1}^1 \otimes \cdots \otimes \phi_{j_n}^n \right\rangle \overset{\text{def}}{=} \left\langle \phi_{i_1}^1, \phi_{j_1}^1 \right\rangle \cdots \left\langle \phi_{i_n}^n, \phi_{j_n}^n \right\rangle$$

and then extended to the whole space by linearity.

It follows that this definition is basis-independent and, if every $\left\{\phi_i^k\right\}_{1 \leqslant i \leqslant \mathbf{dim}(\mathbb{H}_k)}$ is orthonormal, then so is

$$\left\{ \phi_{i_1}^1 \otimes \phi_{i_2}^2 \otimes \cdots \otimes \phi_{i_n}^n \right\}_{1 \leqslant i_1 \leqslant \mathbf{dim}(\mathbb{H}_1), \cdots, 1 \leqslant i_n \leqslant \mathbf{dim}(\mathbb{H}_n)}.$$

For a single Hilbert space $\mathbb{H}$ and for $n > 0$ then we define $\mathbb{H}^{\otimes n} \overset{\text{def}}{=} \overbrace{\mathbb{H} \otimes \cdots \otimes \mathbb{H}}^{n}$. We can also consistently define $\mathbb{H}^{\otimes 0} \overset{\text{def}}{=} \mathbb{C}$, the complex scalar field.

The tensor product $\mathbb{H}_1 \otimes \cdots \otimes \mathbb{H}_n$ satisfies an important *universal mapping property* [138]. Let $\mathbb{K}$ be a complex vector space and $f : \mathbb{H}_1 \times \cdots \times \mathbb{H}_n \to \mathbb{K}$ be a function which is linear in each variable separately. Then there is a unique linear operator $\otimes f : \mathbb{H}_1 \otimes \cdots \otimes \mathbb{H}_n \to \mathbb{K}$ such that

$$(\otimes f)(\psi_1 \otimes \cdots \otimes \psi_n) = f(\psi_1, \cdots, \psi_n)$$

for all $\psi_1 \in \mathbb{H}_1$, ..., $\psi_n \in \mathbb{H}_n$.

In particular, linear operators $\mathbf{A}_1$, ..., $\mathbf{A}_n$ on $\mathbb{H}_1$, ..., $\mathbb{H}_n$ define a unique linear operator $\mathbf{A}_1 \otimes \cdots \otimes \mathbf{A}_n$ on

---

[1]Defining tensor constructs on products of C^*–algebras such as the bounded linear operators on Hilbert spaces is actually much more significant and subtle [137]. For simplicity of presentation, we purposely avoided this construction.

$\mathbb{H}_1 \otimes \cdots \otimes \mathbb{H}_n$ satisfying

$$\left(\mathbf{A}_1 \otimes \cdots \otimes \mathbf{A}_n\right)\left(\psi_1 \otimes \cdots \otimes \psi_n\right) \stackrel{\text{def}}{=} \left(\mathbf{A}_1 \psi_1\right) \otimes \cdots \otimes \left(\mathbf{A}_n \psi_n\right),$$

for all $\psi_1 \in \mathbb{H}_1, \ldots, \psi_n \in \mathbb{H}_n$. If $\mathbf{A}_1, \ldots, \mathbf{A}_n$ are bounded then clearly $\mathbf{A}_1 \otimes \cdots \otimes \mathbf{A}_n$ is as well with $\|\mathbf{A}_1 \otimes \cdots \otimes \mathbf{A}_n\| = \|\mathbf{A}_1\| \cdots \|\mathbf{A}_n\|$.

Example 12. Suppose $\left\{\phi_i^k \mid 1 \leqslant i \leqslant d_k\right\}$ is a basis for $\mathbb{H}_k$ in which $\mathbf{A}_k$ has coefficient matrix $\left[a_{ij}^k \mid 1 \leqslant i, j \leqslant d_k\right]$, for $k = 1, \ldots, n$. Then, in basis $\{\phi_{i_1} \otimes \cdots \otimes \phi_{i_n} \mid 1 \leqslant i_1 \leqslant d_1, \cdots, 1 \leqslant i_n \leqslant d_n\}$, the operator $\mathbf{A}_1 \otimes \cdots \otimes \mathbf{A}_n$ has coefficient matrix

$$\left[a_{(i_1 \cdots i_n)(j_1 \cdots j_n)} \mid 1 \leqslant i_1, j_1 \leqslant d_1, \cdots, 1 \leqslant i_n, j_n \leqslant d_n\right]$$

where

$$a_{(i_1 \cdots i_n)(j_1 \cdots j_n)} = a_{i_1 j_1}^1 \cdots a_{i_n j_n}^n. \tag{B.1}$$

This follows from uniqueness by verifying the universal property on basis elements then extending to the whole space.

Definition 35. Let $\mathbf{A}$ be a bounded linear operator on $\mathbb{H}_1 \otimes \cdots \otimes \mathbb{H}_n$. Let $1 \leqslant k \leqslant n$ and $\phi \in \mathbb{H}_k$ be fixed. By the Reisz Representation Theorem [111] there is a unique bounded linear operator $\mathbf{A} \restriction_k \phi$ on $\mathbb{H}_1 \otimes \cdots \otimes \widehat{\mathbb{H}}_k \otimes \cdots \otimes \mathbb{H}_n$ such that for all $\psi_1, \chi_1 \in \mathbb{H}_1, \ldots, \psi_{k-1}, \chi_{k-1} \in \mathbb{H}_{k-1}, \psi_{k+1}, \chi_{k+1} \in \mathbb{H}_{k+1}$, $\ldots, \psi_n, \chi_n \in \mathbb{H}_n$ we have

$$\langle \psi_1 \otimes \cdots \otimes \psi_{k-1} \otimes \psi_{k+1} \otimes \cdots \otimes \psi_n | \left(\mathbf{A} \restriction_k \phi\right)\left(\chi_1 \otimes \cdots \otimes \chi_{k-1} \otimes \chi_{k+1} \otimes \cdots \otimes \chi_n\right)\rangle$$

$$= \psi_1 \otimes \cdots \otimes \psi_{k-1} \otimes \phi \otimes \psi_{k+1} \otimes \cdots \otimes \psi_n$$

$$\mathbf{A}\left(\chi_1 \otimes \cdots \otimes \chi_{k-1} \otimes \phi \otimes \chi_{k+1} \otimes \cdots \otimes \chi_n\right),$$

where the caret $\widehat{}$ above a symbol indicates an item missing from a list; that is, ϕ is inserted into both k^{th} places prior to the application of $\mathbf{A}$ and the inner product. We call $\mathbf{A} \restriction_k \phi$ a **restriction of A** along the kth

dimension.

Definition 36. Let $\mathbf{A}$ be a trace class operator [111] on $\mathbb{H}_1 \otimes \cdots \otimes \mathbb{H}_n$ and let $\phi_1, \phi_2, \cdots$ be an orthonormal basis for $\mathbb{H}_k$ with $1 \leqslant k \leqslant n$. Then the **partial trace of $\mathbf{A}$** along the kth dimension is

$$\mathbf{tr}_k(\mathbf{A}) \stackrel{\text{def}}{=} \sum_{i=1}^{\mathbf{dim}(\mathbb{H}_k)} (\mathbf{A} \restriction_k \phi_i),$$

where the convergence is in the operator norm. Note that $\mathbf{tr}_k(\mathbf{A})$ is a bounded linear operator on $\mathbb{H}_1 \otimes \cdots \otimes \widehat{\mathbb{H}}_k \otimes \cdots \otimes \mathbb{H}_n$.

Remark 31. Since $\mathbf{A}$ is a trace class operator it can be shown that $\mathbf{tr}_k(\mathbf{A})$ exists and is independent of the orthonormal basis chosen.

Example 13. For trace class operators, $\mathbf{A}_1, \ldots, \mathbf{A}_n$, it is easy to check that

$$\mathbf{tr}_k(\mathbf{A}_1 \otimes \cdots \otimes \mathbf{A}_n) = \mathbf{tr}(\mathbf{A}_k) \cdot \mathbf{A}_1 \otimes \cdots \otimes \widehat{\mathbf{A}}_k \otimes \cdots \otimes \mathbf{A}_n$$

APPENDIX C: POISSON RATE FUNCTIONS

This appendix describes various forms of functional data needed for the continous time channel model of Sec. 4.4.3. Note that we use the Markov rate matrix / Poisson rate formulation discussed in Sec. 2.1.2.3.

As input data in the "analysis" direction Sec. 4.4.1, we are given the voltage-gated Markov rate matrix at a fixed temperature $\mathbf{K}\left(V, T_0\right)$, from which we need to derive both the Poisson rate function $\lambda\left(V, T\right)$ and the structural-energy operator $\mathcal{E}\left(V\right)$. This is done in Sec. C.1 for the non-voltage-gated situation. Then Sec. C.2 adjusts the definitions to handle voltage-gating.

In the "synthesis" direction Sec. 4.4.3, we are given the structural-energy operator $\mathcal{E}\left(V\right)$ from which $\lambda\left(V, T\right)$ and the Markov rate matrix $\mathbf{K}\left(V, T\right)$ must be obtained. This is done in Sec. C.3.

Finally, Sec. C.4 shows that these definitions satisfy the model constraints in Sec. 4.4.3.

For any vector $\boldsymbol{\mu}$, let $\mathbf{D}\left[\boldsymbol{\mu}\right]$ denote the diagonal matrix whose diagonal is $\boldsymbol{\mu}$ and for any matrix $\mathbf{A}$, $\mathbf{diag}\left[\mathbf{A}\right]$ is the column vector consisting of the diagonal entries of $\mathbf{A}$.

C.1 $\ \boldsymbol{\lambda}\left(\boldsymbol{T}\right)$ and $\mathbf{E}$ from $\mathbf{K}\left(\boldsymbol{T_0}\right)$

Let $\mathbf{K}\left(T_0\right)$ be a given standard real kinetic rate matrix at a base temperature T_0. Let $\kappa_i\left(T_0\right)$, $i = 1, \ldots, M$ denote the eigenvalues of $\mathbf{K}\left(T_0\right)$. By this is meant that

- All $\kappa_i\left(T_0\right) \geqslant 0$.

- Precisely one $\kappa_i\left(T_0\right) = 0$.

- $\mathbf{1}_M \cdot \mathbf{K}\left(T_0\right) = \mathbf{0}$, where $\mathbf{1}_M \overset{\text{def}}{=} \overbrace{\left[1, 1, \cdots, 1\right]}^{M}$.

- There is a unique vector $\boldsymbol{\pi}_\infty$ (the **equilibrium distribution**) whose entries are all positive, which sums to 1, and for which $\mathbf{K}\left(T_0\right) \cdot \boldsymbol{\pi}_\infty = \mathbf{0}$.

- The **detailed balance** (also called **reversibility**) condition $\mathbf{K}\left(T_0\right) \cdot \mathbf{D}\left[\boldsymbol{\pi}_\infty\right] = \mathbf{D}\left[\boldsymbol{\pi}_\infty\right] \cdot \mathbf{K}\left(T_0\right)^{\mathrm{T}}$ holds.

117

Fix $d > 0$ with dimension temperature and dimensionless $Q_d > 0$ such that

$$Q_d^{1/d} > \left(\frac{\kappa_{\max}(T_0)}{\kappa_{\mathrm{avg}}(T_0)} \right)^{1/T_0},$$

where $\kappa_{\max}(T_0)$ is the largest eigenvalue and $\kappa_{\mathrm{avg}}(T_0)$ is the geometric average of the non-zero eigenvalues: $\kappa_{\mathrm{avg}}(T_0) = \det(\mathbf{K}(T_0) + \boldsymbol{\pi}_\infty \cdot \mathbf{1})$. Note that Hodgkin-Huxley use

$$\begin{cases} T_0 = 279.15^\circ \mathrm{K} \\ d = 10^\circ \mathrm{K} \\ Q_d = 3 \end{cases}$$

so that $Q_d^{T_0/d} \approx 2.1 \times 10^{13}$.

Then $\kappa_{\max}(T_0) < \kappa_{\mathrm{avg}}(T_0) \cdot Q_d^{T_0/d}$. Choose λ_0 such that

$$\kappa_{\max}(T_0) < \lambda_0 < \kappa_{\mathrm{avg}}(T_0) \cdot Q_d^{T_0/d}. \tag{C.1}$$

Definition 37. Define $\mathbf{a}_\infty$ to be the positive vector such that $\mathbf{a}_\infty(i)^2 = \boldsymbol{\pi}_\infty(i)$, for $i = 1, \dots, M$ (which might be written informally as $\mathbf{a}_\infty = \sqrt{\boldsymbol{\pi}_\infty}$). The energy operator is then

$$\mathbf{E} \stackrel{\mathrm{def}}{=} \mathbf{D}[\mathbf{a}_\infty]^{-1} \left(\frac{1}{\lambda_0} \mathbf{K}(T_0) + \boldsymbol{\pi}_\infty \cdot \mathbf{1} \right) \mathbf{D}[\mathbf{a}_\infty]. \tag{C.2}$$

We have

$$-\log \left(\frac{\kappa_{\mathrm{avg}}(T_0)}{\lambda_0} \right) < \frac{T_0}{d} \log Q_d$$

so that

$$E_{\mathrm{avg}} \stackrel{\mathrm{def}}{=} -k_B T_0 \log \left(\frac{\kappa_{\mathrm{avg}}(T_0)}{\lambda_0} \right) < \frac{k_B T_0^2}{d} \log Q_d.$$

Since $\lambda_0 > \kappa_{\max}(T_0) \geqslant \kappa_{\mathrm{avg}}(T_0)$, we can also define

$$E_i \stackrel{\mathrm{def}}{=} -k_B T_0 \log \left(\frac{\kappa_i(T_0)}{\lambda_0} \right),$$

118

for $i = 1, \ldots, M$. Note that E_{avg} is the arithmetic average of the E_i. Thus

$$0 < E_{\text{avg}} < \frac{k_B T_0^2}{d} \log Q_d$$

and we can choose $E_0 > 0$ such that

$$E_{\text{avg}} + E_0 < \frac{k_B T_0^2}{d} \log Q_d.$$

Since

$$\frac{E_{\text{avg}} + E_0}{k_B T_0^2 \log Q_d} < \frac{1}{d}$$

define $d^* > 0$ by

$$\frac{1}{d^*} + \frac{E_{\text{avg}} + E_0}{k_B T_0^2 \log Q_d} = \frac{1}{d}. \tag{C.3}$$

Now, for any $T > 0$, define the Poisson rate and eigenvalues to be

Definition 38.

$$\begin{cases} \lambda(T) \overset{\text{def}}{=} \lambda_0 \, Q_d^{(T-T_0)/d^*} \, e^{-E_0/k_B \cdot (1/T - 1/T_0)} \\ \kappa_i(T) \overset{\text{def}}{=} \lambda(T) \, e^{-E_i/k_B T}, \text{ for } i = 1 \ldots, M. \end{cases} \tag{C.4}$$

C.2 $\boldsymbol{\lambda(V, T)}$ and $\mathbf{E}(V)$ from $\mathbf{K}(V, T_0)$

When the kinetic rate matrix $\mathbf{K}(V, T_0)$ depends on a gating variable V, fix constants $0 < \rho_0, \epsilon_0 < 1$ and modify Eq. C.1 and Eq. C.2 to make uniform choices as follows:

$$\begin{cases} \lambda_0(V) = (1 - \rho_0) \cdot \kappa_{\max}(V, T_0) + \rho_0 \cdot \kappa_{\text{avg}}(V, T_0) \cdot Q_d^{T_0/d} \\ \mathbf{E}(V) \overset{\text{def}}{=} \mathbf{D}\left[\mathbf{a}_\infty(V)\right]^{-1} \left(\mathbf{K}(V, T_0)/\lambda_0 + \boldsymbol{\pi}_\infty(V) \cdot \mathbf{1}\right) \mathbf{D}\left[\mathbf{a}_\infty(V)\right], \end{cases} \tag{C.5}$$

where $\boldsymbol{\pi}_\infty(V)$ is the equilibrium distribution $\mathbf{K}(V, T_0) \cdot \boldsymbol{\pi}_\infty(V) = \mathbf{0}$ at gating level V and $\mathbf{a}_\infty(V) \overset{\text{def}}{=} \sqrt{\mathbf{a}_\infty(V)}$.

Define the number

$$E_0\left(V\right) \stackrel{\text{def}}{=} \epsilon_0 \cdot \left(\frac{k_B\, T_0^2}{d}\, \log Q_d - E_{\text{avg}}\left(V\right)\right),$$

where $E_{\text{avg}}\left(V\right) \stackrel{\text{def}}{=} -k_B T_0 \log\left(\kappa_{\text{avg}}\left(V, T_0\right)/\lambda_0\left(V\right)\right)$.

Then replace the definition Eq. C.3 by

$$\frac{1}{d^*(V)} + \frac{E_{\text{avg}}\left(V\right) + E_0\left(V\right)}{k_B\, T_0^2\, \log Q_d} = \frac{1}{d}$$

and those in Eq. C.4 by

$$\begin{cases} \lambda\left(V, T\right) \stackrel{\text{def}}{=} \lambda_0\left(V\right)\, Q_d^{(T-T_0)/d^*(V)}\, e^{-E_0(V)/k_B \cdot (1/T - 1/T_0)} \\ \kappa_i\left(V, T\right) \stackrel{\text{def}}{=} \lambda\left(V, T\right)\, e^{-E_i(V)/k_B T},\, \text{for } i = 1\ldots, M. \end{cases}$$

C.3 $\boldsymbol{\lambda\left(V, T\right)}$ and $\mathbf{K}\left(\boldsymbol{V, T}\right)$ from $\mathbf{E}\left(V\right)$

Suppose we are given the gated energy matrix $\mathbf{E}\left(V\right)$ and function $E_0\left(V\right) > 0$ such that

$$\frac{E_{\text{avg}}\left(V\right) + E_0\left(V\right)}{k_B\, T_0^2\, \log Q_d} < \frac{1}{d}$$

for every V, where $E_{\text{avg}}\left(V\right)$ is the arithmetic average of the non-zero eigenvalues of $\mathbf{E}\left(V\right)$; i.e., $E_{\text{avg}}\left(V\right) = \mathbf{tr}\left(\mathbf{E}\left(V\right)\right)/\left(M - 1\right)$.

Let $\mathbf{a}_\infty\left(V\right) > 0$ be the unique positive equilibrium distribution $\mathbf{E}\left(V\right) \cdot \mathbf{a}_\infty\left(V\right) = \mathbf{0}$.

Define $d^*(V) > 0$ by

$$\frac{1}{d^*(V)} + \frac{E_{\text{avg}}\left(V\right) + E_0\left(V\right)}{k_B\, T_0^2\, \log Q_d} = \frac{1}{d}.$$

In addition, suppose we are given $\lambda_0\left(V\right) > 0$. Then define

Definition 39.

$$\begin{cases} \lambda\left(V,T\right) \overset{\text{def}}{=} \lambda_0\left(V\right) Q_d^{\left(T-T_0\right)/d^*(V)} e^{-E_0(V)/k_B \cdot \left(1/T - 1/T_0\right)} \\ \mathbf{K}\left(V,T\right) \overset{\text{def}}{=} \lambda\left(V,T\right) \mathbf{D}\left[\mathbf{a}_\infty\left(V\right)\right] e^{-\mathbf{E}(V)/k_B T} \left(\mathbf{I} - \boldsymbol{\pi}_\infty\left(V\right) \cdot \mathbf{1}\right) \mathbf{D}\left[\mathbf{a}_\infty\left(V\right)\right]^{-1}. \end{cases}$$

We now need to verify the $\mathbf{K}\left(V, T_0\right)$ eigenvalue inequalities

$$\kappa_{\max}\left(V, T_0\right) < \lambda_0\left(V\right) < \kappa_{\mathrm{avg}}\left(V, T_0\right) \cdot Q_d^{T_0/d}. \tag{C.6}$$

By diagonalizing we have $\kappa_i\left(V, T_0\right) = \lambda_0\left(V\right) e^{-E_i(V)/k_B T_0}$ so

$$\begin{cases} \kappa_{\max}\left(V, T_0\right) = \lambda_0\left(V\right) e^{-E_{\min}(V)/k_B T_0} \\ \kappa_{\mathrm{avg}}\left(V, T_0\right) = \lambda_0\left(V\right) e^{-E_{\mathrm{avg}}(V)/k_B T_0}. \end{cases}$$

Since $E_{\min}\left(V\right) > 0$, we have $e^{-E_{\min}(V)/k_B T_0} < 1$ so

$$\kappa_{\max}\left(V, T_0\right) = \lambda_0\left(V\right) e^{-E_{\min}(V)/k_B T_0} < \lambda_0\left(V\right)$$

which is the first part of Eq. C.6.

Since

$$\frac{E_{\mathrm{avg}}\left(V\right)}{k_B T_0^2 \log Q_d} < \frac{E_{\mathrm{avg}}\left(V\right) + E_0\left(V\right)}{k_B T_0^2 \log Q_d} < \frac{1}{d},$$

we have $e^{E_{\mathrm{avg}}(V)/k_B T_0} < Q_d^{T_0/d}$ and so

$$1 < e^{-E_{\mathrm{avg}}(V)/k_B T_0} Q_d^{T_0/d} = \kappa_{\mathrm{avg}}\left(V, T_0\right) Q_d^{T_0/d}.$$

Multiplying through by $\lambda_0\left(V\right)$ yields

$$\lambda_0\left(V\right) < \lambda_0\left(V\right) e^{-E_{\mathrm{avg}}(V)/k_B T_0} Q_d^{T_0/d},$$

which is the second part of Eq. C.6.

C.4 Properties of $\boldsymbol{\lambda}\left(\boldsymbol{T}\right)$ and $\boldsymbol{\kappa}_i\left(\boldsymbol{T}\right)$

- For temperatures $T_1 < T_2$ we have

$$
\begin{aligned}
\frac{\kappa_i\left(T_2\right)}{\kappa_i\left(T_1\right)} &= Q_d^{(T_2-T_1)/d^*}\, e^{-(E_i+E_0)/k_B\cdot(1/T_2-1/T_1)} \\
&= Q_d^{(1/d^*+(E_i+E_0)/(k_BT_1T_2))\cdot(T_2-T_1)}.
\end{aligned}
$$

When $T_1, T_2 \approx T_0$, the expression $\left(E_i + E_0\right)/\left(k_BT_1T_2\right)$ cannot differ by much from $\left(E_\text{avg} + E_0\right)/\left(k_BT_0^2\right)$ which, by definition, is $1/d - 1/d^*$. Thus

$$
\frac{\kappa_\text{avg}\left(T_2\right)}{\kappa_\text{avg}\left(T_1\right)} \approx Q_d^{(T_2-T_1)/d}
$$

which is the well-known Q_d rule-of-thumb for reaction rates [26].

- As $T \to 0$,
$$
\lambda\left(T\right) \to \lambda_0\, Q_d^{T_0/d^*}\, e^{E_0/k_BT_0}\, e^{-E_0/k_BT} \to 0
$$

since $E_0 > 0$. So every non-zero eigenvalue

$$
\kappa_i\left(T\right) = \lambda\left(T\right) e^{-E_i/k_bT} \to 0
$$

hence $\mathbf{K}\left(T\right) \to 0$ as $T \to 0$. The channel is **frozen** into its initial state.

- As $T \to \infty$, every $\kappa_i\left(T\right) \to \lambda\left(T\right) \cdot e^0 = \lambda\left(T\right)$ so $\mathbf{K}\left(T\right) \to \lambda\left(T\right)\left(\mathbf{I} - \boldsymbol{\pi}_\infty \cdot \mathbf{1}\right)$. The conformation distributions $\boldsymbol{\pi}\left(t\right)$ associated with these reaction rate matrices thus satisfy

$$
\boldsymbol{\pi}\left(t\right) \to \boldsymbol{\pi}\left(0\right) \cdot e^{-\lambda(T)} + \boldsymbol{\pi}_\infty \cdot \left(1 - e^{-\lambda(T)}\right)
$$

for large T. Since $\lambda\left(T\right) \to \infty$ as $T \to \infty$, $\boldsymbol{\pi}\left(t\right)$ very rapidly transitions from its initial value $\boldsymbol{\pi}\left(0\right)$

to the equilibrium value $\boldsymbol{\pi}_\infty$. For very large T, we thus have

$$\boldsymbol{\pi}\left(t\right) \approx \boldsymbol{\pi}\left(0\right) \cdot \delta\left(t\right) + \boldsymbol{\pi}_\infty \cdot \left(1 - \delta\left(t\right)\right);$$

that is, there is so much available thermal energy that the channel transitions from its structural energy minimum almost instantaneously.

APPENDIX D: PROOFS FOR THE CHANNEL MODELS

Before proving Thm. 5, we prove a lemma which is also used in Sec. 4.4.2. Recall that, for any vector $\boldsymbol{\mu}$, $\mathbf{D}[\boldsymbol{\mu}]$ is the diagonal matrix whose diagonal is $\boldsymbol{\mu}$ and, for any matrix $\mathbf{A}$, $\mathbf{diag}[\mathbf{A}]$ is the column vector consisting of the diagonal entries of $\mathbf{A}$. Also, if A is a complex matrix of any order, then $A^{|2|}$ denotes the real matrix of the same order whose entries are the squared moduli $|a|^2$ of the entries a of A.

Definition 40. A **transition generator** $\mathbf{P}$ is a real $(M \times M)$ matrix with nonnegative eigenvalues, a right 0-eigenvector $[1, \ldots, 1]^{\mathrm{T}}$, and a left 0-eigenvector $[\phi_1, \ldots, \phi_M]$ for which all $\phi_i \geqslant 0$.

A transition generator is **irreducible** if it is of rank $(M-1)$ and all $\phi_i > 0$. It is **reversible** if it satisfies the **Kolmogoroff condition** $P_{ij} \cdot \phi_i = P_{ji} \cdot \phi_j$, for all $1 \leqslant i, j \leqslant M$.

For an irreducible $\mathbf{P}$, the vector $[\phi_1, \ldots, \phi_M]$, normalized to satisfy $\phi_1 + \cdots + \phi_M = 1$, is unique and is called the **equilibrium (or steady-state) probability vector**.

Lemma 5. *Let* $\mathbf{P}$, $\mathbf{E}$ *be* $(M \times M)$ *matrices and* $\boldsymbol{\phi}$, $\boldsymbol{a}$ *be* M-*dimensional row vectors such that* $a_i \neq 0$ *for* $1 \leqslant i \leqslant M$.

Suppose the matrices and vectors are related as

$$
\begin{cases}
\mathbf{P} = \mathbf{D}\left[\boldsymbol{a}^{\mathrm{H}}\right]^{-1} \cdot \mathbf{E} \cdot \mathbf{D}\left[\boldsymbol{a}^{\mathrm{H}}\right] \\
\boldsymbol{\phi} = \boldsymbol{a}^{|2|}.
\end{cases}
$$

Then $\mathbf{P}$ *is an irreducible and reversible transition generator with steady-state probability vector* $\boldsymbol{\phi}$ *if and only* $\mathbf{E}$ *is the matrix of an activation energy operator with resting coefficient vector* $\boldsymbol{a}$.

Proof. Note that, by the assumptions on $\boldsymbol{\phi}$ and $\boldsymbol{a}$, we have $\mathbf{D}[\boldsymbol{\phi}] = \mathbf{D}\left[\boldsymbol{a}^{\mathrm{H}}\right] \cdot \mathbf{D}[\boldsymbol{a}] = \mathbf{D}[\boldsymbol{a}] \cdot \mathbf{D}\left[\boldsymbol{a}^{\mathrm{H}}\right]$.

Also note that the Kolmogoroff condition on $\mathbf{P}$ can be written as $\mathbf{D}[\boldsymbol{\phi}] \cdot \mathbf{P} = \mathbf{P}^{\mathrm{T}} \cdot \mathbf{D}[\boldsymbol{\phi}]$ while the detailed balance condition on $\mathbf{E}$ is $\mathbf{D}[\boldsymbol{s}] \cdot \mathbf{E} = \mathbf{E}^{\mathrm{T}} \cdot \mathbf{D}[\boldsymbol{s}]$, where $s_i \stackrel{\text{def}}{=} a_i/a_i^*$, $1 \leqslant i \leqslant M$.

Finally, when $a_i \neq 0$ for $1 \leqslant i \leqslant K$, it is clear that $\mathbf{P}$ and $\mathbf{E}$ have the same eigenvalues since the eigenvectors are mapped onto each other by the invertible matrix $\mathbf{D}\left[\boldsymbol{a}^{\mathrm{H}}\right]$.

So if $\mathbf{P}$ is irreducible and reversible with steady-state probability vector ϕ then

$$\mathbf{D}\left[a\right] \cdot \mathbf{D}\left[a^{\mathrm{H}}\right] \cdot \mathbf{P} = \mathbf{P}^{\mathrm{T}} \cdot \mathbf{D}\left[a\right] \cdot \mathbf{D}\left[a^{\mathrm{H}}\right]$$

$$\Rightarrow \mathbf{E} = \mathbf{D}\left[a\right]^{-1} \cdot \mathbf{P}^{\mathrm{T}} \cdot \mathbf{D}\left[a\right].$$

By applying the hermitian transpose operator and noting that $\mathbf{P}$ is real by assumption, we obtain

$$\mathbf{E}^{\mathrm{H}} = \mathbf{D}\left[a^{\mathrm{H}}\right] \cdot \mathbf{P} \cdot \mathbf{D}\left[a^{\mathrm{H}}\right]^{-1} = \mathbf{E}$$

and thus $\mathbf{E}$ is hermitian. Also, since $\mathbf{P}$ has positive eigenvalues except for the single eigenvalue 0 of multiplicity 1, the same is true of $\mathbf{E}$. Moreover,

$$\mathbf{D}\left[a\right] \cdot \mathbf{E} = \mathbf{D}\left[a\right] \cdot \mathbf{D}\left[a^{\mathrm{H}}\right] \cdot \mathbf{P} \cdot \mathbf{D}\left[a^{\mathrm{H}}\right]^{-1} = \phi \cdot \mathbf{P} \cdot \mathbf{D}\left[a^{\mathrm{H}}\right]^{-1} = 0 \cdot \mathbf{D}\left[a^{\mathrm{H}}\right]^{-1} = \mathbf{0}$$

so a is a 0-eigenvector of $\mathbf{E}$.

Finally, since we have shown $\mathbf{E} = \mathbf{D}\left[a^{\mathrm{H}}\right]^{-1} \cdot \mathbf{P}^{\mathrm{T}} \cdot \mathbf{D}\left[a^{\mathrm{H}}\right]$, we thus have

$$\mathbf{E} = \mathbf{D}\left[a\right]^{-1} \cdot \left(\mathbf{D}\left[a^{\mathrm{H}}\right]^{-1} \cdot \mathbf{E} \cdot \mathbf{D}\left[a^{\mathrm{H}}\right]\right)^{\mathrm{T}} \cdot \mathbf{D}\left[a\right] = \mathbf{D}\left[s\right]^{-1} \cdot \mathbf{E}^{\mathrm{T}} \cdot \mathbf{D}\left[s\right]$$

since $\mathbf{D}\left[s\right] = \mathbf{D}\left[a^{\mathrm{H}}\right]^{-1} \cdot \mathbf{D}\left[a\right]$ from which detailed balance follows. Therefore $\mathbf{E}$ is the matrix of an activation energy operator with resting coefficient vector a as claimed.

The converse is proved in similar fashion. $\square$

Corollary 5. *Let $\mathbf{P}$ be an irreducible and reversible $(M \times M)$ transition generator with steady-state probability vector ϕ. Then there exist rank-1 matrices $\mathbf{P}_1, \ldots, \mathbf{P}_M$ and positive real numbers $\mu_1, \ldots, \mu_{M-1}$*

satisfying

$$
\begin{cases}
\mathbf{P} = \displaystyle\sum_{i=1}^{M-1} \mu_i \mathbf{P}_i \\[2ex]
\mathbf{I} = \displaystyle\sum_{i=1}^{M} \mathbf{P}_i \\[2ex]
\mathbf{P}_i^2 = \mathbf{P}_i, \quad 1 \leqslant i \leqslant M \\[2ex]
\mathbf{P}_i \cdot \mathbf{P}_j = \mathbf{0}, \ 1 \leqslant i, j \leqslant M, i \neq j.
\end{cases}
$$

Moreover, $\mathbf{P}_M = [1, \ldots, 1]^{\mathrm{T}} \cdot \boldsymbol{\phi}$.

Proof. Define $a_{Mi} \stackrel{\text{def}}{=} \sqrt{\phi_i}$, for $1 \leqslant i \leqslant M$. By Lem. 5, $\mathbf{E} \stackrel{\text{def}}{=} \mathbf{D}\left[\boldsymbol{a}_M\right] \cdot \mathbf{P} \cdot \mathbf{D}\left[\boldsymbol{a}_M\right]^{-1}$ is a real non-negative-definite symmetric matrix of rank $(M-1)$. Moreover, $\boldsymbol{a}_M$ is a norm-1 row eigenvector of eigenvalue 0. Therefore, we can extend $\boldsymbol{a}_M$ to an orthonormal basis $\boldsymbol{a}_1, \ldots, \boldsymbol{a}_{M-1}, \boldsymbol{a}_M$ of row eigenvectors such that $\boldsymbol{a}_i$ has eigenvalue $\mu_i > 0$ for $i \leqslant (M-1)$. Defining the rank-1 matrices $\mathbf{E}_i \stackrel{\text{def}}{=} \boldsymbol{a}_i^{\mathrm{T}} \cdot \boldsymbol{a}_i$ for $1 \leqslant i \leqslant M$, we have

$$
\begin{cases}
\mathbf{E} = \displaystyle\sum_{i=1}^{M-1} \mu_i \mathbf{E}_i \\[2ex]
\mathbf{I} = \displaystyle\sum_{i=1}^{M} \mathbf{E}_i \\[2ex]
\mathbf{E}_i^2 = \mathbf{E}_i, \quad 1 \leqslant i \leqslant M \\[2ex]
\mathbf{E}_i \cdot \mathbf{E}_j = \mathbf{0}, \ 1 \leqslant i, j \leqslant M, i \neq j.
\end{cases}
$$

from which the corollary follows by applying the operator $\mathbf{D}\left[\boldsymbol{a}_M\right]^{-1} (\,\cdot\,) \mathbf{D}\left[\boldsymbol{a}_M\right]$. $\qquad\square$

Proof of Thm. 5. First note that, because $\mathcal{E}$ is irreducible, every $a_{\mathcal{E}i} = \langle \boldsymbol{\phi}_{\mathcal{E}} | \boldsymbol{\psi}_i \rangle \neq 0$ so Constraint 6. holds by definition. Also $\mathbf{D}\left[\boldsymbol{a}_{\mathcal{E}}^{\mathrm{H}}\right]^{-1}$ exists and thus $\boldsymbol{\Pi}\left(\mathcal{E}, T\right)$ is well-defined.

By definition, $\boldsymbol{\phi}_{\mathcal{E}}$ satisfies $\boldsymbol{\phi}_{\mathcal{E}} \cdot \mathcal{E} = 0$ so that $\boldsymbol{a}_{\mathcal{E}} \cdot \mathbf{E} = [0, \ldots, 0]$ and $\mathbf{E} \cdot \boldsymbol{a}_{\mathcal{E}}^{\mathrm{H}} = [0, \ldots, 0]^{\mathrm{T}}$. Hence $\boldsymbol{a}_{\mathcal{E}} \cdot e^{-\mathbf{E}/k_B T} = \boldsymbol{a}_{\mathcal{E}}$ and $e^{-\mathbf{E}/k_B T} \cdot \boldsymbol{a}_{\mathcal{E}}^{\mathrm{H}} = \boldsymbol{a}_{\mathcal{E}}^{\mathrm{H}}$. Recalling the definition $\boldsymbol{\phi}_{\mathcal{E}} \stackrel{\text{def}}{=} \left[|a_{\mathcal{E}1}|^2, \ldots, |a_{\mathcal{E}M}|^2\right]$, we have

$$
\mathbf{D}\left[\boldsymbol{a}_{\mathcal{E}}^{\mathrm{H}}\right]^{-1} \cdot \boldsymbol{a}_{\mathcal{E}}^{\mathrm{H}} \cdot \boldsymbol{a}_{\mathcal{E}} \cdot \mathbf{D}\left[\boldsymbol{a}_{\mathcal{E}}\right] = [1, \ldots, 1]^{\mathrm{T}} \cdot \boldsymbol{\phi}_{\mathcal{E}} \tag{D.1}
$$

and therefore

$$\mathbf{\Pi}\left(\mathcal{E}, T\right) = \mathbf{I} - \left(\mathbf{I} - [1, \dots, 1]^{\mathrm{T}} \cdot \boldsymbol{\phi}_{\mathcal{E}}\right) \cdot e^{-\mathbf{P}_{\mathcal{E}}/k_B T}, \tag{D.2}$$

where $\mathbf{P}_{\mathcal{E}} \stackrel{\text{def}}{=} \mathbf{D}\left[a_{\mathcal{E}}^{\mathrm{H}}\right]^{-1} \cdot \mathbf{E} \cdot \mathbf{D}\left[a_{\mathcal{E}}^{\mathrm{H}}\right]$.

By Lem. 5, $\mathbf{P}_{\mathcal{E}}$ is an irreducible and reversible transition generator with steady-state probabilities $\pi_{\mathcal{E}i} = |a_{\mathcal{E}i}|^2$. Since $\boldsymbol{\phi}_{\mathcal{E}} \cdot \mathbf{P}_{\mathcal{E}} = \mathbf{0}$, (D.2) reduces to

$$\begin{aligned}
\mathbf{\Pi}\left(\mathcal{E}, T\right) &= [1, \dots, 1]^{\mathrm{T}} \cdot \boldsymbol{\phi}_{\mathcal{E}} + \mathbf{I} - e^{-\mathbf{P}_{\mathcal{E}}/k_B T} \\
&= [1, \dots, 1]^{\mathrm{T}} \cdot \boldsymbol{\phi}_{\mathcal{E}} + \sum_{i=1}^{M-1} \left(1 - e^{-\mu_{\mathcal{E}i}/k_B T}\right) \mathbf{P}_{\mathcal{E}i}
\end{aligned} \tag{D.3}$$

where all $\mu_{\mathcal{E}i} > 0$ using Cor. 5.

From the first form, we have $\boldsymbol{\phi}_{\mathcal{E}} \cdot \mathbf{\Pi}\left(\mathcal{E}, T\right) = \boldsymbol{\phi}_{\mathcal{E}} \cdot [1, \dots, 1]^{\mathrm{T}} \cdot \boldsymbol{\phi}_{\mathcal{E}} + \boldsymbol{\phi}_{\mathcal{E}} - \boldsymbol{\phi}_{\mathcal{E}} = \boldsymbol{\phi}_{\mathcal{E}}$ which is Constraint 2. From the second form, as $T \to 0$, we have

$$[1, \dots, 1]^{\mathrm{T}} \cdot \boldsymbol{\phi}_{\mathcal{E}} + \sum_{i=1}^{M-1} \left(1 - e^{-\mu_{\mathcal{E}i}/k_B T}\right) \mathbf{P}_{\mathcal{E}i} \to \mathbf{P}_{\mathcal{E}0} + \sum_{i=1}^{M-1} \mathbf{P}_{\mathcal{E}i} = \mathbf{I}$$

which is Constraint 3 while as $T \to \infty$

$$[1, \dots, 1]^{\mathrm{T}} \cdot \boldsymbol{\phi}_{\mathcal{E}} + \sum_{i=1}^{M-1} \left(1 - e^{-\mu_{\mathcal{E}i}/k_B T}\right) \mathbf{P}_{\mathcal{E}i} \to [1, \dots, 1]^{\mathrm{T}} \cdot \boldsymbol{\phi}_{\mathcal{E}}$$

which is Constraint 4.

The Kolmogoroff condition holds for $\mathbf{\Pi}\left(\mathcal{E}, T\right)$ because, by Lem. 5, it holds for $\mathbf{P}_{\mathcal{E}}$ and obviously holds as well for the terms $[1, \dots, 1]^{\mathrm{T}} \cdot \boldsymbol{\phi}_{\mathcal{E}} + \mathbf{I}$. Thus Constraint 5. is satisfied.

Since $[1, \dots, 1]^{\mathrm{T}}$ is a right eigenvector of $\mathbf{P}_{\mathcal{E}}$ of eigenvalue 0, the first equality in (D.3) shows $[1, \dots, 1]^{\mathrm{T}}$ is a right eigenvector of $\mathbf{\Pi}\left(\mathcal{E}, T\right)$ of eigenvalue 1. Let $\Pi_{ij}\left(\mathcal{E}, T\right)$ denote the entries of $\mathbf{\Pi}\left(\mathcal{E}, T\right)$. Constraint 3. implies $\liminf_{T \to \infty} \Pi_{ij}\left(\mathcal{E}, T\right) = \pi_{\mathcal{E}i} > 0$ so there is a T_{ij} such that $\Pi_{ij}\left(\mathcal{E}, T\right) > 0$ for all $T \geqslant T_{ij}$. Defining $T_{\mathcal{E}} \stackrel{\text{def}}{=} \max_{1 \leqslant i, j \leqslant M} T_{ij}$ we conclude that $\mathbf{\Pi}\left(\mathcal{E}, T\right)$ is a valid discrete Markov transition matrix for $T \geqslant T_{\mathcal{E}}$. Therefore Constraint 1. is satisfied. $\qquad\square$

APPENDIX E: PROOF OF THE MAXIMUM ENTROPY NOISE

PROPERTY FOR POPULATIONS OF QUANTUM ION CHANNELS

E.1 The Autocovariance of a Hidden Markov Model

This section presents the general form of the results first derived (incorrectly[1]) by Hill & Chen [32] and widely reproduced thereafter [33, 72].

Let

$$p^{G}_{t_1,\ldots,t_n}(g_1,\ldots,g_n) = \sum_{j_1,\ldots,j_n} f_{j_1}(g_1)\cdots f_{j_n}(g_n)\,\pi_{t_1,\ldots,t_n}(j_1,\ldots,j_n) \tag{E.1}$$

be the distribution function of a hidden Markov model $G(t)$ with hidden Markov process $I(t)$.

Clearly the mean $\mu_G(t)$ is given by

$$\mu_G(t) \overset{\text{def}}{=} \mathsf{E}\left[G(t)\right] = \sum_j \mu_{f,j}\,\pi_t(j),$$

where $\mu_{f,j} \overset{\text{def}}{=} \int g\,f_j(g)\,dg$. We write this as

$$\mu_G(t) = \boldsymbol{\mu}_f \cdot \boldsymbol{\pi}(t), \tag{E.2}$$

for row vector $\boldsymbol{\mu}_f$ and column vector $\boldsymbol{\pi}(t)$.

Because of the Markov property, for $t \neq s$, we easily calculate the moments

$$\mathsf{E}\left[G(t)\,G(s)\right] = \sum_{j,i} \mathsf{E}\left[G(t)\,G(s) \mid I(t) = j, I(s) = i\right]\pi_{t,s}(j,i)$$

$$= \sum_{j,i} \mu_{f,j}\,\mu_{f,i}\,\pi_{t,s}(j,i)$$

which we write as

$$\mathsf{E}\left[G(t)\,G(s)\right] = \boldsymbol{\mu}_f \cdot \boldsymbol{\Pi}(t,s) \cdot \boldsymbol{\mu}_f^{\mathsf{T}}, \tag{E.3}$$

where $\boldsymbol{\Pi}(t,s)$ is the matrix with components $\Pi_{j,i}(t,s) \overset{\text{def}}{=} \pi_{t,s}(j,i)$.

---

[1]Note: Hill & Chen assumed the ergodic property for Markov processes rather than proving it.

When $t = s$, we have

$$\mathsf{E}\left[G\left(t\right)^2\right] = \sum_j \mathsf{E}\left[G\left(t\right)^2 \mid I\left(t\right) = j\right] \pi_t\left(j\right) = \boldsymbol{\mu}_f^{(2)} \cdot \boldsymbol{\pi}\left(t\right), \tag{E.4}$$

where $\mu_{f,j}^{(2)} \overset{\text{def}}{=} \int g^2 f_j\left(g\right) dg$.

Using Eq. E.3 and Eq. E.4, we can derive the autocovariance function

$$R_G\left(t, s\right) = \begin{cases} \boldsymbol{\mu}_f \cdot R_I\left(t, s\right) \cdot \boldsymbol{\mu}_f^{\mathrm{T}} & t \neq s \\ \boldsymbol{\mu}_f^{(2)} \cdot \boldsymbol{\pi}\left(t\right) - \left(\boldsymbol{\mu}_f \cdot \boldsymbol{\pi}\left(t\right)\right)^2 & t = s, \end{cases}$$

where $R_I\left(t, s\right) \overset{\text{def}}{=} \boldsymbol{\Pi}\left(t, s\right) - \boldsymbol{\pi}\left(t\right) \cdot \boldsymbol{\pi}\left(t\right)^{\mathrm{T}}$. By calculating the discontinuity in these cases as $t \to s$, we can write this as

$$R_G\left(t, s\right) = \boldsymbol{\mu}_f \cdot R_I\left(t, s\right) \cdot \boldsymbol{\mu}_f^{\mathrm{T}} + \boldsymbol{\sigma}_f^2 \cdot \boldsymbol{\pi}\left(s\right) \delta\left(t - s\right),$$

where $\boldsymbol{\sigma}_f^2$ is the row vector of standard deviations calculated from all the $f_j\left(g\right)$ condtional distributions.

Letting $\mathbf{K}$ be the Markov rate matrix, the Chapman-Kolmogoroff Equations imply, for $t \geqslant s$,

$$R_G\left(t, s\right) = \boldsymbol{\mu}_f \cdot e^{-(t-s)\mathbf{K}} \cdot R_I\left(s\right) \cdot \boldsymbol{\mu}_f^{\mathrm{T}} + \boldsymbol{\sigma}_f^2 \cdot \boldsymbol{\pi}\left(s\right) \delta\left(t - s\right), \tag{E.5}$$

where $R_I\left(s\right) \overset{\text{def}}{=} \boldsymbol{\Pi}\left(s, s\right) - \boldsymbol{\pi}\left(s\right) \cdot \boldsymbol{\pi}\left(s\right)^{\mathrm{T}}$.

Now, when the the system is initiated in the equilibrium distribution $\boldsymbol{\pi}\left(0\right) = \boldsymbol{\pi}_\infty$, then $R_I\left(s\right) = R_\infty \overset{\text{def}}{=} \boldsymbol{\Pi}_\infty - \boldsymbol{\pi}_\infty \cdot \boldsymbol{\pi}_\infty^{\mathrm{T}}$ independent of s, where $\boldsymbol{\Pi}_\infty$ is the diagonal matrix with diagonal $\boldsymbol{\pi}_\infty$. So $G\left(t\right)$ is 2nd–order stationary with autocovariance function

$$R_G\left(t\right) = \boldsymbol{\mu}_f \cdot e^{-|t|\mathbf{K}} \cdot R_\infty \cdot \boldsymbol{\mu}_f^{\mathrm{T}} + \boldsymbol{\sigma}_f^2 \cdot \boldsymbol{\pi}_\infty \delta\left(t\right). \tag{E.6}$$

Remark 32. The term $\boldsymbol{\sigma}_f^2 \cdot \boldsymbol{\pi}_\infty \delta\left(t\right)$ adds a white noise floor to the spectrum of $G\left(t\right)$ caused by "sputter" $\boldsymbol{\sigma}_f^2$ in the conductances. That is, some channel conformations may be neither fully open nor fully closed to

the passage of ions.

E.2 Proof of Thm. 6

We prove the single-species form of the GVZM formula Eq. 5.1. A slightly more sophisticated argument will yield the multi-channel. Let the species have M conformations. Fix a gating level V. Let $\mathbf{D}[\psi]$ denote the diagonal matrix with diagonal ψ.

Let X be a population of statistically independent ion channels in contact with a thermal bath at temperature T and let ρ be a probability measure on X [80] representing the channel density. Extend ρ to the "neurological measure space" $\mathbb{X} \overset{\text{def}}{=} \{1, \ldots, M-1\} \times X$ by using the counting measure [78] on the first factor. Let the suffix "(x)" indicate parameterization by $x \in X$.

Let the eigenvalues of $\mathcal{E}(x)$ be $E_0(x), \ldots, E_{M-1}(x)$, where $E_0(x)$ is the minimum energy value corresponding to the eigenvector $\phi_{\mathcal{E}(x)}$. From Sec. 4.4.2, Def. 17 and Sec. 4.4.3, Def. 18, we can extract the rate matrix $\mathbf{K}(x)$ (cf. Sec. 2.1.2.3), in a coherence basis for $\mathcal{E}(x)$ in which $\phi_{\mathcal{E}(x)}$ is the first basis element:

$$
\begin{aligned}
\mathbf{K}(x) &= \lambda(T)(\mathbf{I} - \mathbf{\Pi}(\mathcal{E}(x), T)) \\
&= \lambda(T)\,\mathbf{J}(x) \cdot \left(e^{-(\mathcal{E}(x) - E_0(x)\mathbf{I})/k_B T} - \mathbf{\Phi}_{\mathcal{E}(x)} \right) \cdot \mathbf{J}(x)^{-1} \\
&= \lambda(T)\,\mathbf{J}(x) \cdot \mathbf{U}(x) \cdot \mathbf{J}(x)^{-1},
\end{aligned}
\tag{E.7}
$$

where

$$
\mathbf{U}(x) \overset{\text{def}}{=} \mathbf{D}\left[0, e^{-(E_1(x) - E_0(x))/k_B T}, \ldots, e^{-(E_{M-1}(x) - E_0(x))/k_B T} \right]
$$

and $\mathbf{\Phi}_{\mathcal{E}(x)} = |\phi_{\mathcal{E}(x)}\rangle \cdot \langle \phi_{\mathcal{E}(x)}|$. We leave $\mathbf{J}(x)$ unspecified for now except for the defining conditions from Sec. 4.4.2, Eq. 4.5.

Define

$$
\tau_i(x) \overset{\text{def}}{=} \frac{1}{\lambda(T)}
\begin{cases}
e^{(E_i(x) - E_0(x))/k_B T}, & i = 1, \ldots, M-1 \\
\infty, & i = 0
\end{cases}
\tag{E.8}
$$

132

so we can write $\lambda\left(T\right)\mathbf{U}\left(x\right) = \mathbf{D}\left[1/\tau_0\left(x\right), \ldots, 1/\tau_{M-1}\left(x\right)\right]$.

Using Eq. E.6 (without the white noise term due to sputter), we have autocovariance

$$R_G\left(x,t\right) = \boldsymbol{\mu}_f \cdot e^{-|t|\mathbf{K}\left(x\right)} \cdot R_\infty\left(x\right) \cdot \boldsymbol{\mu}_f^{\mathrm{T}}, \tag{E.9}$$

where $R_\infty\left(x\right) \stackrel{\text{def}}{=} \mathbf{\Pi}_\infty\left(x\right) - \boldsymbol{\pi}_\infty\left(x\right) \cdot \boldsymbol{\pi}_\infty\left(x\right)^{\mathrm{T}}$ with $\mathbf{\Pi}_\infty\left(x\right) \stackrel{\text{def}}{=} \mathbf{D}\left[\boldsymbol{\pi}_\infty\left(x\right)\right]$. (Note that the conductance means $\boldsymbol{\mu}_f$ do not depend on x since we are assuming a single channel species.) Using Eq. E.7 and the equation $\mathbf{K}\left(x\right) \cdot \boldsymbol{\pi}_\infty\left(x\right) = \mathbf{0}$, after some simplification this becomes

$$R_G\left(x,t\right) = \left(\boldsymbol{\mu}_f \cdot \mathbf{J}\left(x\right)\right) \cdot \mathbf{V}\left(x\right) \cdot \left(\mathbf{J}\left(x\right)^{-1} \cdot \boldsymbol{\mu}_f^{\mathrm{T}}\right) - \left(\boldsymbol{\mu}_f \cdot \boldsymbol{\pi}_\infty\left(x\right)\right)^2, \tag{E.10}$$

where $\mathbf{V}\left(x\right) \stackrel{\text{def}}{=} \mathbf{D}\left[e^{-|t|/\tau_0\left(x\right)}, \ldots e^{-|t|/\tau_{M-1}\left(x\right)}\right]$. (Note $e^{-|t|/\tau_0\left(x\right)} = 1$ for every t.) Since the channels are independent with population density ρ, the total autocovariance is

$$R_G\left(t\right) = \int_X R_G\left(x,t\right) d\rho\left(x\right). \tag{E.11}$$

Now, define the partition function [105]

$$Z\left(\theta\right) \stackrel{\text{def}}{=} \int_{\mathbb{X}} \frac{1}{\tau_i\left(x\right)^{2-\theta}} \, d\rho\left(i,x\right), \tag{E.12}$$

where $\tau_i\left(x\right)$ was defined by Eq. E.8. Let $\theta\left(\overline{\Delta E}\right) \in \mathbb{R}$ solve the rate equation

$$\int_{\mathbb{X}} \frac{\log\left(\tau_i\left(x\right)\right)}{\tau_i\left(x\right)^{2-\theta}} \, d\rho\left(i,x\right) = Z\left(\theta\right)\left(\frac{\overline{\Delta E}}{k_B T} - \log\left(\lambda\left(T\right)\right)\right) \tag{E.13}$$

for energy parameter $\overline{\Delta E}$. It is well-known [106] that the parameterized distribution function

$$g\left(\overline{\Delta E}, i, x\right) \stackrel{\text{def}}{=} \frac{1}{Z\left(\theta\right)} \frac{1}{\tau_i\left(x\right)^{2-\theta}} = \frac{1}{Z\left(\theta\right)} e^{-(2-\theta)\log\left(\tau_i\left(x\right)\right)} \tag{E.14}$$

with $\theta = \theta(\overline{\Delta E})$ is the maximum entropy distribution function under the constraint Eq. E.15. But this constraint is easily seen to be equivalent to the energy equation

$$\int_{\mathbb{X}} (E_i(x) - E_0(x)) \, g\left(\overline{\Delta E}, i, x\right) \, d\rho(i, x) = \overline{\Delta E}. \tag{E.15}$$

Therefore: $g\left(\overline{\Delta E}, i, x\right)$, as defined by Eq. E.14, is the maximum entropy distribution solving the required energy constraint.

Now, for each $x \in X$, choose the matrix $\mathbf{J}(x)$ not only to satisfy defining conditions

$$\begin{cases} \mathbf{1} \cdot \mathbf{J}(x) = \phi_{\mathcal{E}}^{\mathrm{H}} \\ \mathbf{J}(x) \cdot \phi_{\mathcal{E}} = \phi_{\mathcal{E}}^{|2|} \end{cases}$$

from Sec. 4.4.2, Eq. 4.5 but, in addition,

$$\begin{cases} \boldsymbol{\mu}_f \cdot \mathbf{J}(x) = \left[\boldsymbol{\mu}_f \cdot \boldsymbol{\pi}_\infty(x), \sqrt{g\left(\overline{\Delta E}, 1, x\right)}, \dots \sqrt{g\left(\overline{\Delta E}, M-1, x\right)}\right] \\ \mathbf{J}(x) \cdot \left[\boldsymbol{\mu}_f \cdot \boldsymbol{\pi}_\infty(x), \sqrt{g\left(\overline{\Delta E}, 1, x\right)}, \dots \sqrt{g\left(\overline{\Delta E}, M-1, x\right)}\right]^{\mathrm{T}} = \boldsymbol{\mu}_f^{\mathrm{T}}. \end{cases} \tag{E.16}$$

Substituting Eq. E.16 into Eq. E.10 and Eq. E.11 then yields

$$\begin{aligned} R_G(t) &= \int_{\mathbb{X}} e^{-|t|/\tau_i(x)} g\left(\overline{\Delta E}, i, x\right) \, d\rho(i, x) \\ &\propto \int_{\mathbb{X}} e^{-|t|/\tau_i(x)} \frac{1}{\tau_i(x)^{2-\theta}} \, d\rho(i, x), \end{aligned} \tag{E.17}$$

the GVZM autocovariance function with spectral exponent $\theta = \theta(\overline{\Delta E})$. $\qquad\square$

Remark 33. Equations Eq. E.8, Eq. E.14, and Eq. E.15 show the precise mechanism by which the spectral exponent θ is determined. It is seen to arise from entropy equilibrium rather than any purported self–similarity or dynamical system structure (Sec. 2.2.1). Its temperature– and energy–dependence also suggests various experimental procedures to test the theory. Moreover, Thm. 6 reveals Hill & Chen (Sec. 2.2.5) to have

been mistaken in their assertion that ion channel kinetics could not account for $1/f$–type noise. We have shown that, if channels are controlled by hidden quantum layers, then such noises may be generated by simple mechanisms.

Remark 34. It is interesting to observe that the entire theory of energy–gated, quantum–controlled ion channels was developed simply to create sufficiently–many degrees of freedom to obtain Eq. E.16 and thus make Hill & Chen's classic channel autocovariance function Sec. 5.1, Eq. 5.4 look like Eq. E.17. However, having solved the technical problem of generating $1/f^\theta$–type noise, we expect the quantum channel model to have applications in many areas of theoretical and applied neuroscience.

APPENDIX F: THE PERIODOGRAM DISTRIBUTION OF PERIODIC ARMA PROCESSES

This appendix[1] presents the background for a useful class of random processes we call $ARMA(P, Q, N)$ processes.

Definition 41. For this article, the single-epoch **periodogram** of a discrete-time signal $x(n)$, $0 \leqslant n \leqslant N - 1$, is defined by

$$S_x(k) \overset{\text{def}}{=} \frac{2\pi}{N} |X(k)|^2, \quad 0 \leqslant k \leqslant N - 1,$$

where

$$X(k) \overset{\text{def}}{=} \sum_{n=0}^{N-1} x(n) \; e^{-i(2\pi/N)kn}$$

is the DFT of $x(n)$ [16]. The factor 2π converts the frequency unit from radians/sec to Hz.

Definition 42. A real Gaussian $\boldsymbol{ARMA\,(P, Q, N)}$ **process** is a zero-mean, stationary random process $\{x(n)\}_{n=-\infty}^{\infty}$ satisfying

$$\sum_{p=0}^{P} a_p \, x(n - p) = \sum_{q=0}^{Q} b_q \, \nu(n - q), \tag{F.1}$$

where $a_0 = b_0 = 1$ and $\{\nu(n)\}_{n=-\infty}^{\infty}$ is an iid zero-mean, Gaussian process which is N-periodic: $\nu(n + N) = \nu(n)$, for all n. The equality in the periodicity condition is meant to be exact; i.e., there are really only N distinct random processes $\nu(0), \ldots, \nu(N - 1)$.

We note that the stationarity condition excludes transient solutions. Any stationary solution $x(n)$ of (F.1) must then be N–periodic as well. (The issue of existence and uniqueness of these solutions will not be discussed here. See [56] for a discussion of the $N = \infty$ case). For simplicity, we always assume the polynomials $A(z) = \sum_{p=0}^{P} a_p z^p$ and $B(z) = \sum_{q=0}^{Q} b_q z^q$ have no common zeros.

Definition 43. An $ARMA\,(P, Q, N)$ system is **causal** [56] if the polynomial $A(z)$ defined above has no zeros on or inside the unit circle.

Definition 44. The single-epoch **periodogram** of a discrete-time signal $x(n)$, $0 \leqslant n \leqslant N - 1$, is defined as

---

[1]Portions of this appendix have appeared in [2].

137

$$S_x(k) \stackrel{\text{def}}{=} \frac{2\pi}{N} |X(k)|^2, \quad 0 \leqslant k \leqslant N-1,$$

where

$$X(k) \stackrel{\text{def}}{=} \sum_{n=0}^{N-1} x(n) \; e^{-i(2\pi/N)kn}$$

is the discrete Fourier transform (DFT) of x [16].

Theorem 10. *Let $x(0), \ldots, x(N-1)$ be one period of a causal Gaussian $ARMA(P, Q, N)$ process and let $S_x(k)$, $0 \leqslant k \leqslant N-1$ be its periodogram. Then*

$$S_x(k) = 2\pi \sigma_\nu^2 \cdot \frac{\left| B\left(e^{-i(2\pi k/N)}\right) \right|^2}{\left| A\left(e^{-i(2\pi k/N)}\right) \right|^2} \cdot (1/2) \, \Xi(k),$$

where $\Xi(k)$, $0 \leqslant k \leqslant N-1$, is a sequence of $\chi^2(2)$ distributed [93] random variables which are independent for $0 \leqslant k, l < N/2$ when $k \neq l$ and σ_ν^2 is the variance of $\nu(n)$.

Proof. By N–periodicity, the summations in (F.1) are circular convolutions [16] of length N. Standard results on the discrete Fourier transform then imply

$$S_x(k) = \frac{\left| B\left(e^{-i(2\pi k/N)}\right) \right|^2}{\left| A\left(e^{-i(2\pi k/N)}\right) \right|^2} \cdot S_\nu(k),$$

where $S_\nu(k)$ is the periodogram of the random period $\nu(0), \ldots, \nu(N-1)$. It is therefore sufficient to prove

$$S_\nu(k) = \pi \sigma_\nu^2 \cdot \Xi(k),$$

where $\Xi(k)$, $k = 0, \ldots, N-1$ is as in the theorem.

Since $\nu\,(\,\cdot\,)$ is real we have

$$
\begin{cases}
\mathbf{Re}\,[S_\nu\,(k)] = \displaystyle\sum_{n=0}^{N-1} \nu\,(n)\,\cos\,(2\pi k/N) \\[4mm]
\mathbf{Im}\,[S_\nu\,(k)] = -\displaystyle\sum_{n=0}^{N-1} \nu\,(n)\,\sin\,(2\pi k/N).
\end{cases}
\tag{F.2}
$$

The equations

$$
\begin{cases}
\displaystyle\sum_{n=0}^{N-1} \cos\,(2\pi l/N)\cos\,(2\pi k/N) = \dfrac{N}{2}\,(\delta\,(k-l) + \delta\,(k+l)) \\[4mm]
\displaystyle\sum_{n=0}^{N-1} \sin\,(2\pi l/N)\sin\,(2\pi k/N) = \dfrac{N}{2}\,(\delta\,(k-l) - \delta\,(k+l)) \\[4mm]
\displaystyle\sum_{n=0}^{N-1} \sin\,(2\pi l/N)\cos\,(2\pi k/N) = 0,
\end{cases}
\tag{F.3}
$$

where $k-l$ and $k+l$ are computed $\mathrm{mod}\,N$, follow from the inverse DFT equations.

Since $\nu\,(0),\ldots,\nu\,(N-1)$ are independent, zero-mean Gaussians with variance σ_ν^2, we have $\mathsf{E}\,[\nu\,(n)\,\nu\,(m)] = \sigma_\nu^2\delta\,(n-m)$. Together with (F.2) and (F.3), this implies $\mathbf{Re}\,[S_\nu\,(k)]$ and $\mathbf{Im}\,[S_\nu\,(k)]$ are uncorrelated, hence independent, Gaussians with variance $N\sigma_\nu^2/2$. Moreover, the same reasoning shows that all $\mathbf{Re}\,[S_\nu\,(k)]$ are independent of all $\mathbf{Im}\,[S_\nu\,(l)]$ and that the pairs $\mathbf{Re}\,[S_\nu\,(k)]$, $\mathbf{Re}\,[S_\nu\,(l)]$ and $\mathbf{Im}\,[S_\nu\,(k)]$, $\mathbf{Im}\,[S_\nu\,(l)]$ are independent for $0 \leqslant k, l < N/2$ when $k \neq l$.

Then, by definition of the $\chi^2\,(2)$ distribution [93],

$$
S_\nu\,(k) = \frac{2\pi}{N}\left(\mathbf{Re}\,[S_\nu\,(k)]^2 + \mathbf{Im}\,[S_\nu\,(k)]^2\right) \sim \pi\sigma_\nu^2 \cdot \chi^2\,(2)
$$

with the independence results following from the previous paragraph.

$\square$

APPENDIX G: SYMBOLS AND CONVENTIONS

- "$\stackrel{\text{def}}{=}$" means "equal by definition" and "$\stackrel{\text{def}}{\Longleftrightarrow}$" means "logically equivalent by definition."

- The symbol "$\subseteq$" will be used for subset containment (rather than "$\subset$"). The symbol "$\backslash$" will denote set difference.

- For a function $f : X \to Y$ and $E \subseteq Y$, $f^{-1}[E] \stackrel{\text{def}}{=} \{x \in X \mid f(x) \in E\}$.

- $\chi_E(x)$ denotes the characterstic or indicator function of the set E: $\chi_E(x) = 1$, if $x \in E$, while $\chi_E(x) = 0$ otherwise.

- The $\mapsto$ arrow abbreviates "maps to."

- Function composition may be made explicit using the symbol $\circ$.

- Non-italic superscript $(\,\cdot\,)^{\text{T}}$ denotes the matrix transpose without complex conjugation.

- Unless otherwise indicated, the scalar field is the complex numbers $\mathbb{C}$.

- $\mathbb{N}$ are the non-negative integers.

- $\aleph_0$ is the smallest infinite cardinal; i.e., cardinality of $\mathbb{N}$.

- $\mathbb{H}$ denotes a general Hilbert space and $\mathbb{H}^{\otimes n} \stackrel{\text{def}}{=} \overbrace{\mathbb{H} \otimes \cdots \otimes \mathbb{H}}^{n}$.

- $\mathcal{B}(\mathbb{H})$ are the bounded linear operators on $\mathbb{H}$, $\mathcal{T}(\mathbb{H}) \subseteq \mathcal{B}(\mathbb{H})$ are the trace class operators, and $\mathcal{S}(\mathbb{H}) \subseteq \mathcal{T}(\mathbb{H})$ are the states. $\mathbf{I}_\mathbb{H}$ is the identity operator on $\mathbb{H}$.

- $(\,\cdot\,)^*$ is complex conjugation applied to scalars, vectors, or matrices, $|z| = \sqrt{z \cdot z^*}$ is absolute value, and $\mathbf{sgn}(z) \stackrel{\text{def}}{=} z^*/|z|$ is the complex sign function.

- $(\,\cdot\,)^{\text{H}}$ is the hermitian transpose $((\,\cdot\,)^*)^{\text{T}}$.

- If A is a complex matrix of any order, then $A^{|2|}$ denotes the real matrix of the same order whose entries are the squared moduli $|a|^2$ of the entries a of A. (cf. Thm. 3 for the use of this operation.)

- $\mathbf{I}_M$ is the $(M \times M)$ identity matrix or operator with the subscript omitted if it is clear from context.

- $\mathbf{det}(\,\cdot\,)$ is the determinant.

- $\mathbf{D}\left[\boldsymbol{\mu}\right]$ is the diagonal matrix whose diagonal is the (row or column) vector $\boldsymbol{\mu}$. For any square matrix $\mathbf{A}$, $\mathbf{diag}\left[\mathbf{A}\right]$ is the column vector of the diagonal elements of $\mathbf{A}$. Thus $\mathbf{diag}\left[\mathbf{D}\left[\boldsymbol{\mu}\right]\right] = \boldsymbol{\mu}$.

- $\mathbf{tr}\left(\,\cdot\,\right)$ is the trace operator on square matrices or trace class operators.

- For any $M > 1$, $\mathbf{1}_M$ is the row vector $\mathbf{1}_M \overset{\text{def}}{=} \overbrace{[1, 1, \cdots, 1]}^{M}$.

- $\mathbf{Sp}\left(\mathbf{A}\right)$ is the spectrum of the normal operator A: $\mathbf{Sp}\left(\mathbf{A}\right) \overset{\text{def}}{=} \{\alpha \in \mathbb{C} \mid (\alpha \cdot \mathbf{I}_{\mathbb{H}} - \mathbf{A}) \text{ has no inverse}\}$.

- Unless otherwise indicated, "vector" means "column vector." Note this is the dual of the most common convention for Markov processes so certain expressions such as the Chapman-Kolmogoroff Equations ([79]) may appear transposed.

- $\delta\left(t\right)$ is the delta function.

- $\mathsf{E}\left[\,\cdot\,\right]$ is the expected-value operator, $\mathsf{Var}\left[\,\cdot\,\right]$ is variance, and $\mathsf{Prob}\left(\,\cdot\,\right)$ will be used informally for "the probability of".

- The caret $\widehat{\cdot}$ above a symbol indicates a item removed from a list. Thus $w, x, \widehat{y}, z$ is the list w, x, z. The empty-set symbol $\emptyset$ also denotes an empty list.

- The symbols "i, j" will always be used as integer indices and never to denote the imaginary unit $\sqrt{-1}$.

- When required, Hilbert spaces will be assumed to be separable and all bounded normal operators will be assumed to be compact [109] so that an orthonormal basis of eigenvectors and a countable spectral decomposition exist.

- h is Planck's constant with units Joule-sec.

- k_B is Boltzmann's constant with units Joule/°K.

- η is a dimensionless Markov transition efficiency.

- Italic "T" denotes absolute temperature with units °K.

LIST OF REFERENCES

[1] A. Paris, G. Atia, A. Vosoughi, and S. Berman, "Formalized Quantum Stochastic Processes and Hidden Quantum Models with Applications to Neuron Ion Channel Kinetics," [Online], 2015, Available: http://arXiv.org/abs/1511.00057.

[2] ——, "A New Statistical Model of Electroencephalogram Noise Spectra for Real-time Brain-Computer Interfaces," *IEEE Trans. Biomed. Eng.*, 2016, [To Appear] ©2016 IEEE.

[3] ——, "Causal filtering for $1/f^\alpha$-type noise in single-electrode EEG signals," in *Proc. 38th Annual International Conference of the IEEE EMBS*, Orlando, FL, USA, 2016.

[4] D. J. McFarland and J. R. Wolpaw, "Brain-computer interfaces for communication and control," *Communications of the ACM*, vol. 54, no. 5, pp. 60–66, 2011.

[5] Y. Wang, R. Wang, X. Gao, B. Hong, and S. Gao, "A practical VEP-based brain-computer interface," *IEEE Trans. Biomed. Eng.*, vol. 14, no. 2, pp. 234–239, 2006.

[6] B. Z. Allison, D. J. McFarland, G. Schalk, S. D. Zheng, M. M. Jackson, and J. R. Wolpaw, "Towards an independent brain-computer interface using steady state visual evoked potentials," *Clin. Neurophysiol.*, vol. 119, no. 2, pp. 399–408, 2008.

[7] J. J. Daly and J. R. Wolpaw, "Brain-computer interfaces in neurological rehabilitation," *Lancet Neurology*, vol. 7, no. 11, pp. 1032–1043, Nov. 2008.

[8] G. R. Muller-Putz, R. Scherer, C. Brauneis, and G. Pfurtscheller, "Steady-state visual evoked potential (SSVEP)-based communication: impact of harmonic frequency components," *J. of Neural Eng.*, vol. 2, no. 4, pp. 123–130, Dec. 2005.

[9] C. S. Herrmann, "Human EEG responses to 1-100 Hz flicker: Resonance phenomena in visual cortex and their potential correlation to cognitive phenomena," *Exper. Brain Res.*, vol. 137, no. 3-4, pp. 346–353, Apr. 2001.

[10] G. G. Molina and V. Mihajlovic, "Spatial filters to detect steady-state visual evoked potentials elicited by high frequency stimulation: BCI application," *Biomedizinische Technik*, vol. 55, no. 3, pp. 173–182, June 2010, Special Issue.

[11] S. M. M. Torres, P. F. Diez, T. Bastos-Filho, M. Sarcinelli-Filho, V. Mut, and E. Laciar, "SSVEP-BCI implementation for 37-40 Hz frequency range," in *Conf. Proc. IEEE EMBS*, 2011, pp. 6352–6355.

[12] P. F. Diez, V. A. Mut, E. M. A. Perona, and E. L. Leber, "Asynchronous BCI control using high-frequency SSVEP," *J. of NeuroEngineering and Rehabilitation*, vol. 8, pp. 1–8, 2011, article No. 39.

[13] I. Volosyak, D. Valbuena, T. Luth, T. Malechka, and A. Graser, "BCI demographics II: How many (and what kinds of) people can use a high-frequency SSVEP BCI?" *IEEE Trans. Neural Sys. and Rehab. Eng.*, vol. 19, no. 3, pp. 232–239, June 2011.

[14] R. Scherer, F. Lee, A. Schlogl, R. Leeb, H. Bischof, and G. Pfurtscheller, "Towards self-paced brain-computer communication: Navigation through virtual worlds," *IEEE Trans. Biomed. Eng.*, vol. 55, no. 2, pp. 675–682, February 2008.

[15] [Personal communication], 2013, Cristoph Kappeller, g.tec Medical Engineering GMBH.

[16] A. V. Oppenheim and R. W. Schafer, *Digital Signal Processing*. Englewood Cliffs, N.J: Prentice-Hall, 1975, includes bibliographical references.

[17] S. J. Luck, *An Introduction to the Event-Related Potential Technique*, 2nd ed. Cambridge, MA: MIT Press, 2014.

[18] M. X. Cohen, *Analyzing Neural Time Series Data*. Cambridge, MA: MIT Press, 2014.

[19] A. Paris, G. Atia, A. Vosoughi, and S. Berman, "Hidden Quantum Models of Neuron Ion Channels as a Source of 1/f-Type Noise," 2017, iEEE Trans. Biomed. Eng. [To appear].

[20] ——, "Final Report on National Science Foundation Grant CCF-1525990," [Online], 2017.

[21] N. Wiener, *Cybernetics or Control and Commmunication in the Animal and Machine*. Cambridge, MA: MIT Press, 1948.

[22] S. Albeverio, "Wiener and Feynman path integrals and their applications," in *Proceedings of the Norbert Wiener Centenary Congress, 1994*, ser. Proceedings of Symposia in Applied Mathematics, V. Mandrekar and P. Masani, Eds., vol. 52. American Mathematical Society, 1994, pp. 163–194.

[23] N. Wiener, *I Am a Mathematician*. Cambridge, MA: MIT Press, 1956.

[24] ——, *Time Series*. Cambridge, MA: MIT Press, 1949.

[25] A. Hodgkin and A. Huxley, "A quantitative description of membrane current and its application to conduction and excitation in nerve," *J. Physiol.*, vol. 117, pp. 500–544, 1952.

[26] A. Hodgkin, A. Huxley, and B. Katz, "Measurement of current-voltage relations in the membrane of the giant axon of *Loligo*," *J. Physiol.*, vol. 116, pp. 424–448, 1952.

[27] R. Penrose, *Quantum Physics and Conscious Thought*. London: Routledge & Kegan Paul, 1987, pp. 105–120.

[28] R. Penrose and S. Hameroff, *Conciousness in the Universe: Neuroscience, Quantum Space-Time Geometry, and Orch OR Theory*. Cambridge, MA: Cosmology Science Publishers, 2011, pp. 3–42.

[29] C. Koch and K. Hepp, "Quantum mechanics in the brain," *Nature*, no. (7084):611, 2006.

[30] L. K. McKemmish, J. R. Reimers, R. H. McKenzie, A. E. Mark, and N. S. Hush, "Penrose-Hameroff orchestrated objective-reduction proposal for human consciousness is not biologically feasible," *Phys. Review E*, no. 021912, pp. 1–6, 2009.

[31] M. Tegmark, "The importance of quantum decoherence in brain processes," *Physica Rev E*, no. 61, pp. 4194–4206, 2000.

[32] T. Hill and Y.-D. Chen, "On the theory of ion transport across the nerve membrane, IV. Noise from the open-close kinetics of K^+ channels," *Biophys. J.*, vol. 12, pp. 948–959, 1972.

[33] A. Manwani and C. Koch, "Detecting and estimating signals in noisy cable structures, I: Neuronal noise sources," *Neural Computation*, vol. 11, pp. 1797–1829, 1999.

[34] B. Hille, *Ion Channels of Excitable Membranes*, 3rd ed. Sunderland, MA: Sinauer Associates, Inc., 2001.

[35] K. Diba, H. Lester, and C. Koch, "Intrinsic noise in cultured hippocampal neurons: Experiment and modeling," *J. of Neuroscience*, vol. 24, no. 43, pp. 9723–9733, October 27, 2004.

[36] P. L. Nunez and R. Srinivasan, *Electric fields of the brain: The neurophysics of EEG*, 2nd ed. Oxford: Oxford University Press, 2006.

[37] H. Bakardjian, T. Tanaka, and A. Cichocki, "Optimization of SSVEP brain responses with application to eight-command brain computer interface," *Neurosci Lett.*, vol. 469, no. 1, pp. 34–38, 2010. [Online]. Available: http://www.bakardjian.com/work/ssvep_data_Bakardjian.html

[38] A. Destexhe and M. Rudolph-Lilith, *Neuronal Noise*, ser. Springer Series in Computational Neuroscience, Vol. 8. Springer, 2012.

[39] R. Tetzlaff, T. Niederhofer, and P. Fischer, "Automated detection of a preseizure state: Non-linear EEG analysis in epilepsy by cellular nonlinear networks and Volterra systems," *Int. J. Circuit Th. and Applications.*, vol. 34, no. 1, pp. 89–108, Jan-Feb 2006.

[40] L. Rankine, N. Stevenson, M. Mesbah, and B. Boashash, "A nonstationary model of newborn EEG," *IEEE Trans. Biomed. Eng.*, vol. 54, no. 1, pp. 19–28, January 2007.

[41] L. J. DeFelice, *Introduction to Membrane Noise*. New York: Plenum, 1981.

[42] S. Bezrukov and I. Vodyanoy, "Noise in biological-membranes and relevant ionic systems," in *Biomembrane Electrochemistry*, M. Blank and I. Vodyanoy, Eds. Oxford UP, 1994, pp. 375–399.

[43] J. A. White, J. T. Rubinstein, and A. R. Kay, "Channel noise in neurons," *Trends. Neurosci.*, vol. 23, no. 2, 2000.

146

[44] Z. Mainen and T. Sejnowski, "Influence of dendritic structure in firing pattern in model neocortical neurons," *Nature*, vol. 382, pp. 363–366, July 25, 1996.

[45] A. Herz, T. Gollisch, C. Machens, and D. Jaeger, "Modeling single-neuron dynamics and computations: A balance of detail and abstraction," *Science*, vol. 314, no. 80, pp. 80–85, October 6, 2006.

[46] A. Manwani and C. Koch, "Detecting and estimating signals in noisy cable structures, II: Information theoretical analysis," *Neural Computation*, vol. 11, pp. 1831–1873, 1999.

[47] W. J. Freeman, M. Holmes, B. C. Burke, and S. Vanhatalo, "Spatial spectra of scalp EEG and EMG from awake humans," *Clin. Neurophysiol.*, vol. 114, no. 6, pp. 1053–1068, Jun. 2003.

[48] A. F. Strassberg and L. J. DeFelice, "Limitations of the Hodgkin-Huxley formalism: Effects of single channel kinetics on transmembrane voltage dynamics," *Neural Computation*, vol. 5, pp. 843–855, 1993.

[49] D. Mak and W. Webb, "Conductivity noise in transmembrane ion channels due to ion concentration fluctuations via diffusion," *Biophys. J.*, vol. 72, pp. 1153–1164, 1997.

[50] T. N. Palmer and M. O'Shea, "Neuronal noise as a physical resource for human cognition," December 2014. [Online]. Available: http://arxiv.org/abs/1412.4920

[51] R. Legenstein and W. Maass, "Ensembles of spiking neurons with noise support optimal probabilistic inference in a dynamically changing environment," *PLoS Computational Biology*, vol. 10, no. 10, pp. 1–27, 10 2014.

[52] G. Buzsáki, *Rhythms of the brain*. Oxford University Press, 2006.

[53] B. Katz and R. Miledi, "The statistical nature of the acetycholine potential and its molecular components," *J. Physiol.*, vol. 224, pp. 665–699, 1972.

[54] A. Díez, V. Suazo, P. Casado, M. Martín-Loeches, and V. Molina, "Spatial distribution and cognitive correlates of gamma noise power in schizophrenia," *Psychological Medicine*, vol. 43, no. 6, pp. 1175–1185, June 2013.

[55] O. Vysata, A. Procházka, J. Mares, R. Rusina, L. Pazdera, M. Valis, and J. Kukal, "Change in the characteristics of EEG color noise in Alzheimer's disease," *Clinical EEG And Neuroscience*, vol. 45, no. 3, pp. 147–151, July 2014.

[56] P. J. Brockwell and R. A. Davis, *Time Series: Theory and Methods*, 2nd ed. New York: Springer-Verlag, 1991.

[57] K. D. Miller and T. W. Troyer, "Neural noise can explain expansive, power-law nonlinearities in neural response functions," *J. Neurophysiol.*, vol. 87, pp. 653–659, 2002.

[58] V. Gribkoff and L. Kaczmarek, Eds., *Structure, Function, and Modulation of Neuronal Voltage-Gated Ion Channels*. Hoboken: Wiley, 2009.

[59] W. McColloch and W. Pitts, "A logical calculus of the ideas immanent in nervous activity," *Bull. Math. Biophysics*, vol. 5, pp. 115–133, 1943.

[60] J. Woodbury, "Eyring rate theory model of the current-voltage relationships of ion channels in excitable membranes," in *Advances in Chemical Physics, Volume XVI*. John Wiley and Sons Ltd., 1969, pp. 601–617.

[61] D. Sigg, "Modeling ion channels: Past, present, and future," *J. Gen. Physiol.*, vol. 144, no. 1, pp. 7–26, 2014.

[62] D. Johnston and S. M.-S. Wu, *Foundations of Cellular Neurophysiology*. Cambridge, MA: MIT Press, 1995.

[63] A. Destexhe, Z. F. Mainen, and T. J. Sejnowski, "Synthesis of models for excitable membranes, synaptic transmission and neuromodulation using a common kinetic formalism," *J. of Comp. Neurosci.*, vol. 1, pp. 195–230, 1994.

[64] R. Fitzhugh, "A kinetic model of the conductance changes in nerve membrane," *J. Cell. Comp. Physiol.*, vol. 66, Suppl., pp. 111–117, 1965.

[65] T. Hill and Y.-D. Chen, "Cooperative effects in models of steady-state transport across membranes, I," *Proc. Nat. Acad. of Sci. USA*, vol. 65, no. 4, pp. 1069–1076, April 1970.

[66] ——, "On the theory of ion transport across the nerve membrane, II. Potassium ion kinetics and cooperativity (with x = 4)," *Proc. Nat. Acad. of Sci. USA*, vol. 68, no. 8, pp. 1711–1715, August 1971.

[67] ——, "On the theory of ion transport across the nerve membrane, III. Potassium ion kinetics and cooperativity (with x = 4,6,9)," *Proc. Nat. Acad. of Sci. USA*, vol. 68, no. 10, pp. 2488–2492, October 1971.

[68] ——, "On the theory of ion transport across the nerve membrane, VI. Free energy and activation free energies of conformal change," *Proc. Nat. Acad. of Sci. USA*, vol. 69, no. 7, pp. 1723–1726, July 1972.

[69] ——, "On the theory of ion transport across the nerve membrane, VII. Cooperativity between channels of a large square lattice," *Proc. Nat. Acad. of Sci. USA*, vol. 70, no. 1, pp. 62–65, January 1973.

[70] ——, "Fluctuations and noise in kinetic systems: Application to K^+ channels," *Biophys. J.*, vol. 13, pp. 1276–1295, 1973.

[71] F. Conti, L. DeFelice, and E. Wanke, "Potassium and sodium ion current noise in the membrane of the squid giant axon," *J. Physiol. (London)*, vol. 248, pp. 45–82, 1975.

[72] J. Clay and L. DeFelice, "Relationship between membrane excitability and single-channel open-close kinetics," *Biophys. J.*, vol. 42, pp. 151–157, May 1983.

[73] J. H. Morals-Cabral, Y. Zhou, and R. MacKinnon, "Energetic optimization of ion conduction rate by the K^+ selectivity filter," *Nature*, vol. 414, pp. 37–42, 1 November 2001.

[74] S. Bernèche and B. Roux, "Energetics of ion conduction through the K^+ channel," *Nature*, vol. 414, pp. 73–76, 1 November 2001.

[75] Y. Zhou, J. H. Morals-Cabral, A. Kaufman, and R. MacKinnon, "Chemistry of ion coordination and hydration revealed by a K^+ channel–Fab complex at 2.0 Å resolution," *Nature*, vol. 414, pp. 43–48, 1 November 2001.

[76] G. Bernroider and S. Roy, "Quantum entanglement of K^+ ions, multiple channel states, and the role of noise in the brain," in *Proc. SPIE 5841, Fluctuations and Noise in Biological, Biophysical, and Biomedical Systems III, 205.* SPIE, 2005, pp. 5841–29:205–14.

[77] A. Sudbery, *Quantum Mechanics and the Particles of Nature.* Cambridge: Cambridge University Press, 1988.

[78] H. Royden, *Real Analysis*, 2nd ed. New York: Macmillan Publishing Co., 1968.

[79] J. Lamperti, *Stochastic Processes: A Survey of the Mathematical Theory*, ser. Applied Mathematical Sciences. New York: Springer-Verlag, 1977, vol. 23.

[80] A. Rényi, *Foundations of Probability.* San Francisco: Holden-Day, 1970.

[81] R. J. Elliot, L. Aggoun, and J. B. Moore, *Hidden Markov Models: Estimation and Control.* New York: Springer-Verlag, 1995.

[82] N. G. Van Kampen, *Stochastic Processes in Physics and Chemistry*, Rev. and enl. ed. Amsterdam ; New York: North-Holland, 1992.

[83] R. Feynman, *Negative probabilities.* London: Routledge & Kegan Paul, 1987, pp. 235–248.

[84] B. Mandelbrot, "Some noises with 1/f spectrum: A bridge between direct current and white noise," *IEEE Trans. Information Th.*, no. 2, pp. 289–298, April 1967.

[85] D. A. Bell, "A survey of 1/f noise in electrical conductors," *J. Phys. C.: Solid State Phys.*, vol. 13, pp. 4425–4437, 1980.

[86] P. Dutta and P. M. Horn, "Low-frequency fluctuations in solids: 1/f noise," *Rev. Modern Phys.*, vol. 53, no. 3, pp. 497–516, July 1981.

[87] M. S. Keshner, "1/f noise," *Proc. IEEE*, vol. 70, no. 3, pp. 212–218, March 1982.

[88] B. Mandelbrot, *Multifractals and 1/f Noise.* New York: Springer-Verlag, 1999.

[89] D. T. Gillepsie, "The mathematics of Brownian motion and Johnson noise," *Am. J. of Phys.*, vol. 64, no. 3, pp. 225–240, March 1996.

[90] J. Bernamont, "Fluctuations in the resistance of thin films," *Proc. Phys. Soc. Lond.*, vol. 49, p. 138, 1937.

[91] K. Linkenhaer-Hansen, V. V. Nikouline, J. M. Palva, and R. Ilmoniemi, "Long-range temporal correlations and scaling behavior in human brain oscillations," *J. of Neuroscience*, no. 4, pp. 1370–1377, February 2001.

[92] A. P. Liavas, G. V. Moustakides, G. Henning, E. Psarakis, and P. Husar, "A periodogram-based method for the detection of steady-state visually evoked potentials," *IEEE Trans. Biomed. Eng.*, vol. 45, no. 2, pp. 242–248, Feb. 1998.

[93] A. M. Mood, F. A. Graybill, and D. C. Boes, *Introduction to the Theory of Statistics*, 3rd ed. New York: McGraw-Hill, 1974.

[94] A. M. L. F. M. de Sá, A. F. C. Infantosi, and V. V. Lazarev, "Evaluating the event-related synchronization and desynchronization by means of a statistical frequency test," in *29th Annual International Conference of the IEEE Engineering in Medicine and Biology Society*, Cité Internationale, Lyon, France, 2007.

[95] A. L. McWhorter, "1/f noise and related surface effects in Germanium, MIT Lincoln Laboratory Report No. 80," in *Semiconductor Surface Physics*, R. Kingston, Ed. Univ. of Penns. Press, 1957, p. 207.

[96] V. der Ziel, "On the noise spectra of semiconductor noise and flicker effect," *Physica*, vol. 16, no. 4, pp. 359–372, 1950.

[97] F. Du Pre, "A suggestion regarding the spectral density of flicker noise," *Phys. Rev.*, vol. 78, p. 615, 1950.

[98] C. Suh and V. der Ziel, "A noise spectrum described by a distribution in time constants," *Appl. Phys. Lett.*, vol. 37, no. 6, pp. 565–566, 1980.

[99] A. van der Ziel, "Noise in solid-state devices and lasers," *Proc. IEEE*, vol. 58, no. 8, pp. 1178–1206, 1970.

[100] R. F. Voss and J. Clarke, "1/f noise in music and speech," *Nature*, vol. 258, no. 5533, pp. 317–318, November 27, 1975.

[101] F.-B. Vialette, M. Marice, J. Dauwels, and A. Cichocki, "Steady-state evoked potentials: Focus on essential paradigms and future perspectives," *Progress in Neurobiology*, no. 90, pp. 418–438, 2010.

[102] D. Bohm and B. Hiley, *The Undivided Universe*.   London: Routledge, 1993.

[103] W. Thirring, *Quantum Mechanics of Atoms and Molecules*, ser. A Course in Mathematical Physics. New York; Wien: Springer-Verlag, 1979, vol. 3.

[104] D. Bohm, *Quantum Theory*.   New York: Dover Publications, 1989.

[105] R. C. Tolman, *The Principles of Statistical Mechanics*.   New York: Dover Publications, 1979.

[106] M. C. Mackey, *Time's Arrow: The Origins of Thermodynamic Behavior*, Dover Publications paperback 2003 ed.   New York: Springer-Verlag, 1992.

[107] D. Bohm, *Wholeness and the Implicate Order*.   London: Routledge and Kagan Paul, 1980.

[108] R. Penrose, *The Emperor's New Mind: Concerning Computers, Minds and the Laws of Physics*. Oxford University Press, 1989.

[109] J. K. Hunter and B. Nachtergaele, *Applied Analyis*.   Singapore: World Scientific, 2001.

[110] P. A. M. Dirac, *Principles of Quantum Mechanics*, 4th ed.   Oxford: Oxford Science Publications, 1958.

[111] M. Reed and B. Simon, *Methods of Modern Mathematical Physics, Vol I. Functional Analysis*, Revised and Enlarged ed.   San Diego: Academic Press, 1980.

[112] S. K. Berberian, *Lectures in Functional Analysis and Operator Theory*, ser. Graduate Texts in Mathematics 15.   New York: Springer-Verlag, 1974.

[113] L. Accardi, A. Frigerio, and J. Lewis, "Quantum stochastic processes," *Pub. Res. Inst. Math. Sci. Kyoto Univ.*, vol. 18, pp. 97–133, 1982.

[114] W. Słomczyński and K. Życzkowski, "Quantum chaos: An entropy approach," *J. Math. Physics*, vol. 32, no. 1, pp. 5674–5700, 1994.

[115] L. Accardi, "Nonrelativistic quantum mechanics as a noncommutative Markof process," *Advances in Mathematics*, vol. 20, pp. 329–366, 1976.

[116] J. Heo, V. Belavkin, and U. Ji, "Monotone quantum stochastic processes and covariant dynamical hemigroups," *J. Functional Analysis*, vol. 261, pp. 3345–3365, 2011.

[117] S. Gudder, "Transition effect matrices and quantum markov chains," *Found. Phys.*, vol. 39, pp. 573–592, 2009.

[118] H. R. Brown and R. Harré, Eds., *Philosophical Foundations of Quantum Field Theory*. Oxford: Clarendon Press, 1990.

[119] G. B. Folland, *Quantum Field Theory: A Tourist Guide for Mathematicians*, ser. Mathematical Surveys and Monographs. Providence: American Mathematical Society, 2008, vol. 149.

[120] R. Bower, B. Bowman, and J. Kenyon, "Theory of the kinetic analysis of patch-clamp data," *Biophys. J.*, vol. 52, no. 6, pp. 961–978, 1987.

[121] A. Paris, G. Atia, A. Vosoughi, and S. Berman, "A New Statistical Model of EEG Noise Spectra for Real-Time, Low–γ–band SSVEP Brain-Computer Interfaces," in *Proc. Sixth International BCI Meeting*, 2016.

[122] L. Liebovitch and J. Sullivan, "Fractal analysis of a voltage-dependent potassium channel from cultured mouse hippocampal neurons," *Biophys. J.*, vol. 52, pp. 979–988, 1987.

[123] R. A. Horn and C. R. Johnson, *Matrix Analysis*, paperback ed. Cambridge; New York: Cambridge University Press, 1985.

[124] A. Paris, A. Vosoughi, and G. Atia, "Whitening 1/f-type noise in electroencephalogram signals for steady-state visual evoked potential brain-computer interfaces," in *48th Asilomar Conf. on Signals, Systems and Computers*, 2014, ©2014 IEEE.

[125] I. M. Gel'fand and N. Y. Vilenkin, *Generalized Functions*. New York: Academic Press, 1964, vol. 4: Applications of Harmonic Analysis.

[126] A. van der Ziel, *Appl. Phys. Lett.*, pp. 883–884, 1978.

[127] B. C. Levy, *Principles of Signal Detection and Parameter Estimation*. New York: Springer Science+Business Media, 2008.

[128] J. L. Doob, *Stochastic Processes*. New York: John Wiley & Sons, 1953.

[129] Y. Benjamini and Y. Hochberg, "Controlling the false discovery rate: a practical and powerful approach to multiple testing," *J. Royal Statistical Soc., Series B*, vol. 57, no. 1, pp. 289 – 300, 1995.

[130] Y. Benjamini, A. M. Krieger, and D. Yekutieli, "Adaptive linear step-up procedures that control the false discovery rate," *Biometrika*, vol. 93, no. 3, pp. 491 – 507, 2006.

[131] T. Fawcett, "An introduction to ROC analysis," *Pattern Recognition Letters*, no. 27, pp. 861 – 871, 2006.

[132] B. Efron and R. J. Tibshirani, *An Introduction to the Bootstrap*, ser. Monographs on Statistics and Applied Probability 57. New York: Chapman & Hall, 1993.

[133] Q. Wei, M. Xiao, and Z. Lu, "A comparative study of correlation analysis and power spectral density analysis for SSVEP detection," in *Third International Conference on Intelligent Human-Machine Systems and Cybernetics*, 2011, pp. 7–10.

[134] R. Kuś, A. Dusyk, P. Milanowski, M. Łabęcki *et al.*, "On the quantification of SSVEP frequency responses in human EEG in realistic BCI conditions," *PLoS ONE*, vol. 8, no. 10, pp. e77 536:1–9, October 2013.

[135] L. Ljung, *System Identification – Theory for the User*. Englewood Cliffs, N.J: Prentice-Hall, 1987.

[136] R. von Mises, *Probability, Statistics, and Truth*. New York: Dover Publications, 1981.

[137] F. M. Brückler, "Tensor products of C*–algebras, operator spaces, and Hilbert C*–modules," *Mathematical Communications*, vol. 4, pp. 257–268, 1999.

[138] J. J. Rotman, *An Introduction to Homological Algebra*. New York: Academic Press, 1979.